THE RESISTANCE OF CIRCULATING TUMOR CELLS TO LARGE FLUID SHEAR STRESS IN HEMATOGENOUS DISSEMINATION BY REDUCING MECHANOSENSITIVITY VIA NUCLEAR MECHANOSENSING MEDIATED MYOSIN CYTOPLASMIC REDISTRIBUTION

ZHANG CUNYU

PhD

The Hong Kong Polytechnic University

2024

The Hong Kong Polytechnic University

Department of Biomedical Engineering

The resistance of circulating tumor cells to large fluid shear stress in hematogenous dissemination by reducing mechanosensitivity via nuclear mechanosensing mediated myosin cytoplasmic redistribution

ZHANG CUNYU

A thesis submitted in partial fulfilment of the requirements for the degree of Doctor of Philosophy

Aug. 2023

CERTIFICATE OF ORIGINALITY

I hereby declare that this thesis is my own work and that, to the best of my knowledge and belief, it reproduces no material previously published or written, nor material that has been accepted for the award of any other degree or diploma, except where due acknowledgement has been made in the text.

_____ _____ (Signed)

ZHANG Cunyu (Name of student)

Abstract

Tumor cells metastasize to distant organs mainly through hematogenous dissemination, where circulating tumor cells (CTCs) experience varying levels of fluid shear stress (FSS) in capillaries, veins, and arteries. Although FSS is one critical rate-limiting factor of cell survival, there are always a small subpopulation of CTCs persisting within the vasculature, which may eventually generate metastatic tumors that contribute to the majority of cancer-related death. It is well known that living cells that adhere to solid substrates can perceive mechanical cues through mechanotransduction. However, how CTCs in suspension respond to varying levels of FSS remains unclear. Importantly, limited knowledge of how CTCs mechanically adapt to FSS impedes our understanding of CTCs' survival during hematogenous dissemination.

In this study, we found that the apoptosis of suspended breast tumor cells (SBTCs) showed weaker increase rate under high FSS compared to low FSS range, suggesting that SBTCs may exhibit reduced mechanosensitivity under high FSS, which could serve as a protective mechanoadaptation mechanism for their survival. Mechanistically, the phosphorylated myosin light chain (P-MLC), representative of myosin II activation, was predominantly localized in the cortex under low FSS and re-distributed to the cytoplasm under high FSS. Similar phenomena were observed in SBTCs that were attached to Poly-L-Lysine (PLL) coated glass, which could mimic the suspension status. Further, we defined the ratio of the resultant nuclear strain and the applied FSS as force transmission efficiency (FTE) from the cell membrane to nucleus, which was relatively high under low FSS but decreased under high FSS in both suspended and PLL-adhered tumor cells. Inhibition of cytoplasmic but not cortical P-MLC pharmacologically and specifically restored the FTE under high FSS and enhanced shear-induced DNA damage and cell apoptosis.

To elucidate the mechanism underlying P-MLC subcellular relocalization, we discovered that Lamin A/C-mediated nuclear mechanosensing increased nuclear

envelop tension and triggered calcium release from endoplasmic reticulum, which further activated cortical and cytoplasmic P-MLC through myosin light chain kinase (MLCK) and Rho associated protein kinase (ROCK) under low and high FSS, respectively. Targeting ROCK but not MLCK rescued shear-induced decease in FTE and increased the shear-induced apoptosis of SBTCs both *in vitro* and *in vivo*. In addition, high cytoplasmic P-MLC was also found in cancer stem cells (CSCs) and blood cells that held the survival advantage under FSS. Pharmacologic inhibition of ROCK significantly increased the shear-induced cell apoptosis.

Collectively, our results unveiled a previously unappreciated role of nuclear mechanosensing mediated cytoplasmic myosin II activation in regulating force transmission and mechanosensitivity of SBTCs, by which CTCs mechanically adapted to large FSS, providing new insights into the survival of CTCs during hematogenous metastasis.

List of publications

- Xi Chen[#], Zichen Xu[#], Kai Tang[#], Guanshuo Hu, Pengyu Du, Junfan Wang, **Cunyu Zhang**, Ying Xin, Keming Li, Qianting Zhang, Jianjun Hu, Zhuxue Zhang, Mo Yang, Guixue Wang, Youhua Tan. The Mechanics of Tumor Cells Dictate Malignancy via Cytoskeleton-Mediated APC/Wnt/β-Catenin Signaling *Research (Wash D C).* 2023 Sep 21:6:0224.

- Junfan Wang, Bai Zhang, Xi Chen, Ying Xin, Keming Li, **Cunyu Zhang**, Kai Tang, Youhua Tan. Cell mechanics regulate the migration and invasion of hepatocellular carcinoma cells via JNK signaling. *Acta Biomater.* 2024 Mar 1:176:321-333.

- Chen X, Tang K, Li X, **Zhang C**, Xin Y, Li K, Tan Y. Biomechanics of cancer stem cells. *Essays Biochem.* 2022 Sep 16;66(4):359-369.

- Zhang B, Li X, Tang K, Xin Y, Hu G, Zheng Y, Li K, **Zhang C**, Tan Y. Adhesion to the Brain Endothelium Selects Breast Cancer Cells with Brain Metastasis Potential. *Int J Mol Sci.* 2023 Apr 11;24(8):7087.

Presentations

- **Cunyu Zhang**, Kai Tang, Keming Li, Ying Xi, Youhua Tan. Cytoplasmic myosin II localization regulates force transmission efficiency and mediates the mechanoadaptation of circulating tumor cells to fluid shear flow. PAIR Conference 2023: Research Excellence for Societal Impacts (2023)

- Tan Youhua, Xi Chen, Kai Tang, **Cunyu Zhang**. Do Tumor Cell mechanics Matter in Malignancy. 2023 中国生物医学工程大会暨创新医疗峰会. (2023)

Acknowledgments

Time went by as the flowing water. Three years PhD career was comping to an end. During three years study, it was my good fortune to have a great supervisor, a number of friends and lab mates.

First of all, I want to express my great appreciation to my chief supervisor, Dr TAN Youhua, who guided me the path of research during three years. Before enrolment in PolyU, I knew nothing about tumor mechanics. The meetings with Dr. TAN and Dr. TANG Xin from University of Florida during one year after enrolment undoubtedly enhanced my knowledge about tumor cell and tumor tissue mechanics, both of which were basics of my research. Every time that I discussed with Dr. TAN, his rigorous thinking and practical recommendations always inspired me to think deeper and explore deeper. Meanwhile, I also want to thanks to my co-supervisor, Prof. YANG Mo in supporting me during my research.

Then, I am also extremely grateful to my parents and my folks. My PhD career was accompanied with COVID-19 pandemics, during which I cannot see my parents and folks. At the beginning of my PhD study, your encouragements and comforts were the momentums that I persisted, your deep concern and love were the source of my power. I am sure these experiences were treasure in my whole life.

Finally, I want to take this opportunity to thanks to my lab mates. LI Keming gave me valuable advices and precious assistances in both my research and daily life. It was so fortunate to meet with you, to acquaint with you and to share happiness and sadness with you. In addition, I want to express my gratitude to XIN Ying and WANG Junfan who assisted me in my early PhD study. I also sincerely appreciate for the kind help from TANG Kai, MAO Renwei, CHEN Xi, DU Pengyu, MENG Jianfeng, HU Guanshuo, HU Bing, ZHANG Yufan, ZHANG Bai and LI Xueyi from lab.

Table of contents

List of figures

Chapter 1

Chapter 2

Chapter 3

Chapter 4

Chapter 5

Chapter 6

Chapter 7

Chapter 8

List of abbreviations

4-HAP	4-Hydroxyacetopophenone
ABP	Actin binding protein
ADP	Adenosine diphosphate
AFM	Atomic force microscopy
AJ	Adherent junction
ATP	Adenosine triphosphate
Ble	Blebbistatin
BLI	Bioluminescence Imaging
BM	Basement membrane
BSA	Bovine serum albumin
CAF	Cancer associated fibroblast
cPLA2	Cytosolic phospholipase A2
CSCs	Cancer stem cells
CTCs	Circulating tumor cells
DMEM	Dulbecco's Modified Eagle Medium
DOX	Doxycycline
ECM	Extracellular matrix
EDAC	Epithelial defence against cancer
EGTA	Ethylene glycol-bis (β-aminoethylether)-N,N,N′,N′-tetraacetic acid
ELC	Essential light chains
EMT	Epithelial-mesenchymal transition
EOP_{NE}	Excess of perimeter of the NE
ER	Estrogen receptor
ER	Endoplasmic reticulum
ERM	Ezrin, radixin and moesin
ESCs	Embryonic stem cells
FA	Focal adhesion
F-actin	Filamentous actin
FRET	Fluorescence resonance energy transfer
FSS	Fluid shear stress

FTE	Force transmission efficiency
G-actin	Globular actin
GEF	Guanine nucleotide exchange factors
H2B	Histone 2B
HA	Hyaluronic acid
H3K9	Histone 3 lysine 9
HC	Heavy chains
HER2	Human epidermal growth factor receptor 2
IFs	Intermediate filaments
ISCs	Intestinal stem cells
KASH	Klarsicht/ANC-1/Syne Homology
LADs	Lamin associated domains
Lamin A/C	Lamin A and Lamin C
Lamin B	Lamin B1 and Lamin B2
LINC	Linker of nucleoskeleton and cytoskeleton
MLC	Myosin light chain
MLCK	Myosin light chain kinase
MLCP	Myosin light chain phosphatase
MSCs	Mesenchymal stem cells
MTC	Magnetic twisting cytometry
MYPT	Myosin phosphatase targeting protein
NE	Nuclear envelop
Non-CSCs	Non selected CSCs
NPCs	Nuclear pore complexes
PI	Propidium iodide
PLL	Poly-L-Lysine
PM	Plasma membrane
P-MLC	Phosphorylated myosin light chain
PR	Progesterone receptor
PTMs	Post-Translational Modifications
PVDF	Polyvinylidene difluoride

RBCs	Red blood cells
RGD	Arg-Gly-Asp
RhoA	Ras homolog family member A
RLC	Regulatory light chains
ROCK	Rho associated protein kinase
ROS	Reactive oxygen species
SBTCs	Suspended breast tumor cells
SFs	Stress fibers
Si-RNA	Small interfering RNA
SUN	Sad1p, UNC-84
TAMs	Tumor-associated macrophages
Tg	Thapsigargin
TGF-β	Transforming growth factor beta
Triple negative	ER^-, PR^- and $HER2^-$
uniform FSS	Wall shear stress
Y27	Y-27632
YAP	Yes-associated protein 1

Chapter 1. Introduction and literature review

1.1 Cancer and cancer metastasis

1.1.1 Cancer and cancer progression

Cancer ranks as the second leading cause of human death in the world[1]. According to the report of World Health Organization, there were more than nineteen million new cancer cases occurred during 2020[2]. In united states, the number of cancer diagnoses was estimated to reach two million in 2022 and there was still an increase trend in 2023[3]. Until now, more than two hundred types of cancer were found. Among them, breast cancer, which surpassed lung cancer and became the most commonly diagnosed cancer type in 2020, accounts for 11.7% of total new cancer cases and 6.9% of cancer death[2]. According to the immunohistochemical expression of estrogen receptor (ER), progesterone receptor (PR), human epidermal growth factor receptor 2 (HER2) and proliferation marker Ki67, breast cancer can be divided into five subtypes. Whereas ER^+, PR^+ breast cancer cells such as MCF-7 showed lower malignancy and risk, ER^-, PR^- and $HER2^-$ (Triple negative) breast cancer cells such as MDA-MB-231 had high malignancy and risk[4]. Although great advance had been made in technological evolution of cancer treatments, such as the emerging neoadjuvant chemotherapy[5] and immunotherapy[6], cancer still claimed nearly ten million people life in 2020[7]. Thus, it is urgent to investigate cancer progression thoroughly, which may help cancer drug development and guide clinical cancer therapy.

More than 90% of cancer-related deaths result from cancer metastasis and it is a terrible status that people have to deal with[8, 9]. Actually, previous studies have largely enhanced our knowledge about cancer metastasis. Researchers have attempted to summarize the distinct characteristics of cancer metastasis compared with primary tumor development. The distinct features of cancer metastasis including motility and invasion, plasticity,

modulation of microenvironment and colonization[10]. During metastasis, tumor cells detach from the primary lesion, invade basement membrane and local tumor stroma, intravasate into blood vessel, disseminate along with the circulation system, finally extravasate into and colonize in distant organ[11].

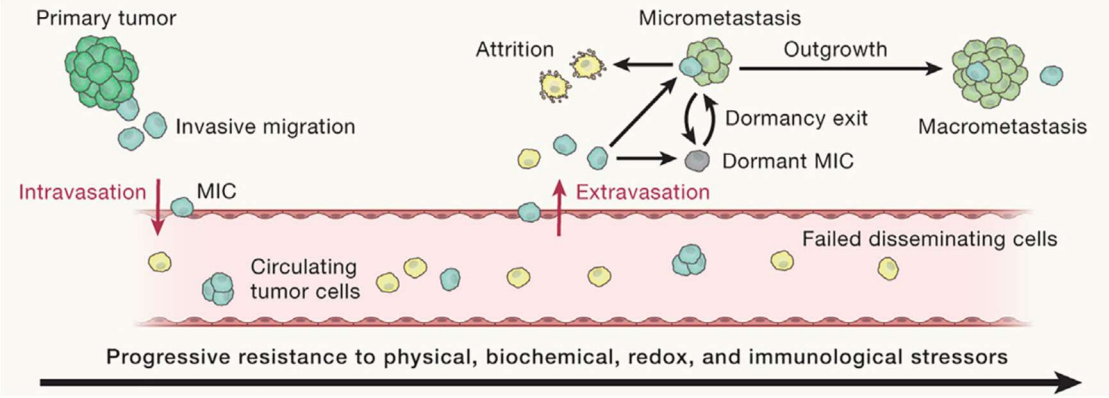

Figure 1-1 Process of cancer metastasis. After shedding from primary tumor, cancer cells migrate and intravasate into blood circulation. With blood flow, cancer cells disseminate into distant organ where they may develop secondary metastasis[11].

Previous studies have unveiled the fundamental roles of biochemical factors that contribute to the cancer progression. For instance, during primary tumor formation, APC-mutant intestinal stem cells (ISCs) outcompete wild type ISCs by continuatively producing WNT antagonists to neighboring wild-type ISCs, thereby promoting differentiation of wild type ISCs and further inhibits their growth[12]. This kind of inhibition is through cell secretion factors, which is quite different from the contact inhibition normally seen in normal epithelial[13]. In addition, while immune system eliminates neoplastic cells that show the unique antigens, chronic and unrestricted inflammation trigged by the caerulein enhances chromatin accessibilities and abnormal epigenetic reprogramming that contributes to the gene mutation of pancreatic epithelial cells[14]. On another hand, during cancer cell invasion, cancer associated fibroblasts (CAF) are activated by transforming growth factor beta (TGF-β) secreted by malignant tumor cells. The activated CAF further degrade underlying matrix through secreting metalloproteinases which facilitates cancer cell invasion[15]. Thus, biochemical cues play vital role in cancer dissemination.

1.1.2 Mechanical cues during cancer metastasis

Aside from biochemical factors whose functions have been wealthy studied during metastasis, the significance of mechanical cues have been highlighted recently[16]. As stated in seed and soil model, the mechanical properties of soil, that is mechanical microenvironment, could influence tumor progression[17]. For example, the stiffness of basement membrane (BM), which consists of primarily of collagen IV and laminin, is a pivotal factor determine whether or not the cancer cells could successfully penetrate BM. While high expression of Netrin-4, a key regulator of BM stiffness, decreases the stiffness of BM and impedes cancer cell penetration, knocking down Netrin-4 significantly enhances the BM stiffness and further facilitates tumor cell penetration and cancer metastasis[18]. Moreover, mechanical stiffening of underlying extracellular matrix (ECM) diminishes epithelial defence against cancer (EDAC) in normal epithelial through irregularly filamin distribution. The diminished ability of EDAC substantially decreases the extrusion of $HRas^{V12}$-transformed cells in normal epithelial layer that further contributes to carcinogenesis[19-21]. Moreover, people begin to realize that successful transformation of non-cancerous cells needs stiff matrix-induced YAP/TAZ activity[22]. In addition to EDAC and cell transformation, tumor tissue stiffening also promotes stromal cell autophagy[23] and extracellular vesicles secretion[24, 25] that further accelerate tumor progression. Intriguingly, similar with stiffness, recent research suggests that extracellular viscosity also influences cancer cell behavior. When cancer cells are cultured under high viscosity fluid, the cell motility is elevated through Ras homolog family member A (RhoA) dependent actomyosin contractility[26].

Aside from tumor tissue mechanics, the mechanics of the seed, that is tumor cells, may actively respond to microenvironment and modify their mechanical properties to aid in their metastatic potential. Recent study shows that reduced plasma membrane (PM) tension facilitates cancer cell invasion and migration through BAR proteins. On the contrary, increasing PM tension through activating ezrin, radixin and moesin (ERM) proteins results in decreased amoeboid 3D migration and reduced metastatic potential[27]. Furthermore, soften cell cytoskeleton through *MYH9* inhibition diminishes T cell-

induced perforin pore formation and granzyme B secretion that endows cancer cells escape from immune attack[28]. More importantly, directly modulating tumor cells stiffness through CRAD based actin depolymerization prevents Yes-associated protein 1 (YAP) nuclear translocation. The inhibited YAP nuclear localization further facilitates stemness genes expression and hybrid epithelial-mesenchymal transition (EMT), both of which increase metastatic potential[29]. Thus, tumor mechanics serve as determinants of both cancer initiation and cancer progression, rather than the byproducts of cancer evolution.

Although increasing evidences have demonstrated the important roles of ECM stiffening during cancer initiation, invasion and migration, the significance of mechanical cues during circulating shear flow in blood vessel are overlooked. Limited knowledge of how CTCs react to shear flow hinders our comprehensive understandings of the physical journal during cancer metastasis.

1.2 Blood circulation and CTCs

1.2.1 The role of CTCs during cancer metastasis

After intravasation, cancer cells need to entry into blood circulation and further disseminate into distant organ. These cells that shed from primary and intravasate into blood vessel are called CTCs[30]. The concept of CTCs was first put forward by Ashworth who found the tumor cells 'flow' in blood stream that had the similar appearance with primary tumor cells[31]. There is estimated to be $1*10^6$ cancer cells per gram of primary tumor can intravasate and shed into bloodstream per day[32]. Nowadays, CTCs are widely seen as the seed of metastasis, as in most cancer types, cancer cells disseminate into distant organ through bloodstream, except for glioblastoma, where cancer cells may migrate into distant organ along brain blood vessels as an alternative way[33].

As the seed of cancer metastasis, CTCs have its own clinical applications. From clinical point of view, the number of CTCs in blood is positively correlated with bad prognosis and poor patient survival[34-36]. Although CTCs are rare events in liquid biopsy, these

CTCs are seen as the culprit of cancer metastasis[37], as CTCs isolated from patient have capacity to induce metastatic outgrowth when they are injected into bone marrow of mice[38]. Furthermore, these detected CTCs are more likely to come from the aggressive subclone in primary tumor compared with other tumor cells, as hundreds of isolated CTCs have potential to form secondary metastasis [38-40]. In line with this idea, clinical data show that the proteomic and genomic messages that CTCs carried may not be detected in primary tumor[41], possibly attributes to strong migration or intravasation abilities, which renders them keep away from primary site. Previous research has found that metastasis may happened prior to the detection of primary tumor, possibly due to the fact that metastasis is an early event[42]. Therefore, the CTCs, which are the intermediate stage of metastasis, can be used as early diagnosis marker and prognostic indicator[43].

In addition to diagnostic values of CTCs during cancer metastasis, CTCs can be targeted more efficiently compared with primary tumor cells. The primary tumor cells are located in complex microenvironment including stiffened matrix, irregular blood vessel and impaired lymphatic drainage, all of which impede drug delivery[44-46]. Compared with primary tumor cells, CTCs are exposed to blood microenvironment including high reactive oxygen species (ROS) and considerable level of blood shear stress, which render them more vulnerable and sensitive to cancer drugs delivered through blood circulation[47].

Based on the saying above, CTCs are not only the culprit of cancer metastasis, but also more druggable than primary tumor cells. Targeting the vulnerability of CTCs in blood circulation may provide novel insight to prevent cancer metastasis.

1.2.2 Responses of CTCs to FSS

During the travel within bloodstream, CTCs are subjected to high level of ROS[48], interact with blood cells and sustain the attack of immune cells[49]. In addition to biochemical microenvironment, they also suffered from FSS during circulation[50].

Unlike passive material, CTCs can actively sense and respond to microenvironment they encountered. There are extensive studies unveil the responses of CTCs to blood cell contact[49]. For example, through interacting with plates, GITRL signaling pathway is activated that further renders CTCs ability to evade the immune surveillance of NK cells[51]. Intrudingly, although it is generally believed that tumor-associated macrophages (TAMs) play immune surveillance functions, contacting with TAMs in bloodstream promotes EMT of CTCs that further enhances their fitness to mechanical distortions. This indicates that CTCs with the presence of these immune cells displays a survival-promoting phenotype known as 'mechanical fitness'[52].

Beyond the extensively investigated interaction between CTCs and blood cells, increasing evidences indicate that mechanical cues within the vascular system also influence the survival and functions of CTCs. The most prevalent biophysical stimulation during circulation is shear stress generated by fluid flow[53]. Shear stress applied to CTCs triggers cell apoptosis through both programmed cell death and necrosis, which are not an exception of cancer cell with high malignancy such as 231-C3 breast cancer cells and chemotherapy-resistant cancer cells[54, 55]. The apoptosis of CTCs is both time and force dependent, as longer shear stress duration and higher shear stress magnitude kill more CTCs[56].

Aside from cell apoptosis, FSS also impacts CTCs' functions. For instance, shear stress application enhances the stemness[57] and decreases the proliferation of CTCs[55] through unknown mechanism. Importantly, 20 dyne/cm^2 shear stress treatment for 12h triggers JNK dependent EMT of breast cancer CTCs that further downregulates pro-apoptosis signaling P53 and increases CTCs' survival[58]. Apart from EMT of CTCs under shear stress, some studies demonstrate that shear stress could tune the adhesion of CTCs to endothelium wall. During CTCs' adhesion, they first slow down its rolling speed, a process called rolling, to minimize the adhesion force required to form tight bond with endothelial cells through Lewisx-P-selectin[59]. After rolling, CTCs further arrest at capillary bed and extravasate from blood vessel[60]. It is found that low shear stress modulates CTCs' ability to arrest at endothelial wall through β1integrin, while high

shear stress promotes CTCs extraversion[61]. This idea is in line with recent study discovers that shear stress activates PAR2 that further facilitates invasion and metastasis formation[62]. In addition, shear stress also enhances migration of breast cancer CTCs through YAP mediated mechanosensing[63].

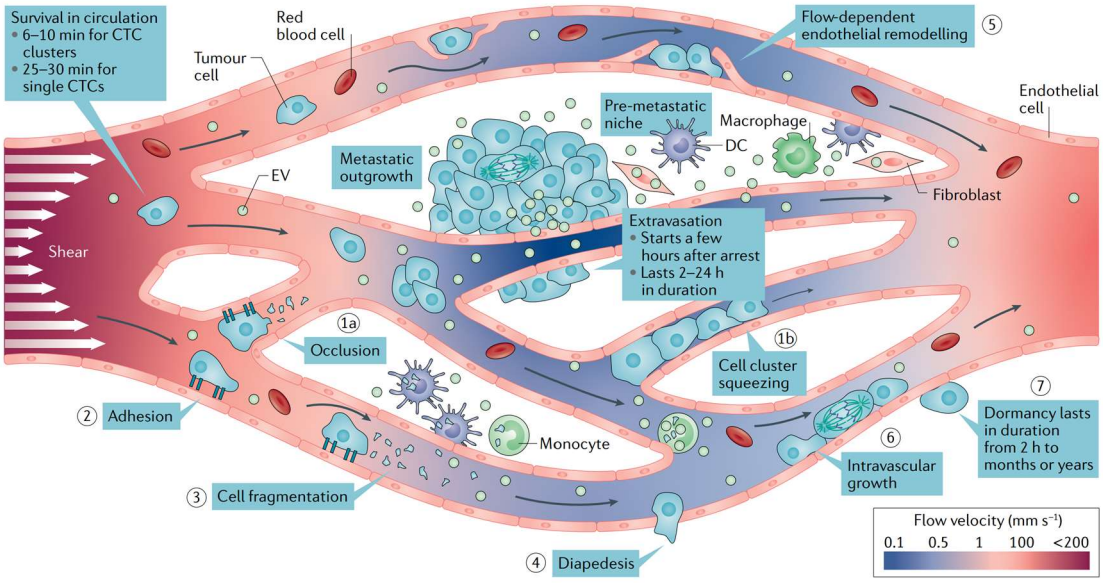

Figure 1-2 Responses of CTCs during bloodstream. CTCs encounter biochemical and biophysical cues during blood circulation and react to it positively[64].

In the terminal of blood vasculature, there are capillaries whose size are smaller than CTCs or even the cell nucleus[65]. When CTCs encounter these microvasculature, they are trapped and deformed for days[66]. While one study demonstrates that such size restrictions are the primary cause of initial arrest of CTCs[66], another study using MDA-MB-435 cell line and intravenous injection model discovers that mechanical constriction is not sufficient for cancer cell arrest.[67] Recent study using microfluidic chip to mimic confined microenvironment finds that confined microenvironment induces DNA damage response of CTCs[68]. Furthermore, mechanical entrapment induced by size restriction triggers pannexin-1dependent adenosine triphosphate (ATP) response that further contributes to CTCs adaptation[69].

Based on saying above, CTCs have capacities to sense and respond to physical microenvironment during blood circulation. Nevertheless, the mechanotransduction

mechanism that CTCs employed to mechanistically adapt to shear stress is still lacking. As the CTCs are seed of metastasis, better understanding of this machinery could provide new target to eliminate CTCs during bloodstream and prevent cancer dissemination.

1.2.3 Survival mechanisms of CTCs under shear stress

The mean shear stress in human being is lowest in the large veins where it is often < 1 dyne/cm^2, and it tends to be 60 to 80 dynes/cm^2 in small arterioles [70]. Such considerable level of shear force kills large amounts of CTCs[55, 58, 71]. Indeed, clinical data show that in spite of numerous CTCs intravasate into blood circulation, less than 0.1% of them could sustain the harsh microenvironment during bloodstream[72], indicating survival of CTCs under shear stress is an inefficiency process. Although the survival rate of CTCs is limited, these survived CTCs may have higher metastatic potential and have chance to further develop into secondary metastasis[30]. Investigating survival mechanism of CTCs under blood shear flow could help us to better target the vulnerability of CTCs, eliminate CTCs during blood flow and prevent cancer metastasis.

Previous studies have provided some insight into how CTCs survive under FSS. For instance, CTC clusters, which are composed of multiple single CTCs (homotypic cluster) or CTC-blood cell aggregates (heterotypic cluster), show fifty folds higher metastasis potential compared with single CTCs[34], partially owing to aggregates confer mechanical shield to protect CTCs from mechanical destruction[73]. Furthermore, compared with less malignant cancer cell type, CTCs with high metastatic potential have higher resistance to shear stress induced mechanical destructions, possibly through more efficient cell membrane repair[74]. Similarly, in comparison to non-malignant epithelial cells, malignant breast tumor cells take advantages of Lamin A/C to survive under fluid shear flow (6,000 dynes/cm^2), as knocking down Lamin A/C diminishes resistance of CTCs to FSS[75]. As such, it is in line with the notion that Lamin A highly expressed cells are likely to metastasis to lymph nodes[76]. In addition, latest research finds the nuclear expansion through histone acetylation promotes CTCs

survival under FSS[77]. Moreover, recent study illustrates the enhanced actomyosin activity increases CTCs apoptosis under circulating shear flow (20 dynes/cm^2)[56]. This is consistent with latest study showing that intracellular resident, tumor-derived microbiota suppresses actomyosin activity through RhoA signaling that further assists in CTCs' survival[78]. Another study, however, shows controversial finding that inhibiting actomyosin reduces CTCs viability under transient and high level of shear force (1 ms, τ_{max} = 6,400 dynes/cm^2)[79]. Therefore, the roles of actomyosin in CTCs' functions under FSS are context-dependent and needs further research.

Although advances have been made in comprehending how mechanical properties of CTCs assist their survival under fluid shear flow, little is known how they mechanically adapt to the shear force. More importantly, as the shear force in the blood vessel varies from 1 to 4 dynes/cm^2 in the veins and over 4 dynes/cm^2 in the artery[50], whether and how CTCs respond to different levels of shear force remains largely unclear. Better understanding of aforementioned questions is urgent to drug development and clinical cancer treatment.

1.3 Mechanotransduction: Linking cell membrane with nucleus

1.3.1 Mechanosensor and cell cortex

Mechanotransduction is a process through which the cells continuously explore the mechanical cues of their surrounding microenvironment and actively respond to it. Mechanical force applied to the cell membrane is first perceived by mechanosensors. Among different membrane mechanosensors, integrin is a well-studied one. The mechanical characteristic of integrin was begun to established in 1993, before which integrin was seen as a biochemical sensor[80]. In 1993, using magnetic beads and magnetic twisting cytometry (MTC) to apply the force to the cell membrane, researchers found cytoskeleton stiffening only happened through Arg-Gly-Asp (RGD) coated magnetic beads instead of others, indicating cells sense external force through RGD binding motif. As RGD is a specific recognition site of integrin, this phenomenon

implies the integrin function as mechanosensor[81]. Similar with integrin that has both extracellular and intracellular domains, GPCR[82] and Piezo1[83] also work as mechanosensors that guide outside-in mechanotransduction process.

After transducing mechanical force inside, the force is further transmitted into spectrin based membrane skeleton and cell cortex. Spectrin is type of cytoskeletal protein whose functions has been extensively studied in red blood cells (RBCs)[84]. More recently, the role of hyaluronic acid (HA)-CD44-specrin mediated mechanotransduction in endothelial cell sensing to FSS has been discovered. When FSS is applied to endothelial cells, HA serves as a mechanosensor that transmits shear stress from microenvironment to CD44, a membrane receptor that directly bind with spectrin cytoskeleton. Further, the force transmitted to spectrin cytoskeleton increases the tension within cell membrane. Finally, the increased membrane tension triggers piezo-1 dependent calcium influx, which regulates endothelial cells alignment and nitrogen oxide production under FSS[85].

Beneath the spectrin cytoskeleton, that is cell cortex. The cell cortex is an approximate 400 nm thick structure that mainly composed of actin filament and myosin motors, which plays critical role in cortical tension generation, as inhibition of myosin II reduces cortical tension by about 80%[86]. The actin filaments in cell cortex are brunched and crosslinked mainly through actin binding protein (ABP) such as Arp2/3 and α-actinin, which enable the formation of hole-like structure in actin cortex[87]. Interestingly, recent study finds the pore size of actin cortex regulates possibility of myosin II penetration and thus cortical tension. While some pores size of actin cortex are smaller than myosin minifilaments that restrict myosin minifilaments penetration, partially inhibition of actin branching through CK666 enlarges pores and facilitates myosin minifilaments penetration, finally leads to more myosin-actin interaction and high cortical tension[88]. As actin cortex physically links PM to ERM protein family, the cortical tension could propagate into cell membrane and influence membrane tension[89].

Both membrane tension and cortical tension have indispensable cellular functions. For

instance, during early differentiation of embryonic stem cells (ESCs), the decreased RhoA activity reduces cell cortical tension that further enhances the endocytosis. Maintaining high membrane tension through constitutively active of Ezrin, a protein that is crucial for maintaining cortical mechanics, impedes normal differentiation process[90, 91]. Moreover, membrane tension also serves as a regulator of membrane ion channel activation[92] and EMT during cancer cell dissemination[27]. In term of cortical tension, it helps the formation of contractile ring that divides daughter cells apart during cytokinesis[93]. Furthermore, in epithelial cell monolayer, high cortical tension facilitates normal epithelial cells eradicate apoptotic cells through extrusion to maintain tissue homeostasis[94]. More recently, outstanding research finds the long-range membrane tension transduction, which plays critical role in membrane recycling[95], differentially determined by membrane-cortex friction from outside-in or inside-out tension propagation. When external force is applied through optically-trapped beads, the membrane-cortex linkage abolishes effective membrane tension propagation. Internal generated force, however, from actin protrusion or actomyosin contractility, could be robustly transmitted across the cell membrane because of membrane-cortex friction[89].

1.3.2 Cell cytoskeleton

Underlying cell cortex, that is cell cytoskeleton. The cytoskeletal structures have been found in all eukaryotes and not an exception for ancient bacterium[96]. Cytoskeleton is composed of three microfilaments including filamentous actin (F-actin), microtubule and intermediate filaments (IFs). While three filaments interact with each other in cytosol, each of them plays the distinct roles in mechanobiology[97].

Among three cytoskeletal filaments, both F-actin and microtubules have a fast-growing plus end and a slow-growing minus end, which conferring filamentous polarity that facilitates fast adaptation of cytoskeleton to external mechanical destruction[98]. The F-actin is polymerized from globular actin (G-actin) monomers through ABP such as Arp2/3 or mDia1[99]. Intriguingly, both G-actin and F-actin are found in cell nucleus that play important role in transcription regulation[100]. After polymerization, F-actin further

interact with myosin motor and crosslinked by alpha-actinin and form the stress fibers (SFs) in adherent cell. The roles of SFs have been well studied in force transmission[101] and tissue scaling[102]. What is interesting is that the alignment of SFs is mainly along the long axis of adherent cell, which called stress fiber anisotropy. The anisotropic alignment of SFs elicits distinct cellular responses with same magnitude but different directions[103].

Compared with F-actin that mainly sustain tensile force, microtubules are responsible for resistance of compressive force[104, 105]. Microtubules are polymers with hollow structures that consist of α, β and γ tubulin, which regulate protein translocation[106], cell extrusion[107] and nuclear positioning during amoeboid migration[108]. The gain-of-functions of microtubules are always accompanied with Post-Translational Modifications (PTMs) including acetylation, glutamination, polyglycylation and detyrosination[109]. The PTMs of microtubules play crucial role in cellular function. For instance, in breast cancer, matrix stiffening stabilizes microtubule through glutamination and further enhances cancer cell proliferation and invasion[110].

In comparison with F-actin and microtubules whose functions in mechanotransduction and mechanobiology have been thoroughly studied, the biomechanical functions of IFs are seldom investigated. Until now, about seventy genes are found to be responsible for transcribe different kinds of IFs that play the distinct roles in cell mechanics[111]. Take type III and type V IFs as an example, while vimentin, a type III IFs which is located throughout the entire cytoskeleton, transmits mechanical signal from focal adhesions (FA) to the cell nucleus[112] and resists relatively high cell deformation under serious mechanical loading[113]; the nuclear Lamins, type V IFs which is located on the inner side of nuclear membrane, is responsible for nuclear stiffness[114] and nuclear mechanosensing[115].

The functions of three cytoskeletal filaments are not independent, instead, they always function together as a synergetic structure. For example, microtubule acetylation promotes the release of guanine nucleotide exchange factors (GEF)-H1 from

microtubules that further actives RhoA and finally increases the actomyosin contractility[116]; vimentin IFs stabilizes microtubules through decreasing catastrophe frequency and increasing rescue events of depolymerizing microtubules[117]. Moreover, vimentin IFs controls SFs stability through RhoA[118]. Thereby, the cytoskeleton should be seen as an integrated structure rather than mutually isolated components[119].

1.3.3 Cell nucleus

When the force travel across the cytoskeleton, it finally reaches the cell nucleus. In fact, the cell cytoskeleton physically links with cell nucleus through linker of nucleoskeleton and cytoskeleton (LINC) complex. The LINC complex is primarily composed of two protein domains: Sad1p, UNC-84 (SUN) domain that mainly locate at inner nuclear membrane, and the conserved C-terminal Klarsicht/ANC-1/Syne Homology (KASH) domain which spans the outer nuclear membrane[120]. On the outer nuclear membrane, Nesprin proteins, including Nesprin-1 to Nesprin-4, interact with cytoskeletal filaments through distinct connections. While Nesprin-1 and 2 connect to F-actin through ABD, Nesprin-3 and Nesprin-4 link IFs and microtubules through and Plectin and Kinesin, respectively[121]. As Nesprin physically links with microfilaments that generate cytoskeletal tension, Nesprin itself is also under conservable level of tension. In line with this concept, inhibition of cytoskeletal tension decreases the tension within LINC complex[122].

Further, Nesprin proteins link underlying SUN proteins through its KASH domain that transmits physical cues into cell nucleus. Based on this structure, researcher design the dominant negative form of KASH (DN-KASH) that disrupts the LINC complex and inhibits mechanotransduction into cell nucleus[123]. Through LINC complex disruption, a number of studies have demonstrated the importance of nuclear mechanosensing[124]. For instance, after chronic exposure of fibroblast to stiff ECM, fibroblast persistence triggers long-term lung fibrotic. Nevertheless, inhibition of nuclear mechanosensing through LINC complex disruption abolishes stiff ECM induced histone acetylation and further fibroblast persistence[125]. Moreover, substrate stiffening induced histone

acetylation promotes mesenchymal stem cells (MSCs) osteogenic differentiation. However, DN-KASH transfection diminishes MSCs differentiation, indicating nuclear mechanosensing plays indispensable role during MSCs differentiation[126].

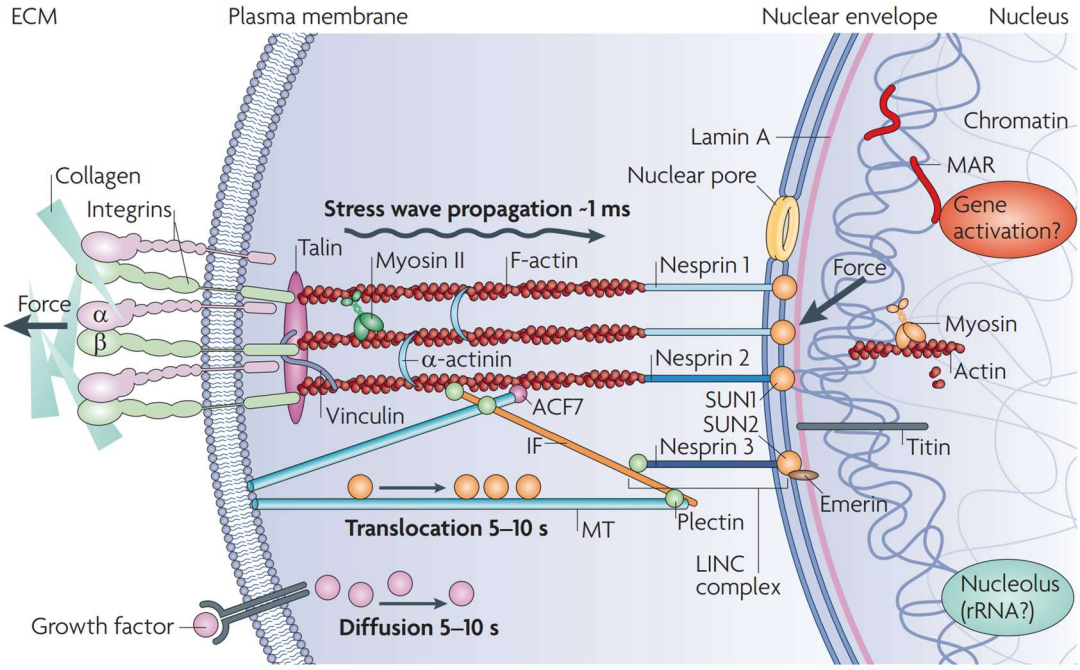

Figure 1-3 Intracellular connections of mechanosensitive molecules and mechanotransduction in adherent cells. Extracellular mechanical signals are transmitted to intracellular receptors by transmembrane protein such as integrins. Then the contractile force generated by the F-actin and myosin II transmits mechanical signals to the LINC complex. Finally, the mechanical force is transmitted to chromatin and induces chromatin displacement[120].

After mechanotransduction through Nesprin-SUN protein complex, mechanical force is further transferred into Lamin protein through Emerin. Lamin protein serves as the scaffold of nuclear envelop (NE) and nucleoskeleton[127]. Further, Lamin protein links chromatin or DNA through HP1[128], BAF[129] or LAP2β[130]. Instead of aforementioned proteins, Lamin proteins could directly interact with chromatin through its Lamin associated domains (LADs)[131]. When LADs dissociate from attached chromatin, the histone 3 lysine 9 (H3K9) me2/3 on chromatin will be replaced by H3/4ac that promotes gene expression[132].

The aforementioned physical linkages from cell surface to nucleus provides a 'high-

speed road' for mechanotransduction. In line with this, previous study using MTC to apply local stress via RGD coated magnetic bead observed that within ~350 ms, the coilin was disassociated from SMN in nuclear Cajal body[133], indicating mechanotransduction could bypass traditional biochemical signaling that directly trigger nuclear responses. More importantly, through same force application method, researchers discover that the force applied on the cell surface is rapidly transmitted into cell nucleus and triggers chromatin stretching, which increases the extent of RNA Polymerase II interacting with the promotor of dihydrofolate reductase gene and finally promotes gene expression[134, 135]. The force induced transcriptional changes takes only 15 seconds, much more rapid than biochemical stimuli which takes hours to days[136], suggesting unique feature of mechanotransduction compared with signaling cascades[137].

While there is a wealth of researches in mechanotransduction pathways of adherent cell, mechanotransduction in suspended cell is still lacking. Revealing mechanotransduction of suspended cells would aid in our understanding of how CTCs sense and respond to FSS, as CTCs are long in suspension status during blood circulation. One limitation to investigate the mechanotransduction in suspended cell is lack of methods to measure cell and nuclear deformation under mechanical force[138]. As suspended cells do not adherent to ECM through specific protein-protein interaction such as fibronectin and integrin $\alpha5\beta1$[139], tracking and measuring nuclear responses under mechanical cues are challenging. Understanding mechanotransduction in suspended cell will undoubtedly enrich our knowledge about force transmission process, which could be further targeted during disease development[140].

1.3.4 Distinct cellular responses to low and high mechanical stimuli

The mechanotransduction units render the cells to sense and respond to external physical stimuli. However, as cells are in a physical microenvironment that spatiotemporally changed, cells need to smartly tackle different magnitudes of mechanical cues in distinct manners to accommodate surrounding physical

microenvironment. For example, soft substrate activates RAP2 and the phosphorylation of Hippo kinases LATS1/2 that retain YAP/TAZ in the cytoplasm[141]. In contrast, stiff substrate enhances cytoskeletal tension and YAP/TAZ nuclear translocation in a Hippo-independent manner[142]. Low spatial confinement mediated cytoplasm but not nuclear deformation has minimal effect on cell contractility, while high confinement leads to nuclear deformation, activates cPLA2, redistributes myosin II into cell cortex, and promotes cell motility[143]. Low uniaxial stretch does not affect tissue realignment but increases perinuclear actin and decreases H3K9 methylation of skin epidermis stem/progenitor cells. However, high stretch rearranges the cytoskeleton perpendicular to the stretch direction and mediates adaptive mechano-responses, which protects cells from stretch-induced DNA damage[144]. Under high mechanical loading, but not low, nucleus shows stronger effective diffusivity[145].

In addition to tensile or compressive force, cells may also have distinct responses to varying magnitudes of shear stress. For instance, for human mesenchymal stromal cells, while 1 dyne/cm^2 FSS induces chromatin condensation, 5 dyne/cm^2 FSS applied for 30 minutes resulted in chromatin decondensatation[146]. More importantly, 15 dyne/cm^2, instead of 2 dyne/cm^2 FSS treatment of lung cancer CTCs for 10 hours upregulates PAR2 cleavage[62]. These findings implicate differential mechanosensing mechanisms of living cells in response to different levels of mechanical stimuli.

Although more attentions are paid into different responses of adherent cell to mechanical stimuli, the molecular mechanism that suspended cells, CTCs in particular, exhibit distinct mechano-responses to different magnitudes of shear stress needs further investigation.

1.4 Non-muscle Myosin II and its roles in tumor progression

1.4.1 Myosin II-Forming basic unit of contractility

The aforementioned mechanosensing and mechanotransduction process strongly depend on actomyosin contractility generated by non-muscle myosin II motors interact

with actin filaments[103, 120]. Non-muscle myosin II is a type of motor protein consisting of three paralogs called myosin IIA, myosin IIB and myosin IIC, encoded by *MYH9*, *MYH10* and *MYH14* respectively. Each of them consists of two essential light chains (ELC), two regulatory light chains (RLC) and two heavy chains (HC)[147]. While the RLC and ELC form the motor domain, the HC form the coil-coil rod domain (or tail domain) of myosin motors[148]. Intriguingly, myosin IIA and myosin IIB are highly expressed in endothelial and epithelial cells[149, 150], while myosin IIC appears to be transcript in lung tissue[151]. The main difference of each other is the HC, while the detailed submicroscopic structure remains to be resovled[152].

While myosin IIA, myosin IIB share similar structure, the duty ratio (e.g., the proportion of ATPase cycle during which myosin II motor domain binds with actin strongly[153]) of them is different. It is reported that myosin IIB has higher duty ratio compared with myosin IIA[153]. In line with the finding, myosin IIA mainly distributes in nascent FA while myosin IIB predominantly localizes near mature FA[154]. The different biochemical properties of myosin isoforms render them distinct cellular functions. For instance, during cleavage furrow formation in cytokinesis, only myosin IIB is recruited into midzone that determines the localization of cleavage furrow[155]. Additionally, during epithelial adherent junction (AJ) assembly, myosin IIA generates higher tugging force that helps AJ maturation and maintained, while myosin IIB assists in E-cadherin recruitment[156]. More importantly, in U2OS cells, myosin IIA and myosin IIB is main contributor of cellular tension generation and stabilization, respectively, while myosin IIC plays critical role in tension restoration under external mechanical distortion[157].

The gain of function or activation of myosin II is mainly through phosphorylation of RLC at Ser19 site, while phosphorylation at Thr18 site contributes in a less extent[158]. In contrast, phosphorylation of RLC in Ser1, Ser2 or Thr9 have adverse effects[159]. As phosphorylation of myosin II primarily happens on myosin light chain (MLC), thus, myosin II activity is represented by amount of P-MLC[160]. The most important function of myosin II is binding with F-actin, forming actomyosin, consuming ATP to sliding on

F-actin and further generating contractile force[161]. During this process, interaction between myosin motors and ATP decreases the binding affinity of myosin motors and F-actin[162]. After myosin activation and ATP hydrolysis into adenosine diphosphate (ADP) and Pi, because of conformational change of RLC, the binding affinity of myosin motors and F-actin significantly increased[163]. Further, through making a power stroke, myosin motors 'walk' on F-actin, contract the actin filaments and finally generate actomyosin contractility[164].

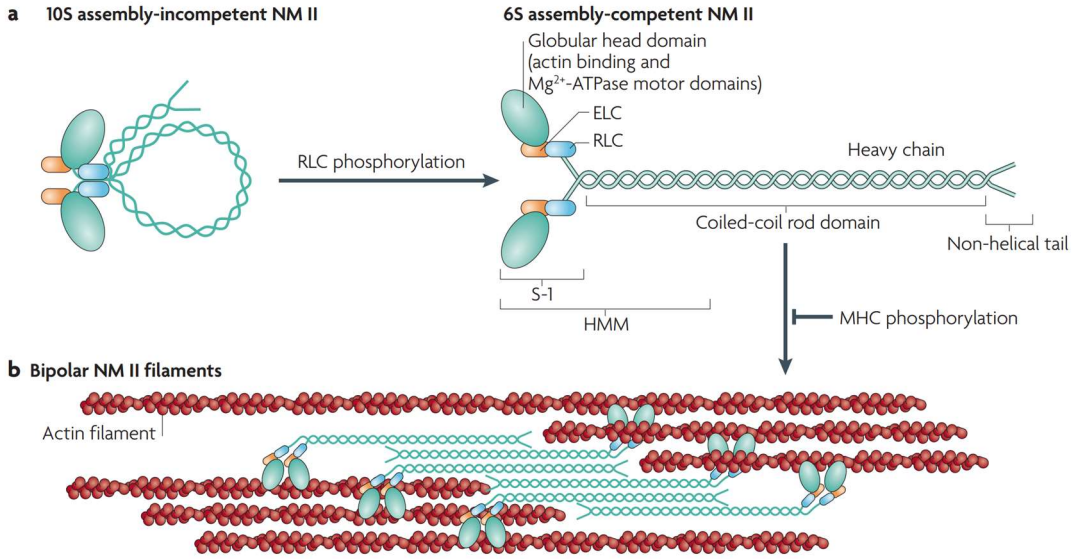

Figure 1-4 Structure and activation of non-muscle myosin II. Myosin II including two RLC, two ELC and two HC. The activation of myosin II mainly through RLC phosphorylation. Interaction between actin filaments and myosin II generates actomyosin contractility which is critical for mechanotransduction[160].

Contractile force generated by actomyosin is critical for cellular behaviours[165, 166]. As the force generated in different subcellular localization plays distinct cellular functions, different myosin II localization is responsible for proceeding distinct downstream biological processes. For instance, in the cell cortex, myosin II activity enhances actin turnover that further keeps actin cortex the steady status[167]. During cytokinesis, myosin II activity in the cortex appears to accelerate the polymerization of actin that further contributes to the cleave furrow formation [168] and facilitates cell rounding under confinement spaces during anaphase[169]. In sharp contrast, myosin II in the cytoplasm

is crucial for mechanotransduction and mechanosensing from cell surface into cell nucleus[103, 170]. Furthermore, the cytoplasmic physical properties, especially viscosity, is influenced by actin crosslinking through motor proteins activity such as myosin II[171]. Considering the saying above, it is not enough to investigate myosin II activity in cortex or cytoplasm alone. Systematically study the functions of myosin II are required to combing the roles of myosin II in cortex and cytoplasm together.

While the roles of myosin II-mediated cellular responses and cell behaviors in adherent cells are fully studied, the function of myosin II activity in mechanotransduction of suspended cells remains largely unsolved. Intrudingly, while it is generally accepted that prestress generated by actomyosin contractility increase cell stiffness in adherent cells[172], myosin II activity soften suspended cells[173], indicating distinct roles of myosin II activity in suspended cells compared with adherent cells. Thus, fully deciphering the functions of myosin II requires a thorough investigation of how suspended cells utilize myosin II activity to respond to and transmit mechanical cues.

1.4.2 Distinct roles of ROCK and MLCK in myosin activation

As mentioned before, myosin II is activated through its RLC phosphorylation. In fact, RLC phosphorylation is predominantly regulated through MLCK and ROCK. While MLCK directly phosphorylates RLC through its myosin binding domain[174], ROCK either directly phosphorylates RLC, or inhibits myosin light chain phosphatase (MLCP) activity through myosin phosphatase targeting protein (MYPT) that in turn enhances RLC phosphorylation[175]. In general, the binding of MLCK and RLC is dominated by Ca^{2+}/calmodulin. Thus, cytosol calcium concentration plays vital role in MLCK induced myosin II activation[176]. Compared with MLCK, little is known whether and how calcium influences ROCK-myosin II interaction, although emerging researches find that calcium ions also influence cellular functions through ROCK mediated cytoskeletal reorganization[26, 177]. ROCK is widely seen as the downstream effector of RhoA, a small GTPase protein belongs to Rho family[178].The Rho protein family including RhoA, Rac1 and Cdc42, play the critical roles in cytoskeletal organization[179].

It has been found that the phosphorylation of ROCK in S1366 site reflects its kinase activity and positively correlates with MLC phosphorylation under RhoA stimulation[180]. Thus, phosphor-ROCK at S1366 is used to represent ROCK activity.

Although MLCK and ROCK both activate myosin II and enhance cell contractility, they have distinct biochemical and biophysical functions[181, 182]. Take cell elastic properties as an example, while ML-7, a MLCK inhibitor decreases cell elasticity, ROCK inhibition through Y27632 shows little change of elasticity[183]. Conversely, ROCK inhibition, but not MLCK, decreases integrin tension near podosome[184]. The predominate role of ROCK in regulating cell contractility can also be seen in RBCs, where ROCK, instead of MLCK, phosphorylates myosin IIA and further manages RBCs shape[185]. Interestingly, previous studies suggested regionally activated myosin II through MLCK and ROCK. Compared with MLCK which activates myosin II in cell periphery through RLC monophosphorylation, ROCK regulates cytoplasmic myosin II activation through RLC diphosphorylation[186, 187], indicating there may be a competition between MLCK and ROCK in myosin II activation[188]. Nevertheless, all aforementioned conclusions are concluded from adherent cells, whether and how MLCK and ROCK in suspended cell have different functions are still unclear. More importantly, the functions of distinct myosin II subcellular distribution need further investigation.

1.4.3 Characteristics of myosin II activity during tumor progression

During tumor progression, cancer cells need to use versatile responses to tackle different microenvironments[189]. Indeed, previous researches have substantially enlarged our knowledge of how myosin II-guide cell mechanics contribute to cancer development, especially in cancer cell migration and invasion[190, 191]. Both cancer cell migration and invasion are based on cell movement including three processes: 1. Protruding the leading edge and form lamellipodia or invadopodia. 2. Adhesion and deadhesion of cell leading edge and trailing edge. 3. Contracting the whole cell body and move forward[192]. In fact, myosin II activity is involved in all three processes during cancer cell movement. For instance, myosin II generated contractile force aids in cell

protrusion or trailing edge retraction through Rho GTPases[193, 194]. MARK2 mediated myosin II RLC phosphorylation promotes FA formation and orientation[195]. Accordingly, myosin II is activated in tumor edge to promote cancer cell invasion[196]. Intriguingly, more and more recent researches highlight the role of myosin II activity during durotaxis, a phenomenon that cells are prone to migrate to stiffer ECM[197, 198].

Except for cell movement, actomyosin contractility also plays vital role during EDAC, where healthy cells need force to extrude apoptotic or mutate cell[19, 94], suggesting myosin II activity as a safeguard during cancer initiation. In addition, TRPV4 channel mediated calcium influx promotes myosin II activity that further contributes to collagen remodeling[199]. Furthermore, Fasudil, a clinically used RhoA inhibitor which inhibits myosin II, prevents initial arrest of CTCs to endothelium[200]. More recently, the importance of myosin II activation induced ROS resistance has been unveiled[201]. These findings suggest that myosin II activity facilitates cancer progression and dissemination.

While the significance of myosin II has been extensively studied in cancer initiation and cancer cell migration, the roles of actomyosin contractility in CTCs under shear stress are still unclear. More importantly, the contradictory roles of myosin II activity in CTCs' survival implying other shear stress-related functions of myosin II[56, 79]. As myosin II activity is crucial for force transmission, further deciphering the roles of myosin II in mechanotransduction of CTCs may help us to better understand the functions of physical cues during cancer metastasis.

1.5 Nuclear mechanosensing and nuclear deformation

1.5.1 Nucleus itself as a mechanosensor

When the cells are suffered from high mechanical force, such as suspended cells under shear flow, the nucleus is substantially deformed[202]. In fact, the nucleus is the largest and almost stiffest organelle in eukaryotes[203]. There are extensive studies demonstrate the nucleus can sense the force transmitted from cytoskeleton as just mentioned[103, 115, 124]. Nevertheless, whether nucleus itself could directly sense the force bypass

cytoskeletal mechanotransduction is a long debate. The first insight that nucleus itself was enough to perceive the mechanical cues was established in 2014[204]. When the authors applied the force to isolated cell nucleus via Nesprin-1 coated magnetic beads, the nuclear stiffening represented by decreased beads displacement was observed, while PLL coated magnetic beads did not elicit downstream nuclear responses[204]. In line with this idea, nuclear stiffening was also seen in direct force application to nucleus through atomic force microscopy (AFM) or magnetic twister[205, 206]. These inspiring researches demonstrate that nucleus itself could sense and response to external biophysical stimuli independent of cytoskeleton. In last decade, much more attentions have been paid into nuclear mechanosensing and a number of studies found that nucleus itself serves as a mechanosensor[207]. One manner that nucleus senses the force is through nuclear pore complexes (NPCs). It has been found that the force directly applied to cell nucleus through AFM tip triggered YAP nuclear localization within minutes regardless of cytoskeleton disruption, likely through NPCs mediated nuclear import[208]. Likewise, osmotic pressure induced nuclear compression regulates YAP translocation independent of actomyosin cytoskeleton[209]. These concepts are consistent with recent study where mechanical force has been proved to regulates the size of NPCs[210] and governs nucleocytoplasmic protein transport[211].

In addition to NPCs, the nucleus can sense the force through NE tension induce calcium release. When spatial confinement is directly applied to cell nucleus, the NE unfold and nuclear envelop tension is increased. The increased NE tension further triggers calcium release from endoplasmic reticulum (ER) and activates cytosolic phospholipase A2 (cPLA2) to catalyzes the formation of fatty acid. The fatty acid, particularly arachidonic acid, activates myosin II and finally increases cancer cell migration to evade confined nicroenvironment[143, 212].

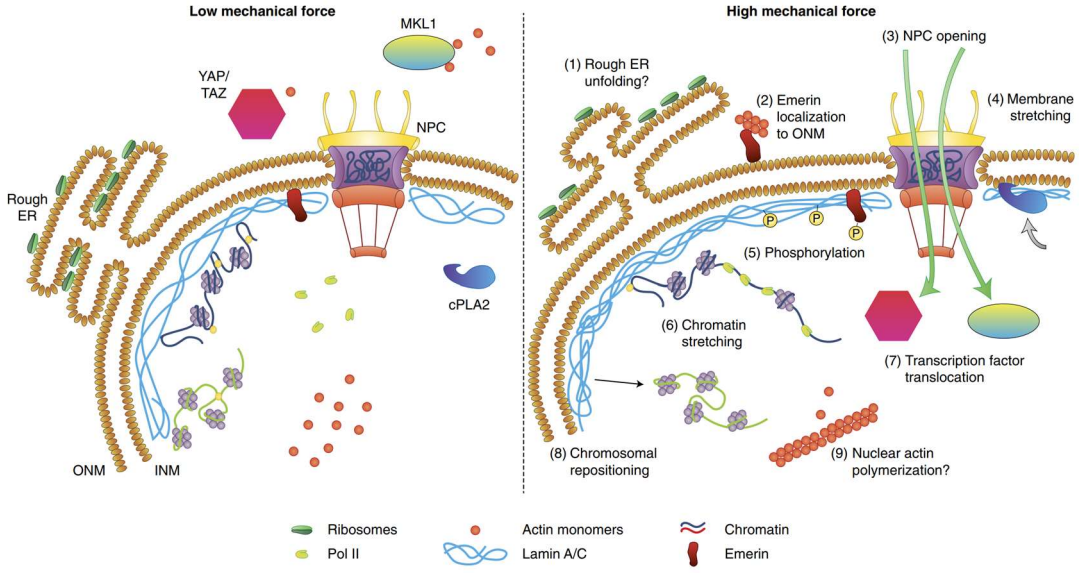

Figure 1-5. The nucleus acts as a mechanosensor responding to physical cues. When the force is directly applied to cell nucleus, NPCs and NE tension serve as responsor that elicit nuclear mechanosensing independent of cytoskeletal mechanotransduction[207].

As mentioned before, when the force is directly applied to cell nucleus, the nucleus is substantially deformed. The consequences of nuclear deformation are quite complex, depending on the specific contexts that cells respond to[213]. For example, during cancer cell migration, cancer cells may encounter narrow spaces that constrict the passage of cell nucleus[214]. In that case, serious nuclear deformation triggers NE rupture, which increases the accessibility of TREX1 with nuclear genomes and induces DNA damage, finally leads to EMT phenotype of cancer cells and enhanced metastatic potential[215-217]. In addition to DNA damage response, nuclear deformation also triggers epigenetic modification such as histone methylation[218] and acetylation[219]. Recently, a high-throughput microfluidic device is utilized to confine the cell nucleus and facilitate mouse fibroblasts to overcome epigenetic barriers, further enhances cell reprogramming efficiency[220].

1.5.2 Lamin A/C and nucleoskeleton

The nuclear mechanosensing mentioned before is strongly rely on nuclear lamina[212].

Nuclear lamina is a 10-30 nm thick meshwork beneath inner nuclear membrane that composed of A-type lamin and B-type lamin. A-type lamin, including Lamin A and Lamin C, is encoded by *LMNA* gene, while B-type lamin, Lamin B1 and Lamin B2 (Lamin B) is encoded by *LMNB1* and *LMNB2* gene, respectively[221]. The mutation of lamins causes serious degenerative disease generally called laminopathies, signed by muscle dystrophy, diabetes and progeria[222, 223]. Strikingly, Lamin A/C expression is negatively correlated with cancer patients' survival, indicating Lamin A/C has oncogenic functions[75].

In addition to biochemical function, lamins also play critical roles in nuclear mechanics and nuclear mechanosensing. The roles of Lamin A/C and Lamin B1 in regulating nuclear mechanic are quite controversial. While some studies demonstrate that Lamin A/C, but not Lamin B1, regulating nuclear stiffness and nuclear strain under biaxial stretch[114, 209, 224], another research suggests that Lamin B serves as an elastic shied and Lamin A/C as a viscous fluid[225]. In addition to nuclear mechanics, Lamin A/C and Lamin B differentially interacts with cytoskeleton and regulates nuclear volume[226]. Whatever the contribute of Lamin A/C or Lamin B to nuclear mechanics, recent study finds that nuclear lamina is indeed under tension[227].

Nuclear lamina, especially Lamin A/C, plays indispensable in cellular functions. During cancer cell 3D migration, high nuclear stiffness induced by Lamin A/C hinders nuclear translocation. Nevertheless, if Lamin A/C is too little, the excessive nuclear softening triggers genomic instability that further limits cancer cell survival after confined migration[228]. In line with this idea, decreased Lamin A/C expression could induce NE rupture and DNA damage during laminopathies development and embryonic hearts stiffening[229, 230].

Intriguingly, while mechanotransduction in cell passes through cytoskeleton to cell nucleus, the lamina, Lamin A/C in particular, could feedback to cytoskeletal components. For instance, during ameboid cancer cell migration in confined space, deficient Lamin A/C level downregulates vimentin expression that subsequently

ensures cell viability during confined migration[231]. Furthermore, suppression of Lamin A/C expression diminishes actin polymerization and MRTF-A nuclear localization, which further abolishes inflammatory responses of macrophages[232]. More importantly, matrix stiffness regulates Lamin A/C phosphorylation, which controls SRF nuclear translocation and alters myosin IIA expression[233]. Strikingly, Lamin A/C-mediated NE tension under spatial confinement triggers cPLA2 induced myosin II cortical localizaion[212].

Previous studies mostly focused on the functions of nucleus when the force directly applied on cell nucleus. However, under some physiological contexts, such as CTCs travel within bloodstream, the nucleus is not directly exposed to shear stress. In that case, whether and how nuclear mechanosensing feedbacks to cytoskeletal reorganization remains an open question.

1.5.3 Mechanoadaptation of nucleus to harsh microenvironment

As mentioned before, when cells are exposed to serious microenvironment or applied with high mechanical loading, not only the cell cytosol, but also the cell nucleus is substantially deformed. As nuclear deformation could trigger DNA damage that threats genome stability, cells must use versatile reactions to accommodate the nucleus to harsh physical environment. The accommodation of cell nucleus to surrounding mechanical microenvironment is called nuclear mechanoadaptation. The nuclear mechanoadaptation is a universal reaction of cells to physical threatens. For instance, under biaxial stretching or FSS, cells either vertically or horizontally aligned their cell cytoskeleton and nucleus to minimalize the force that nucleus expericed[234, 235]. Further, cytoskeletal stiffening through vimentin network confers protection of nucleus[236]. Moreover, precise modulations of actomyosin contractility through PREP1, PPP1R12A and Net39 protect the nucleus from stress overload and DNA damage[237-239].

As the force is transmitted from the cytoskeleton to LINC complex that further into nucleus, LINC complex-associated proteins, including Emerin and LAP1, are critical

in mechanoadaptation of cell nucleus[240, 241]. Interestingly, decoupling of LINC complex from underlying cell nucleus, which impedes force transmission to nucleus, is an alternative way for nuclear mechanoadaptation[242]. In addition to aforementioned blockage or modulation during mechanotransduction, the mechanical property of nucleus also plays important role in nuclear mechanoadaptation. For example, nuclear softening through histone modifications or cytoskeletal managements, has been shown to dissipate mechanical energy within nucleus to afford nuclear protection[144, 243-246].

While the nuclear mechanoadaptation of adherent cells is emerging, whether and how suspended cells, CTCs in particular, accommodate its nucleus to high FSS within blood circulation is still unclear.

1.6 Summary of research gap

Cancer metastasis is the major cause of cancer patients' death. During this journey, cancer cells must overcome serious mechanical threatens, including considerable levels of FSS within the blood vessels. However, limited knowledge of how the CTCs mechanically adapt to the shear force impedes our understanding of CTCs' survival mechanism under fluid shear flow. Furthermore, as the shear force in the blood vessel changes from 1 to 4 dynes/cm^2 in the veins and over 4 dynes/cm^2 in the arteries[50], there is a lack of clarity regarding whether and how CTCs respond differently to varying magnitudes of shear stress. Moreover, the roles of myosin II in the mechanotransduction of suspended CTCs and its influences on the CTCs' survival remain largely unknown. Importantly, a comprehensive understanding of how nuclear mechanosensing involves in nuclear mechanoadaptation of suspended cells is still lacking. Addressing these fundamental questions can substantially enlarge our comprehensive understanding of CTCs' survival under fluid shear flow. Further targeting this mechanoadaptation mechanism can better eliminate CTCs in blood circulation and improve patient survival.

Chapter 2. Materials and Methods

2.1 Cell culture and maintenance

Breast cancer cell line MCF-7 and MDA-MB-231 were bought from ATCC and cultured with Gibco™ Roswell Park Memorial Institute (RPMI) 1640 Medium and Dulbecco's Modified Eagle Medium (DMEM), respectively. Both RPMI 1640 and DMEM were supplemented with 10% FBS (HyClone) and 1% PS (HyClone) at standard culture environment. Human T-cell leukaemia cell line Jurkat E6.1 was purchased from Procell company and authenticated by short tandem repeat. Jurkate E6.1 cell line was cultured by RPMI 1640 medium supplemented with 10% FBS (HyClone) and 1% PS. To maintain cell status, cells were passaged every 2 to 3 days using 0.25% Trypsin (HyClone) depend on the concentration. The cell passaged over twenty will not be used. The short tandem repeat analysis was performed to verify all cell lines were negative for mycoplasma contamination during experiments.

2.2 Application of circulatory shear stress

The circulatory pump system was used to reconstitute blood microenvironment and apply the FSS to SBTCs[56]. This system consisted of a peristaltic pump, a silicone micro-tubing which was about 0.51 mm diameter and 1.5 m length, and a syringe that used as the cell solution reservoir. Before experiments, the whole system was washed by 75% ethanol and rinsed with 4 mL phosphate buffered saline (PBS, HyClone). The FSS in tube wall $\boldsymbol{\tau}$ (dyne/cm^2) was calculated by $\boldsymbol{\tau=4\mu Q/(\pi R^3)}$, where $\boldsymbol{Q}$ was the flow rate, $\boldsymbol{\mu}$ was the dynamic viscosity of the liquid (calculated for 0.01 dyne·s/cm^2 for cell culture media), and $\boldsymbol{R}$ was the tube radius (0.255 mm used in this research). To decrease the attachment of suspended cells to the micro-tubing and syringe, the system was rinsed with 4 mL 1% bovine serum albumin (BSA, VWR Life Science). During experiments, 2 mL cell suspension solution (2*10^5 cells/mL) was added into circulatory system and subjected to varying magnitudes of shear stress for different durations in the cell culture incubator at 37°C and 5%

CO_2 [56].

2.3 Application of uniform FSS

The microfluidic chip (Ibidi µ-Slide $I^{0.2}$ Luer, Cat. No. 80166) coupled with a peristaltic pump (P-230, Harvard Apparatus) and 0.51 mm micro-tubing were used to apply the uniform FSS. To keep suspension status during shear stress treatment, PLL (Sigma-Aldrich) was used to let suspended tumor cells attach to but not spreading on the microfluidic chip. Before experiments, PLL (0.1 % (w/v)) was precoated on microfluidic chip and cultured in room temperature overnight. Next, PLL was aspirated and the channel was washed by PBS for twice. After trypsinization, 100 µl cell suspended solution (10^6 cells/mL) was add it to microfluidic chip. Then, the microfluidic chip containing cell solution was cultured in chamber at 37℃ and 5% CO_2 for fifteen minutes to let suspended cells attach to the chip. Finally, the microfluidic chip was connected with micro-tubing and the uniform FSS was applied to suspended cells by a peristaltic pump. The calculation of shear force magnitude was strictly following the manufacturer's instructions as $\boldsymbol{\tau}\ [dyn/cm^2] = \boldsymbol{\eta}\ [dyn \cdot s/cm^2] \cdot 512.9 \cdot \boldsymbol{\Phi}\ [min/mL]$, where $\boldsymbol{\eta}$ was the viscosity of liquid (calculated for 0.01 dyne·s/cm^2 for cell culture media), $\boldsymbol{\Phi}$ was the flow rate. The system setup can be seen in Figure 2-1.

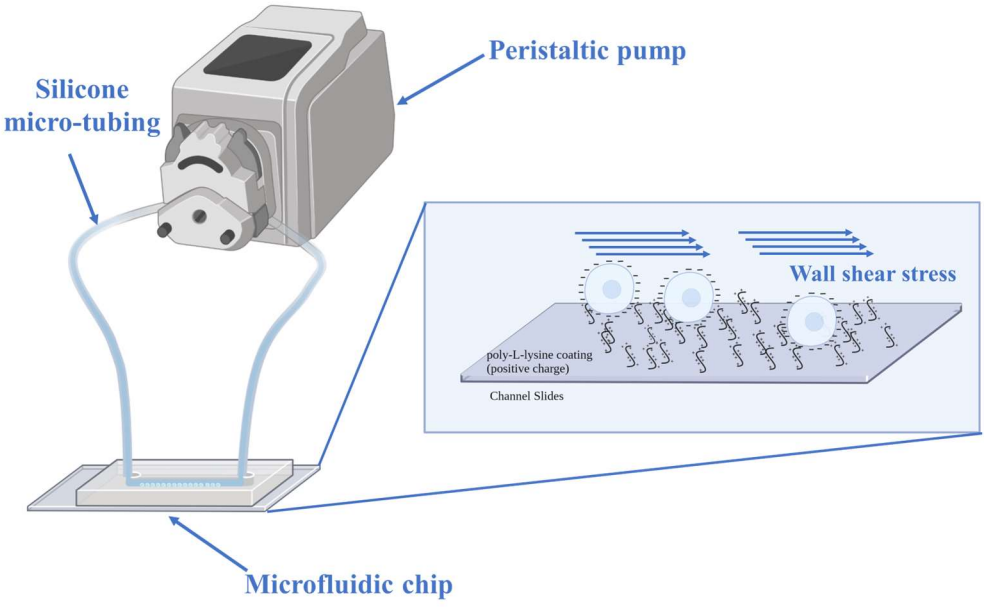

Figure 2-1 System setup of applying uniform FSS. The whole system consists of a peristaltic pump, a silicone micro-tubing and a microfluidic chip. The chip is precoated with the PLL to let suspended tumor cell keep its suspension status when applying the uniform FSS.

2.4 Pharmacologic treatment

Cells were treated with 50 μM 4-Hydroxyacetopophenone (4-HAP, Sigma-Aldrich), 20 μM Blebbistatin (Ble, Sigma-Aldrich), 2 or 20 μM Y-27632 (Y27, Sigma-Aldrich), 20 μM ML-7 (Sigma-Aldrich), 20 nM calyculin A (MCE, Cat. No HY-18983/CS-54), 10 μM si*LMNA* (Thermo Fisher Scientific, Cat. No 4390824), 50 nM Thapsigargin (Tg, Thermo Fisher Scientific, Cat. No 2403704) for given time before or after applying FSS. 1 mM ethylene glycol-bis (β-aminoethylether)-N,N,N′,N′-tetraacetic acid (EGTA, Sigma-Aldrich, Cat. No E3889) was used to chelate calcium in cell culture medium for an hour. All the drugs except 4-HAP were dissolved in DMSO to prepare the stock solution following the manufacturer's instructions and then diluted with the full medium into working solution. 4-HAP was dissolved in 95% ethanol to prepare the stock solution following the manufacturer's instructions and then diluted with the full medium into working solution.

2.5 Quantitative RT-PCR

Total RNA from target cells was isolated using Aurum Total RNA Mini Kit (Bio-Rad). cDNAs were synthesized with the cDNA Synthesis Kit (Thermo Fisher Scientific). GAPDH was used as internal controls for the quantification of gene expression. Real-time PCR was performed with CFX96 Real-Time System (Bio-Rad). Relative mRNA expression was calculated using the ΔΔCT method. The siRNA was designed and synthesized by Hanbio Bio-technology. The sequences used to detect the *MYH10* gene expression were used as follows:

Forward sequence GGAAGAAACGCCATGAGATGC, Reverse sequence GTGCATAGAATTGACTGGTCC.

The sequences used for small interfering RNA (Si-RNA) were listed as follows:

si*MYH10* sequence#1: Forward sequence GAGAAGAAGCUGAAAGAAATT, Reverse sequence: UUUCUUUCAGCUUCUUCUCTT

si*MYH10* sequence#2: Forward sequence CCAAAGAUGAUGUGGGAAATT, Reverse sequence: UUUCCCACAUCAUCUUUGGTT

si*MYH10* sequence#3: Forward sequence UGGAAGAAGCAGAGAAGAATT, Reverse sequence: UUCUUCUCUGCUUCUUCCATT

Negative control: Forward sequence UUCUCCGAACGUGUCACGUTT,

Reverse sequence: ACGUGACACGUUCGGAGAATT

GADPH: Forward sequence GUAUGACAACAGCCUCAAGTT,

Reverse sequence: CUUGAGGCUGUUGUCAUACTT

2.6 Immunofluorescence

Suspended cells after shear flow treatment were collected and fixated by 4% paraformaldehyde (Thermo Fisher Scientific) under room temperature for 20 minutes. After washing cells by PBS for twice, 0.5% Triton X-100 (SAFC) in 1% BSA solution was added to permeate cell membrane under room temperature for an hour. After that, PBS was added to cells and incubated with first antibody diluted with 1% BSA. The first antibodies used in this project were listed below: Phospho-Myosin Light Chain 2 Ser19 (P-MLC) antibody (Cell signaling, Cat. No. 3671); Vinculin antibody (abcam, Cat. No 129002); Phospho-Histone H2A.X Ser139 (γ-H2AX) antibody (Cell signaling, Cat. No. 9718); Lamin A+ Lamin C (Lamin A/C) antibody (abcam, Cat. No 238303); MLCK antibody (abcam, Cat. No 76092); Phospho-ROCK (ser 1366) antibody (Thermo Fisher Scientific, Cat. No PA5-34985); Phospho-Lamin A/C (Ser22) antibody (Thermo Fisher Scientific, Cat. No PA5-17113), Cleaved Caspase-3 (Asp 175) antibody (Cell signaling, Cat. No. 9661). The concentration of first antibody was used following the manufacturer's instructions and co-incubated with permeabilized cells in 4℃ overnight. Further, the cells were washed twice by PBS and incubated with secondary antibody of either Goat Anti-Rabbit IgG H&L (Alexa Fluor® 488, Cat. No.

ab150077), Goat Anti-Rabbit IgG H&L (Alexa Fluor® 647, Cat. No. ab150079) or Goat Anti-Mouse IgG H&L (Alexa Fluor® 594, Cat. No. ab150116) for an hour in dark. Finally, after washing twice by PBS, the cells were cultured with Hoechst (Thermo Fisher Scientific) and imaged as soon as possible.

2.7 Microscopy and living cell imaging

Leica SPE confocal microscopy with 63 × 1.4 NA oil-immersion objective was used to immunofluorescence imaging via Leica MM AF software. For each cell, the cross section was chosen for imaging. Leica SPE confocal microscopy excited DAPI, green fluorescence and red fluorescence at 405 nm, 488 nm, 568 and 635 nm, respectively.

2.8 Western blotting

Cells used for western blotting were lysed by RIPA and extraction buffer (Thermo Fisher Scientific) and stocked at -20. After quantifying protein level in each condition, same amount (~50 μg) of total protein was added into polyacrylamide gels and run by gel electrophoresis (BIO-RAD). Further, after separating proteins with different molecular weight, protein in 10% SDS-PAGE gel was transferred to polyvinylidene difluoride (PVDF) western blotting membrane (with a pore size of 0.2/0.44 μm) thorough Trans-Blotting Turbo (BIO-RAD). In order to diminish non-specific protein-antibody binding, blocking through 3% BSA solution was conducted overnight. Further, antibody of desired protein was co-incubated with western blotting membrane. Finally, secondary antibody was added and blotting images were taken using Clarity MAX^{TM} Western ECL Blotting Substrates and ChemiDoc™ MP Imaging System (BIO-RAD).

2.9 Quantification of P-MLC cortex/cytoplasm ratio

Total level of P-MLC was defined as total fluorescence intensity of cell's cross section. To exclude the difference of cell area, we further calculate P-MLC cortex/cytoplasm ratio from intensity density. To get the P-MLC cortex/cytoplasm ratio, P-MLC was quantified in the cell cortex or cytoplasm respectively. We defined that the region within

450 nanometers beneath the cell membrane was cell cortex, and the remaining part of cell was cell cytoplasm. The P-MLC cortex/cytoplasm ratio was defined as average cortical P-MLC fluorescence intensity divided by average cytoplasmic P-MLC fluorescence intensity. The formula used for calculating P-MLC cortex/cytoplasm ratio was listed as follow:

$$\frac{P-MLC_{cortex}}{P-MLC_{cytoplasm}} = \frac{\sum_{cortex}^{I}/A_{cortex}}{(\sum_{cell}^{I} - \sum_{cortex}^{I})/(A_{cell}-A_{cortex})}$$

Here, the $\sum_{cortex}^{I}$ and $\sum_{cell}^{I}$ were sum of fluorescence intensity in each pixel in cell cortex and whole cell, respectively. A_{cortex} and A_{cell} were the area of cell cortex and whole cell, respectively. All the measurements were performed in ImageJ 1.5K.

2.10 Plasmid transfection

Breast cancer cells were transfected by using Lipofectamine 3000 &lipofectamine 3000 (Life Technologies, Carlsbad, CA, USA) following the manufacturer's protocol. Briefly, cells were pre-seeded in a 6-well plate, the transfection can be conducted when the cell confluency reach about 70–90%. During transfection, for each well, 10 μL P3000 reagent and 5 μg siRNA or plasmid were diluted in 125 μL Opti-MEM medium. After that, the diluted siRNA was added into diluted lipofectamine 3000 reagents (3.75 μL lipofectamine 3000 reagents in Opti-MEM medium) at 1:1 (v/v) ratio and incubated for 20 mins at room temperature. The siRNA-lipid solution was then added to cells and cultured at 37°C and 5% CO_2 incubator for two days before the experiments. The plasmids used for cell transfections were listed as follows: Gata3-T2A-H2B-eGFP donor was a gift from Janet Rossant (Addgene plasmid # 113119; http://n2t.net/addgene:113119; RRID: Addgene_113119); PECAM-H2B-GFP was a gift from Victoria Bautch (Addgene plasmid # 14689; http://n2t.net/addgene:14689; RRID: Addgene_14689); pcdna nesprin TS was a gift from Daniel Conway (Addgene plasmid # 68127 ; http://n2t.net/addgene:68127 ; RRID:Addgene_68127); pAAV.CAG.GCaMP6f.WPRE.SV40 was a gift from Douglas Kim & GENIE Project

(Addgene plasmid # 100836 ; http://n2t.net/addgene:100836 ; RRID:Addgene_100836); mRuby2-LaminA-C-18 was a gift from Michael Davidson (Addgene plasmid # 55901 ; http://n2t.net/addgene:55901 ; RRID:Addgene_55901); pinducer 20 DN-KASHΔPPPL was a gift from Daniel Conway (Addgene plasmid # 129280 ; http://n2t.net/addgene:129280 ; RRID:Addgene_129280); pinducer 20 DN-KASH was a gift from Daniel Conway (Addgene plasmid # 125554 ; http://n2t.net/addgene:125554 ; RRID:Addgene_125554); pNLuc was a gift from Koen Venken (Addgene plasmid # 118058 ; http://n2t.net/addgene:118058 ; RRID:Addgene_118058); siMLCK and doxycycline inducible siROCK2 were designed and purchased from Yanming Biotechnology Co., Ltd.

2.11 Quantification of FRET index under shear stress

Fluorescence resonance energy transfer (FRET) index of Nesprin-based tension sensor was quantified through Leica TCS SP8 MP Multiphoton/Confocal Microscope with 63 × 1.4 NA oil-immersion objective under 405 excitation wavelengths. Briefly, cells were transfected with pcdna Nesprin TS and attached to PLL coated chip in suspension status. The cells expressed relative equal level of fluorescence were selected as targes as previous mentioned[122]. Further, during FSS application through peristatic pump, automatic focusing was enabled to avoid possible vibration of cell focus under shear stress. The FRET index was defined as the fluorescence intensity ratio of receptor (yellow) and donor (cyan). FRET images were acquired every 1.2s. As pcdna Nesprin TS predominately expressed near LINC complex, the FRET index of 1.5 μm near nuclear mask was quantified and further analyzed by Leica MM AF software[247].

2.12 Living cell imaging of calcium response under shear stress

The intracellular calcium sensor GCaMP6 was transfected to cells as previously mentioned[248]. Then, cells were attached to PLL coated microfluidic chip and applied with shear stress through peristatic pump. Images of GCaMP6 calcium sensor were taken by Leica SPE confocal microscopy with 63 × 1.4 NA oil-immersion objective

every 1 minute. Quantification of calcium intensity was performed in ImageJ 1.5K.

2.13 Quantification of cross section area, shape factor and excess of perimeter of the NE

The cross section was defined as the largest cell section when the z-scanning of Leica MM AF software was proceeded. The shape factor was calculated by Image J shape factor measurement. The excess of perimeter of the NE (EOP_{NE}) was quantified as follow. First, the length of nuclear mask (labeled by Lamin A/C staining, including invagination and wrinkle) was quantified through Image J and defined as P_m. Then an ellipse with minimal perimeter was used to include whole nucleus and the perimeter of ellipse was defined as P_e. Finally, the EOP_{NE} was defined as follow:

$$EOP_{NE} = \frac{P_m - P_e}{P_e}$$

Fluorescence images were taken by Leica SPE confocal microscopy with 63 × 1.4 NA oil-immersion objective.

2.14 Quantification of histone 2B (H2B) displacement

Before experiment, living cells were pre-transfected with Gata3-T2A-H2B-eGFP donor or labeled by H2B-RFP (Thermo Fisher Scientific) for two days. After trypsinization, cells were attached to PLL coated chip for 15 minutes. Further, the chip was connected with a peristaltic pump and imaged under Leica SPE microscopy with 63 × 1.4 NA oil-immersion objective, automatic focusing was enabled to avoid possible influence of stage vibration. During force application, the cell nucleus, which was transfected by green or red fluorescence, was imaged fifty times during 46.298s. 46.298s was the minimal time that Leica SPE microscopy spent to capture the 50 images in desired resolution. Finally, based on published MATLAB program, H2B displacement map was plotted[249]. The schematic of H2B displacement calculation was listed below:

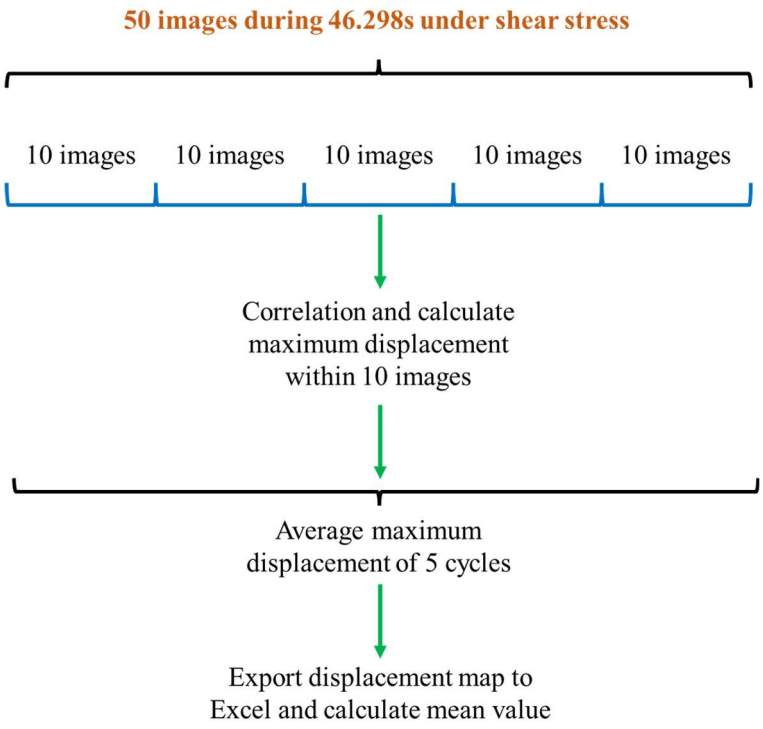

Figure 2-2 Schematic of H2B displacement calculation. During shear stress application, 50 images of H2B were taken within 46.298s. Further, these images were divided into five cycles. For each cycle, MATLAB would correlate and calculate maximum displacement among 10 images. Finally, after averaging maximum displacement of five cycles, the H2B displacement was plotted.

2.15 Definition and quantification of FTE

After getting H2B displacement map, we further exported the figures of H2B displacement in each pixel to the Excel. Further, we used the mean figures of H2B displacement (nm) in the map as the H2B displacement in this cell. Further, in order to compare the ability of force transmission under different conditions, we defined the FTE as follow:

$$Force\ transmission\ efficiency = Normalized\left[{strain}/{stress\ (\frac{dynes}{cm^2})}\right]$$

Here, the strain was the H2B displacement (nm), stress was the shear stress applied on the cell (dyne/cm^2), the FTE was normalized to the CTRL group.

2.16 Propidium iodide (PI) cell apoptosis assay

Cell death after FSS was measured through PI staining. In short, suspended tumor cells after FSS were collected from the tube and centrifuged by 1,500 rpm and 5 mins, then washed by PBS twice. Further, the suspended tumor cells were stained by 1 mL PBS containing 4 μM PI. Finally, after washing for by PBS for twice, the dead cells were stained by the red fluorescence and imaged under Leica SPE confocal microscopy. Quantifying the dead cells number was perform in ImageJ 1.5K.

2.17 CSCs selection through fibrin gel

CSCs of MCF-7 were selected as previously mentioned[250]. In brief, for each well of 24-well plate, MCF-7 solution containing $1*10^5$ cells was mixed with fibrinogen (1 mg/mL, Salmonics LLC) diluted by T7 buffer and the final volume was 150 μL. The mixture of MCF-7 and fibrinogen was further seeded to 24-well plate that was pre-add by 6 μl 0.1U/μL thrombin (Salmonics LLC). After incubating the mixture on 24-well plate in incubator for 30 mins, 1 mL RPMI 1640 supplemented with 10% FBS and 1% PS was added to each well. During following five days culture, cell medium was replaced twice. Finally, the fibrin gel was digested by fibrinase and CSCs can be used.

2.18 Ethics of animal experiments

The animal experiments were approved by THE GOVERNMENT OF THE HONG KONG SPECIAL ADMINISTRATIVE REGION DEPARTMENT OF HEALTH and put on record (22-321) in DH/HT&A/8/2/4 Pt.12. All animal experiments were conducted under supervision of Centralised Animal Facilities of HONG KONG Polytechnic University.

2.19 Tail vein injection and bioluminescence imaging

MDA-MB-231 wild type cells transfected with pNLuc were used to detect cell apoptosis *in vivo*[251]. Briefly, pNLuc were stably transfected to MDA-MB-231 wild type cells and treated with DMSO or Y27632. Next, 100 μL cell suspension containing 10^6 cells was injected into 5-7 weeks female nude mice (Centralised Animal Facilities of HONG KONG Polytechnic University) through tail vein injection. After 12 hours circulation, the whole blood (~1 mL) of mice was collected into vacuum blood collection tube (Lingen Precision Medical Products Co., Ltd.). Further, 20 μM coelenterazine (Sigma-Aldrich) was added into blood with 1:4 ratio (v/v) and incubated for 15 minutes under dark. Finally, 500 μL blood was aspirated into 12 well plate and imaged by Animal Imaging Systems.

2.20 Statistical analysis

For each experiment, at least three independent repeats were performed. Two-tailed student's *t*-test was used to two group comparison, while ANOVA was used to compare the significance between three or more groups. ns=no significant difference, *, $p<0.05$, **, $p<0.01$ ***, $p<0.001$.

Chapter 3. SBTCs show distinct myosin II localization under shear stress

3.1 SBTCs show low mechanosensitivity under high FSS

As mentioned before, adherent cells exhibit distinct responses to different magnitudes of external mechanical stimuli[144, 146, 212], while whether suspended cell respond to different levels of FSS in distinct manners is still unclear. Here, we utilized MCF-7 SBTCs as a model to investigate whether it showed different mechanosensitivity to different levels of FSS. As the force transmitted to cell nucleus could trigger caspase-3 dependent cell apoptosis[252], we thus used caspase-3 expression in cell nucleus to represent cell mechanosensitivity. It is reported that FSS in veins, capillaries, and arteries is 1-4 dyne/cm^2, 10-20 dyne/cm^2, and 4-30 dyne/cm^2, respectively[253]. We therefore chose 0.5 to 20 dyne/cm^2 as the magnitudes of FSS to treat SBTCs. Furthermore, the *in vivo* half-time of breast cancer CTCs is estimated to be one hour[254], we thus applied one hour shear stress to see cell responses under circulatory pump system. The results in Figure 3-1a-b showed that with the levels of FSS gradually increased, caspase-3 nuclear expression exhibited force-dependent responses. Interestingly, while the trend of caspase-3 nuclear expression under low FSS (0-2 dyne/cm^2 FSS) was quite linear, under high FSS (5-20 dyne/cm^2 FSS), caspase-3 nuclear expression seemed increased gently and reached a plateau at 20 dyne/cm^2 FSS (Figure 3-1c). It was apparent that when fitting the caspase-3 nuclear expression with linear regression, the slope of caspase-3 nuclear expression under high FSS was quite lower than low FSS (Figure 3-1d). This result indicated that SBTCs show less mechanosensitivity to high FSS. As caspase-3 dependent cell signaling could trigger cell apoptosis, this phenomenon also indicated that SBTCs exhibited higher resistance to high FSS induced mechanical damage.

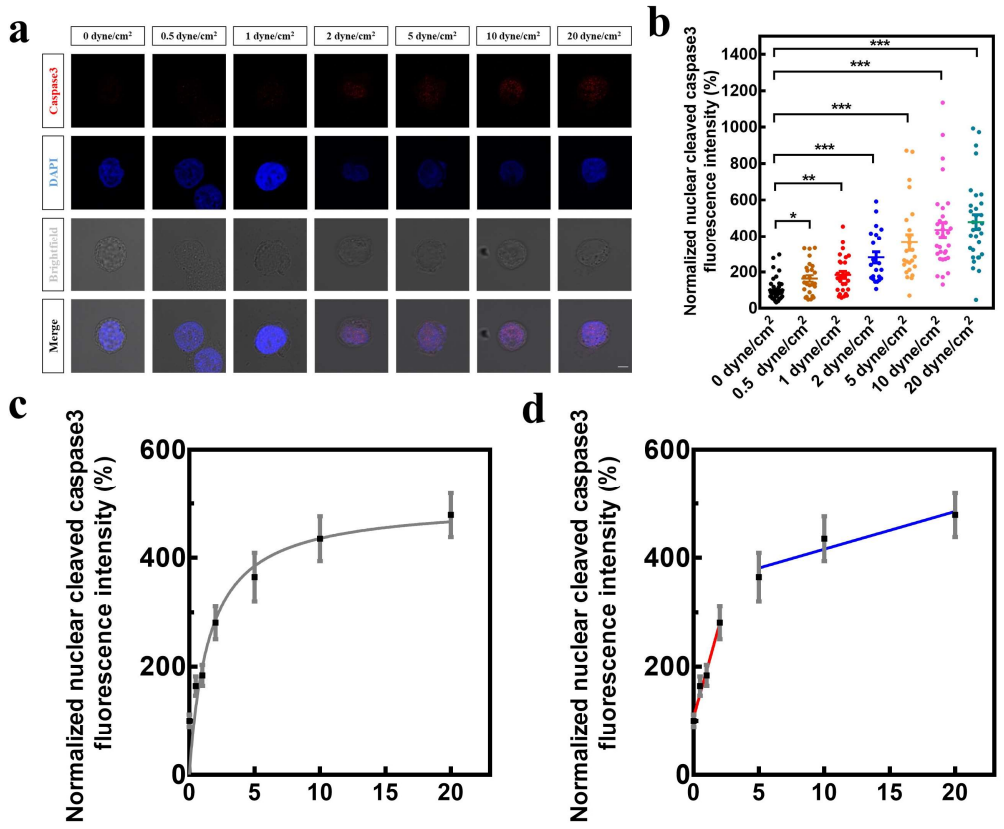

Figure 3-1 Caspase-3 nuclear expression shows distinct trend under low FSS and high FSS. **(a-b)** Representative immunofluorescence images (**a**) and statistic data (**b**) of caspase-3 in cell nucleus after 0.5 dyne/cm^2 to 20 dyne/cm^2 FSS treatment for an hour. **(c-d)** Fitting caspase-3 nuclear expression and magnitudes of FSS with third-order regression (**c**) and linear regression (**d**). Scale bar=5 μm; N = 3 independent experiments; mean ± SEM; *, p <0.05; **, p < 0.01; and ***, p < 0.001

3.2 Myosin II responds to FSS in a time and force dependent manner

Next, we wanted to investigate why SBTCs exhibited distinct mechanosensitivity under varying magnitudes of FSS. As myosin II activity plays indispensable role in cell mechanosensing[103, 198], we thus measured myosin II activity under FSS. Figure 3-2 a-f showed that P-MLC, which represent myosin II activity, responded to varying magnitudes of shear force in time-dependent manner. After FSS for thirty minutes, the P-MLC increased to 118%, 125% and 139% under 2 dyne/cm^2, 5 dyne/cm^2 and 10 dyne/cm^2, respectively. We further put data after an hour FSS treatment together and

observed the clear force dependent manner of P-MLC expression (Figure 3-2 g). While the P-MLC increased to 136% under 2 dyne/cm^2, it further increased to 177% under 10 dyne/cm^2 after one-hour circulation. Based on the data showed above, myosin II activity represented by P-MLC, increased under FSS in time and magnitude dependent manner.

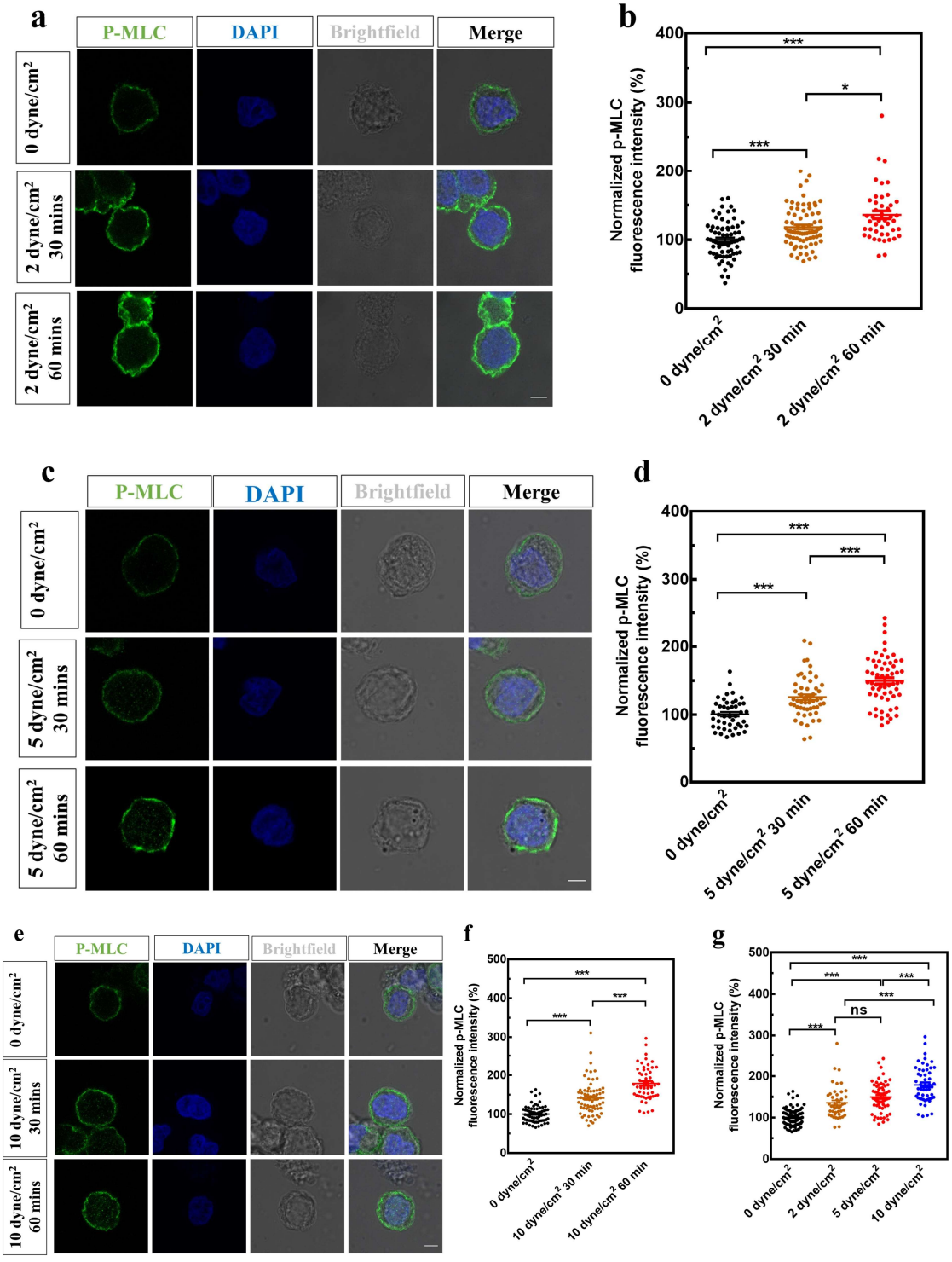

Figure 3-2 Myosin II responds to the FSS in time and force magnitude dependent manner. (a-b) Representative immunofluorescence images (**a**) and statistic data (**b**) of P-MLC after 2 dyne/cm^2 FSS treatment for thirty minutes and an hour. (**c-d)** Representative immunofluorescence images (**c**) and statistic data (**d**) of P-MLC after 5 dyne/cm^2 FSS treatment for thirty minutes and an hour. (**e-f)** Representative immunofluorescence images (**e**) and statistic data (**f**) of P-MLC after 10 dyne/cm^2 FSS treatment for thirty minutes and an hour. (**g**) P-MLC fluorescence intensity after 2 dyne/cm^2, 5 dyne/cm^2 and 10 dyne/cm^2 FSS for an hour. Scale bar=5 μm; N = 3 independent experiments; mean ± SEM; *, p <0.05; **, p < 0.01; and ***, p < 0.001

3.3 Myosin II of SBTCs shows distinct subcellular localization under varying levels of FSS

As different myosin II subcellular localization play distinct cellular functions[212], we thus further investigated whether myosin II showed different localizations under FSS. Hereby, we divided cell into to two parts, one part was cell cortex and another part was cell cytoplasm. At first, we measured cortical thickness to define which part was regarded as cell cortex. Previous study demonstrates that for suspended cell, myosin II is predominantly located in the cell cortex[87]. Based on it, we stained the P-MLC under static condition (no shear stress treatment) and measured the cortex thickness in MCF-7 cells following previous published methods[255]. The results showed that the cortex thickness of suspended MCF-7 was about 450 nm, similar with HeLa cells measured in interphase[86]. Apart from that, cortex thickness remained nearly the same, irrespective of 10 dyne/cm^2 FSS treatment for an hour (Figure 3-3 a). Thus, we used 450 nm as the cortical thickness of suspended MCF-7 in following experiments.

Based on segment of cell cortex and cytoplasm, we wanted to further investigate whether P-MLC under different magnitudes of FSS localized in the different subcellular regions. Intriguingly, P-MLC showed distinct subcellular localization under different magnitudes of FSS. While P-MLC was substantially enhanced in cell cortex under low FSS (2 dyne/cm^2), it relocalized to the cytoplasm after high FSS (5 and 10 dyne/cm^2)

treatment (Figure 3-3 b-c). The contrast was more significant if we comparing the P-MLC cortex/cytoplasm ratio: the P-MLC cortex/cytoplasm ratio was significantly enhanced under low FSS while decreased under high FSS (Figure 3-3 d). This result suggested that myosin II in SBTCs respond differently to smaller and larger FSS: while myosin II mainly localized in cell cortex under low FSS, it redistributed into cell cytoplasm under high FSS.

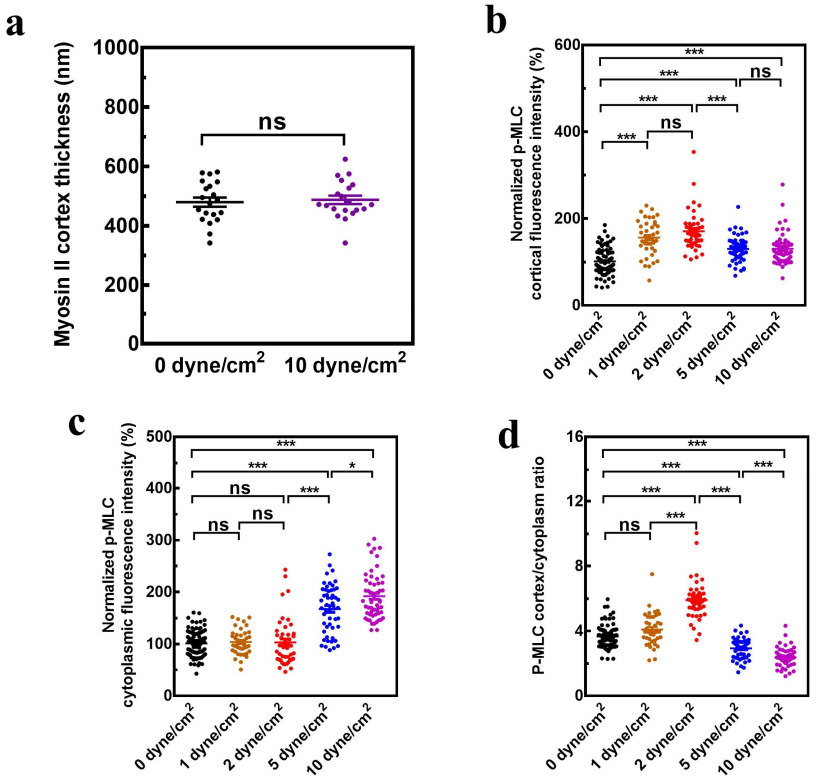

Figure 3-3 SBTCs respond differently to varying levels of FSS. (a) Quantification of cortical thickness under static condition and FSS treatment. **(b-c)** Normalized P-MLC cortical **(b)** and cytoplasmic **(c)** fluorescence intensity after FSS. **(d)** P-MLC cortex/cytoplasm ratio under FSS. N = 3 independent experiments; mean ± SEM; *, p <0.05; **, p < 0.01; and ***, p < 0.001

3.4 PLL coated microfluidic chip recapitulates shear-induced myosin II localization

Now, we have found distinct subcellular distribution of P-MLC responded to low FSS and high FSS. Nevertheless, in circulatory pump system we used, shear stress is equal to viscosity*du/dy, where du/dy is the flow-rate gradient. As the flow-rate gradient

gradually increases from tube center to the wall, the shear stress that the SBTCs experience in the micro-tubing also gradually increases from tube center to the wall[256]. That is to say, the SBTCs experience zero shear stress if they locate in tube center and largest shear stress if they locate in tube wall. Thus, for each the SBTCs, it experiences different levels of shear stress according to their location during circulation and it is hard to quantify the shear stress applied to each of them[256]. The shear stress we mentioned above is the FSS in tube wall (that is to say, highest shear stress that SBTCs may experience). Thereby, it is essential for us to find out a method to ensure the shear force that the cell suffered and quantify SBTCs responses under certain levels of shear stress.

To achieve this goal, we take advantages of PLL, a lysine homopolymers which enhances electrostatic interaction between negatively-charged ions of the cell membrane and positively-charged surface ions of attachment factors on the culture surface[257]. It can bind with cell through non-specific adhesion, which maintains the suspension status of suspended cells for a certain time scale. The PLL coated substrate is widely used in AFM based suspended cells stiffness measurements where the suspension status should be kept[257].

Benefit from the unique adhesion property of PLL, we further coated microfluidic chip with PLL. To justify the PLL coated chip could make suspended tumors cells keep its suspension status within one hour, we compared both morphological parameters and adhesion molecule during an hour attachment. As it can be seen in Figure 3-4 a-b, the morphological parameters including cross section area and shape factor remained unchanged during an hour attachment. In addition, vinculin, an adhesion molecule that is early recruited to the FA[258], remained nearly the same compared with suspended tumor cells (Figure 3-4 c-d). Furthermore, P-MLC that we tested, remained constant within one hour after attachment to PLL coated substrate. (Figure 3-4 e-h). All these results indicated that when the SBTCs attached on PLL coated microfluidic chip, the suspension status could be kept for at least an hour. Furthermore, as SBTCs were attached to the PLL coated substate, when applying the shear flow, the force that the

cells experienced was uniform FSS. In that way, each SBTC was experienced same and certain level of FSS, solving the confusion that SBTCs in circulatory pump system suffered from different levels of FSS.

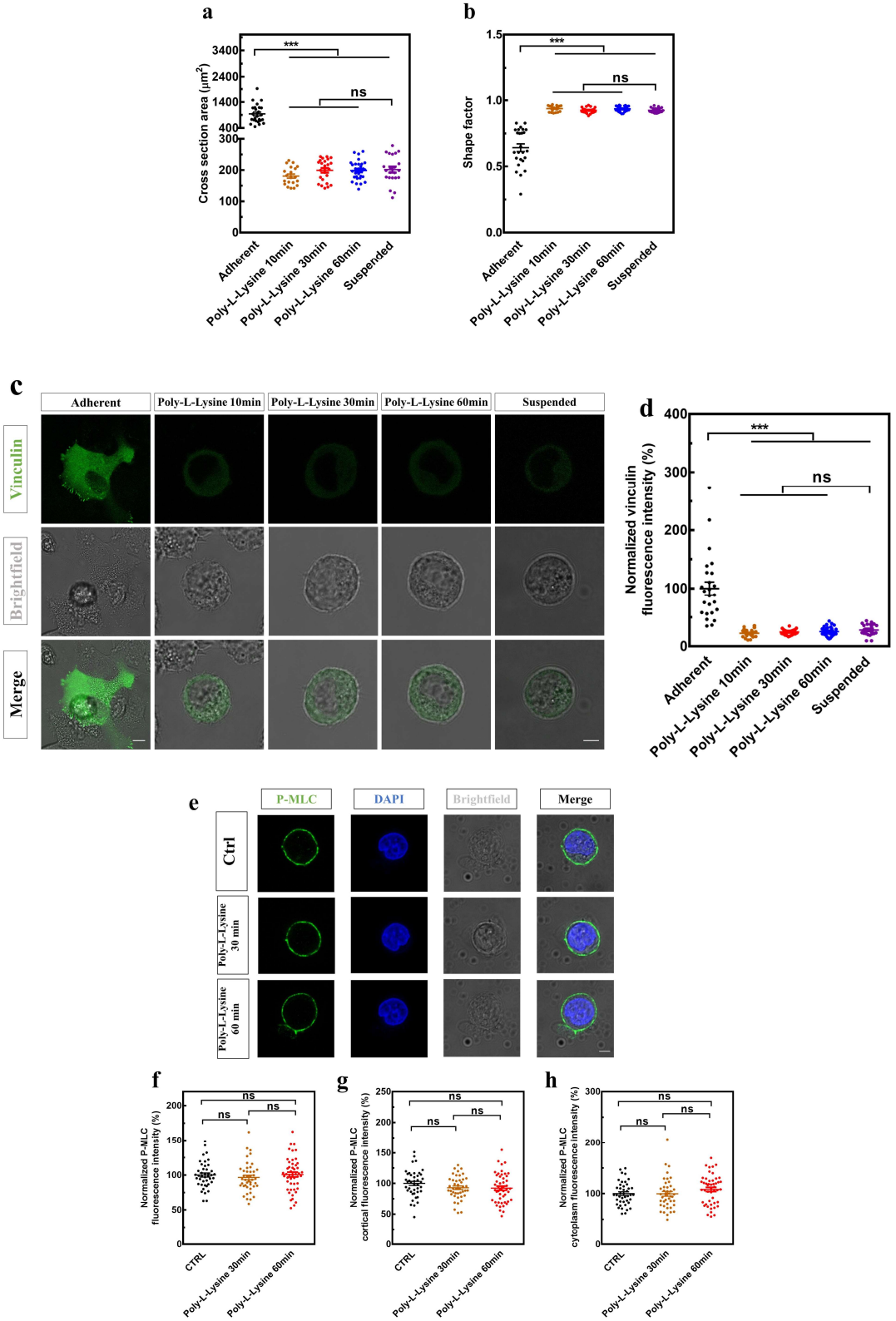

Figure 3-4 PLL coated substate could keep suspension status for an hour. (a) Cross section area of SBTCs on PLL coated substate. **(b)** Shape factor of SBTCs on PLL coated substate. **(c)** Immunofluorescence images of vinculin in adherent and PLL attached suspended cells. **(d)** Vinculin florescence intensity in adherent and PLL attached suspended cells. **(e-f)** Representative immunofluorescence images **(e)** and quantitative data of P-MLC intensity **(f)** of STBCs on PLL coated substate. **(g-h)** Cortical **(g)** and cytoplasmic **(h)** P-MLC intensity of STBCs on PLL coated substate. Scale bar=10 μm for **(c)** and 5 μm for **(e)**; N = 3 independent experiments; mean ± SEM; *, p <0.05; **, p < 0.01; and ***, p < 0.001

Based on PLL coated microfluidic chip, we further confirmed caspase-3 nuclear expression and myosin II subcellular localization under uniform FSS in microfluidic chip as previously done. Herein, we applied lower and higher uniform FSS to SBTCs. As uniform FSS the cells sensed was much higher than FSS we tested above[259], we thus chose 0.25 dyne/cm^2 to 8 dyne/cm^2 uniform FSS and measured cell responses. As it can be seen in Figure 4-5, similar with FSS, capase-3 nuclear expression increased with uniform FSS levels (Figure 3-5 a-b), while increased trend of caspase-3 was slower and almost reached a plateau under high uniform FSS (Figure 3-5 c-d), confirming the lower mechanosensitivity of SBTCs under higher shear stress.

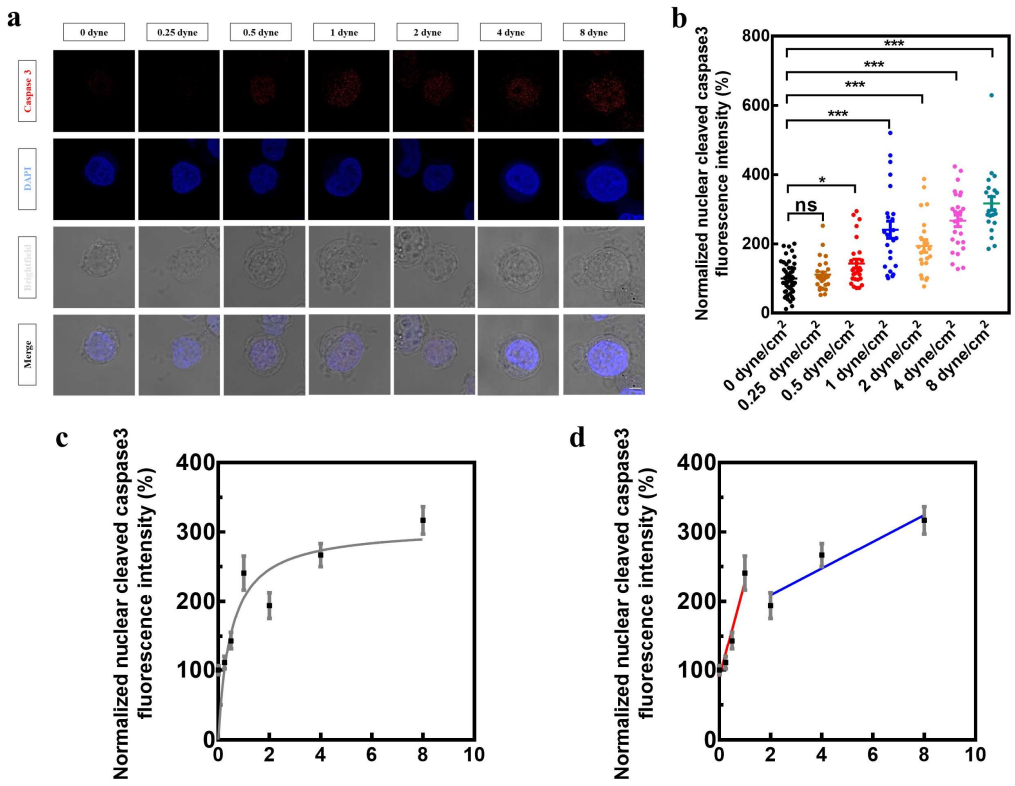

Figure 3-5 Caspase-3 nuclear expression shows distinct trend under low uniform FSS and high uniform FSS. (a-b) Representative immunofluorescence images (**a**) and statistic data (**b**) of caspase-3 in cell nucleus after 0.25 dyne/cm^2 to 8 dyne/cm^2 uniform FSS treatment for an hour. (**c-d)** Fitting caspase-3 nuclear expression and magnitudes of uniform FSS with third-order regression (**c**) and linear regression (**d**). Scale bar=5 μm; N = 3 independent experiments; mean ± SEM; *, p <0.05; **, $p < 0.01$; and ***, $p < 0.001$

In addition to caspase-3, after applying varying levels of uniform FSS to the SBTCs on the microfluidic chip, the similar trends of myosin II subcellular localization were also observed. As it was shown in Figure 3-6 a-d, while P-MLC mainly localized at the cell cortex under low uniform FSS, it redistributed to the cell cytoplasm under high uniform FSS. The distinct responses of SBTCs to different levels of uniform FSS were obvious when comparing P-MLC cortex/cytoplasm ratio. While the ratio increased under low uniform FSS, it decreased under high uniform FSS especially 4 dyne/cm^2 (Figure 3-6 e).

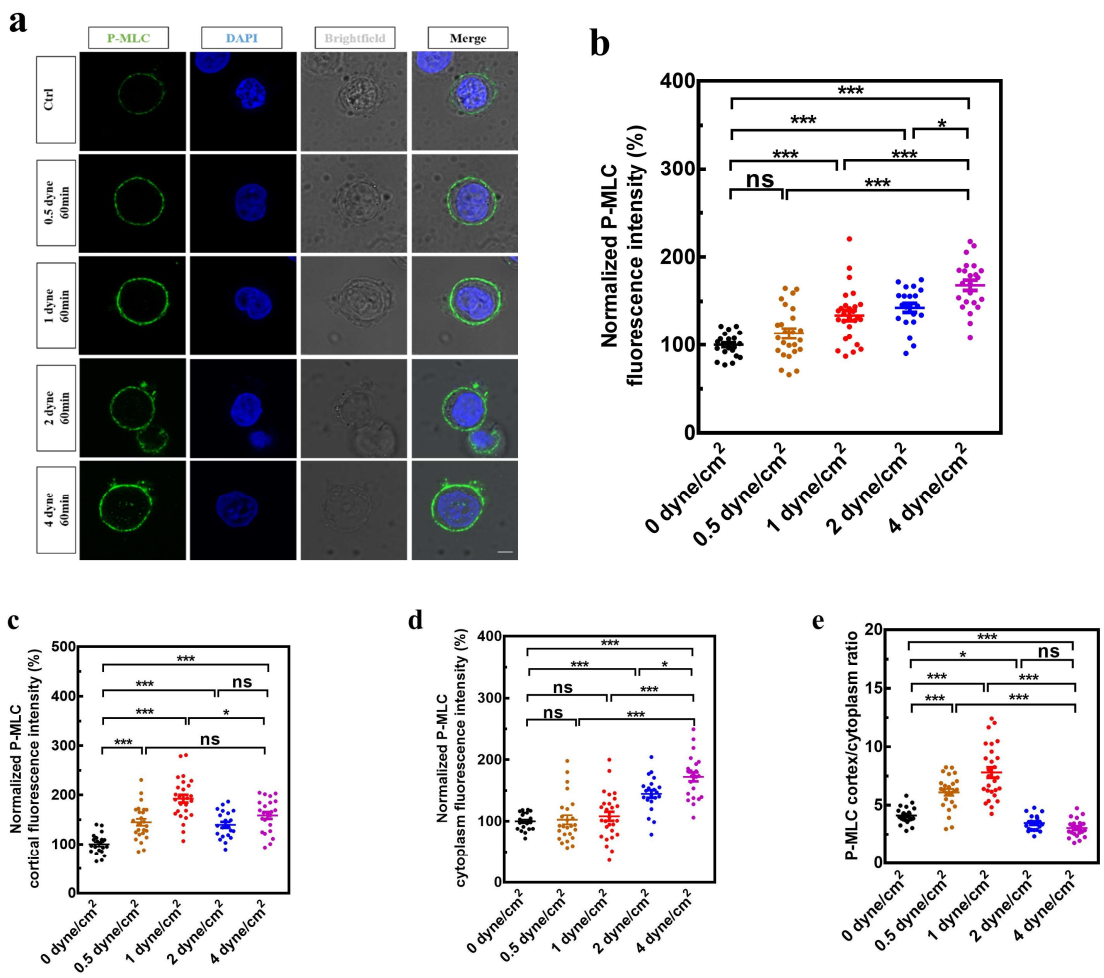

Figure 3-6 Myosin II of SBTCs shows similar responses to uniform FSS compared with FSS. **(a-b)** Representative immunofluorescence images of P-MLC **(a)** and statistic data **(b)** after varying levels of uniform FSS. **(c-d)** P-MLC cortical (**c**) and cytoplasmic **(d)** fluorescence intensity after varying levels of uniform FSS. **(e)** P-MLC cortex/cytoplasm ratio after varying levels of uniform FSS. Scale bar=5 μm; N = 3 independent experiments; mean ± SEM; *, p <0.05; **, p < 0.01; and ***, p < 0.001

In a short summary, myosin II of SBTCs responded differently to both FSS in the circulatory pump system and uniform FSS on the PLL coated microfluidic chip: while myosin II was more activated and localized in the cell cortex under low shear stress, it redistributed and localized to the cell cytoplasm under high shear stress.

Chapter 4. Cytoplasmic myosin II activity reduces FTE under high FSS

4.1 Quantification of nuclear deformation through H2B displacement

So far, we disclosed distinct subcellular localizations of myosin II under lower or higher shear stress. Further, we investigated cellular functions of myosin II subcellular localization in SBTCs. Considering myosin II plays indispensable role in mechanotransduction from cell surface to the cell nucleus[103], we thus speculate myosin II activity of SBTCs may act as a dominant factor that determines force transmission to nucleus. To test this hypothesis, we measured nuclear deformation under shear stress to represent the force transmitted to the cell nucleus as previously published[249]. To this end, we first justified the method of quantifying nuclear deformation through trypsinization. Here, we labeled the H2B of cell nucleus by red fluorescence (Figure 4-1 a). During cell detachment, the striking nuclear deformation represented by higher H2B displacement can be observed (Figure 4-1 b), suggesting H2B displacement calculated from published method well-represent nuclear deformation[249]. Benefit from PLL coated microfluidic chip, we can readily visualize and further calculate H2B displacement of SBTCs under uniform FSS. Here, we first quantified H2B displacement under transient uniform FSS (46s, in order to calculate H2B displacement) from 0 to 4 dyne/cm^2. The representative H2B displacement maps as well as statistical results showed that higher uniform FSS applied on the cell surface elicits higher H2B displacement (Figure 4-1 c and Figure 4-1 d), which was in accordance with our expectation.

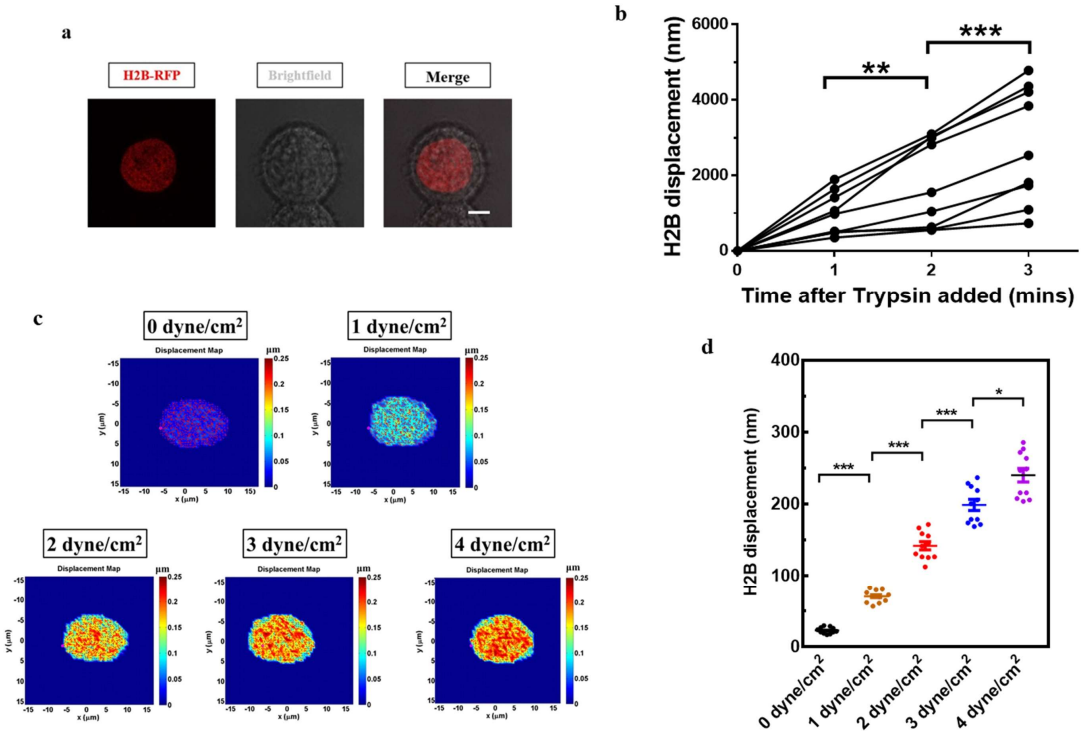

Figure 4-1 Quantification of nuclear deformation via H2B displacement. (a) Representative images of H2B in SBTCs. **(b)** H2B displacement during trypsinization. **(c-d)** Representative H2B displacement maps **(c)** and statistical data of H2B displacement **(d)** under 0 to 4 dyne/cm^2 transient uniform FSS. Scale bar=5 μm; N = 3 independent experiments; mean ± SEM; *, p <0.05; **, p < 0.01; and ***, p < 0.001

4.2 SBTCs show decreased FTE under high FSS

When different levels of shear stress were applied in cell surface, it was not even to comparing the ability of force transmission from cell surface to nucleus through H2B displacement only, as higher force undoubtedly elicit higher nuclear deformation (Figure 4-1 d). Therefore, to comparing the capacity of force transmission to nucleus unbiasedly, we defined a parameter called FTE (ratio of the resultant nuclear strain and the applied FSS, see materials and methods). Higher FTE means under same level of force applied on the cell surface, larger proportion of force would be transmitted into cell nucleus and elicits higher nuclear deformation.

Based on this, we further quantified FTE of SBTCs under different levels of uniform FSS. Intriguingly, after high uniform FSS (2 dyne/cm^2 and 4 dyne/cm^2), but not low

uniform FSS (0.5 dyne/cm^2 and 1 dyne/cm^2) treatment for an hour, FTE substantially dropped from 100% under CTRL (0 dyne/cm^2) to 75% and 58% after 2 dyne/cm^2 and 4 dyne/cm^2 treatment, respectively (Figure 4-2 a-c). The distinct responses of FTE under different levels of uniform FSS was reminiscent of cytoplasmic myosin II localization (Figure 3-6 e). Indeed, when cytoplasmic myosin II activity and FTE were jointly plotted, a clear inverse correlation between myosin II cytoplasmic activity and FTE can be observed: while myosin II activity in cytoplasm and FTE remained nearly constant under low uniform FSS, cytoplasmic myosin II activity increased with declined FTE under high uniform FSS.

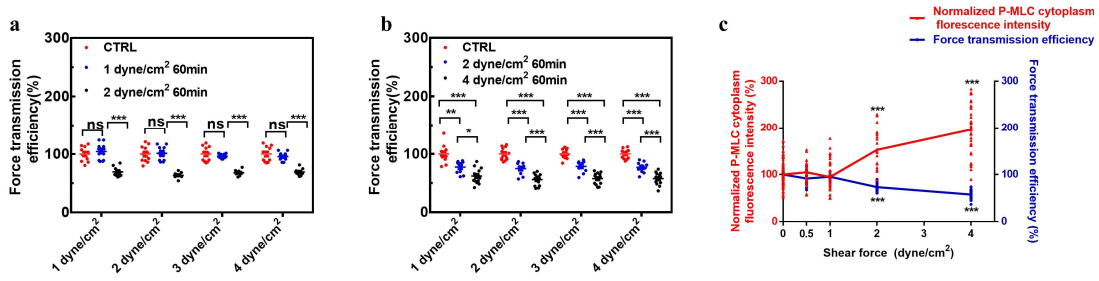

Figure 4-2 SBTCs show decreased FTE under high uniform FSS. (a) Comparing FTE of SBTCs after CTRL (0 dyne/cm^2), 1 dyne/cm^2 and 2 dyne/cm^2 uniform FSS treatment for an hour. **(b)** Comparing FTE of SBTCs after CTRL (0 dyne/cm^2), 2 dyne/cm^2 and 4 dyne/cm^2 uniform FSS treatment for an hour. **(c)** FTE and cytoplasmic myosin II activity of SBTCs show inversed trend under uniform FSS; N = 3 independent experiments; mean ± SEM; *, p <0.05; **, p < 0.01; and ***, p < 0.001

To further confirm the correlation between myosin II cytoplasmic activity and FTE under uniform FSS, we measured dynamic changes of cytoplasmic P-MLC and FTE with time under high uniform FSS. The results showed that under 4 dyne/cm^2 uniform FSS, cytoplasmic P-MLC began to increase at around 20 minutes, together with the decreased FTE (Figure 4-3 a-e). After twenty minutes, cytoplasmic P-MLC further enhanced and FTE further decreased until an hour (Figure 4-3 f). More importantly, both myosin II cytoplasmic activity and FTE remained nearly the same in ninety minutes compared with sixty minutes under high uniform FSS (Figure 4-3 g). These

results unambiguously suggested a strong correlation between cytoplasmic P-MLC and FTE.

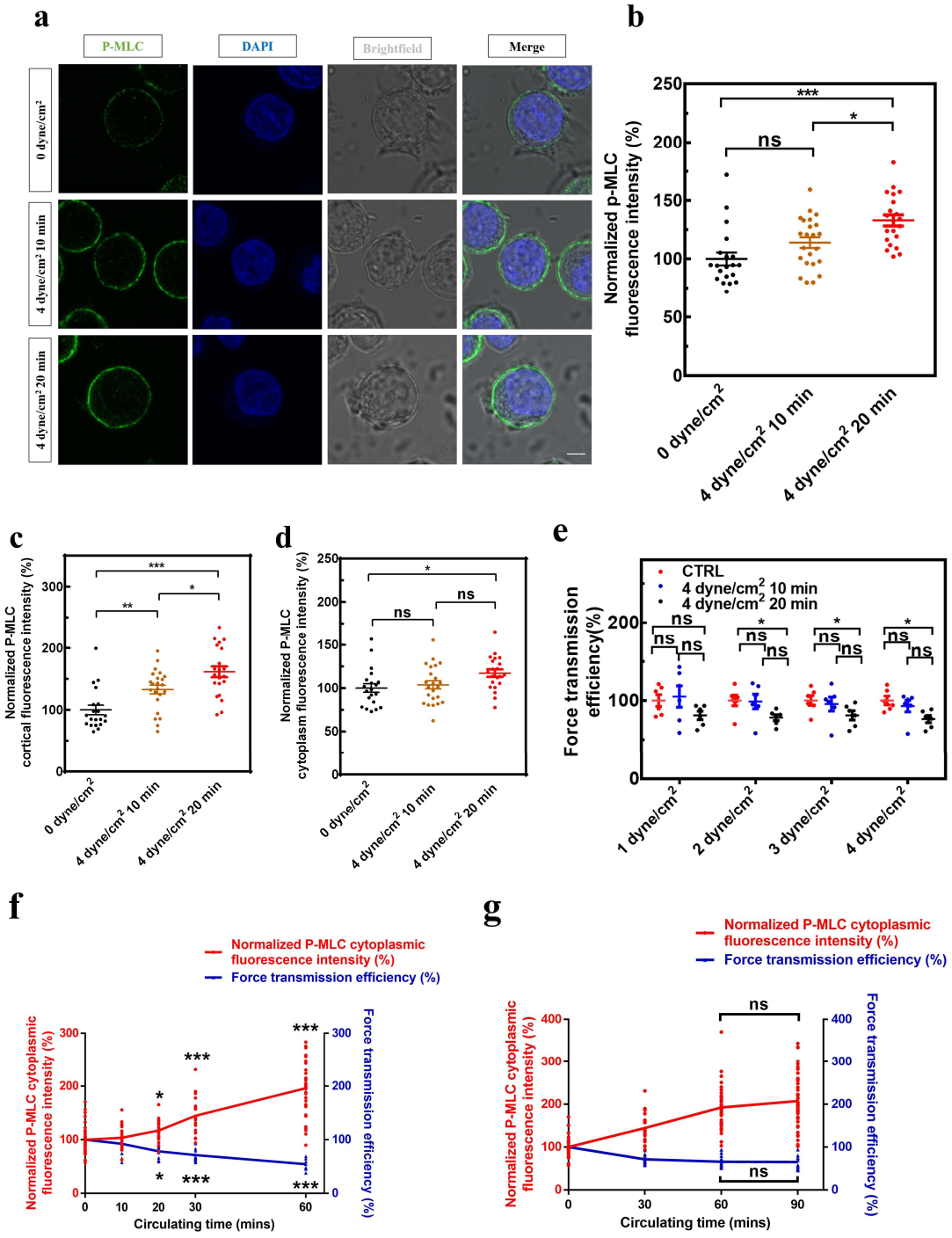

Figure 4-3 Correlation between cytoplasmic P-MLC and FTE under high uniform FSS. (a-b) Representative immunofluorescence images **(a)** and quantitative data of P-MLC intensity **(b)** after 10 and 20 minutes 4 dyne/cm^2 uniform FSS. **(c-d)** Normalized cortical **(c)** and cytoplasmic **(d)** P-MLC fluorescence intensity after 10 and 20 minutes 4 dyne/cm^2 uniform FSS. **(e)** FTE after 10 and

20 minutes 4 dyne/cm^2 uniform FSS. **(f-g)** Dynamic change of FTE and cytoplasmic P-MLC within sixty **(f)** or ninety **(g)** minutes under 4 dyne/cm^2 uniform FSS treatment. Scale bar=5 μm; N = 3 independent experiments; mean ± SEM; *, p <0.05; **, p < 0.01; and ***, p < 0.001

Up to now, we found that FTE was decreased under high uniform FSS with enhanced myosin II cytoplasmic activity. However, the phenomenon we observed was based on PLL coated microfluid chip and uniform FSS. As the PLL coated microfluidic chip cannot reproduce *in vivo* circulatory microenvironment, we thus confirmed the conclusion within circulatory pump system where SBTCs suffered from FSS. In light of this, we applied 10 dyne/cm^2 high FSS to SBTCs and quantified dynamic changes of myosin II subcellular distribution within eight hours. After FSS treatment, we collected SBTCs from the tube and attached them to PLL coated microfluidic chip to measure the FTE as soon as possible. As expected, myosin II activity increased with force duration and remained nearly constant after 2 hours (Figure 4-4 a-e). More importantly, SBTCs also exhibited attenuated FTE after high FSS treatment, the clear negative correlation between FET and myosin II cytoplasmic localization can also be observed (Figure 4-4 f).

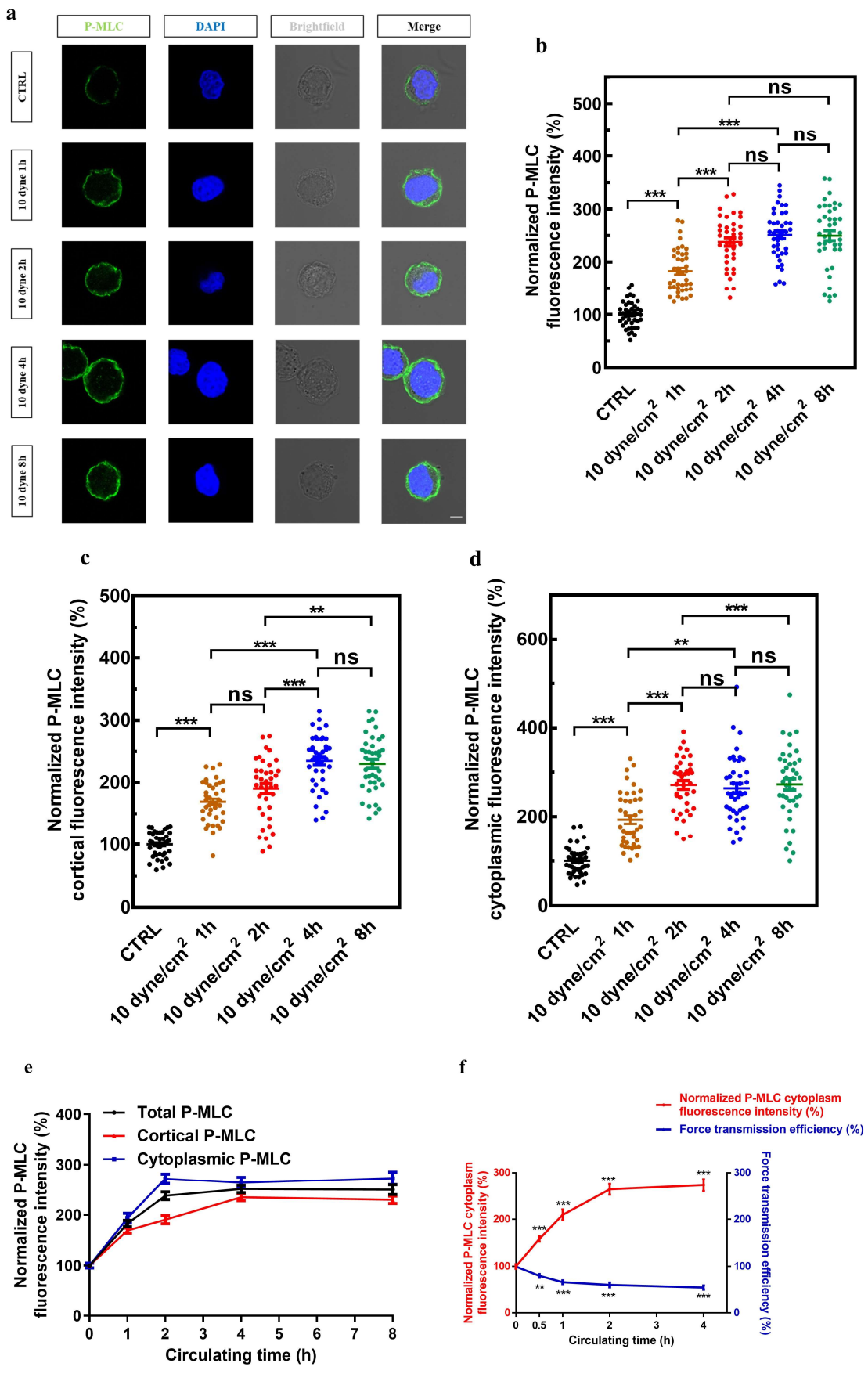
a
P-MLC
DAPI
Brightfield
Merge
CTRL
10 dyne 1h
10 dyne 2h
10 dyne 4h
10 dyne 8h
b
Normalized P-MLC fluorescence intensity (%)
ns
***
**
CTRL
10 dyne/cm2 1h
10 dyne/cm2 2h
10 dyne/cm2 4h
10 dyne/cm2 8h
c
Normalized P-MLC cortical fluorescence intensity (%)
d
Normalized P-MLC cytoplasmic fluorescence intensity (%)
e
Total P-MLC
Cortical P-MLC
Cytoplasmic P-MLC
Normalized P-MLC fluorescence intensity (%)
Circulating time (h)
f
Normalized P-MLC cytoplasm fluorescence intensity (%)
Force transmission efficiency (%)
Normalized P-MLC cytoplasm fluorescence intensity (%)
Force transmission efficiency (%)
Circulating time (h)

Figure 4-4 Correlation between cytoplasmic P-MLC and FTE under high FSS. (a-b) Representative immunofluorescence images **(a)** and quantitative data of P-MLC intensity **(b)** after one to four hours 10 dyne/cm^2 FSS. **(c-d)** Normalized cortical **(c)** and cytoplasmic **(d)** fluorescence intensity after one to four hours 10 dyne/cm^2 FSS. **(e)** Summary of myosin II distribution under10 dyne/cm^2 FSS within four hours. **(f)** Relationship between FTE and cytoplasmic P-MLC under 10 dyne/cm^2 FSS treatment within four hours. Scale bar=5 μm; N = 3 independent experiments; mean ± SEM; *, p <0.05; **, p < 0.01; and ***, p < 0.001

4.3 Cytoplasmic, but not cortical P-MLC regulates FTE

Next, we determined whether there was causal relationship between P-MLC subcellular localization and FTE. Herein, we changed myosin II subcellular distribution instead of its total activity. Previous study suggests that 4-HAP could redistribute myosin II [260], we thus used 4-HAP to treat SBTCs with or without shear stress. Our results demonstrated that without shear stress, 4-HAP treatment enhanced myosin II activity mainly in the cell cortex. Strikingly, under uniform FSS, 4-HAP redistributed cytoplasmic P-MLC to the cortex, while keeping total P-MLC the same (Figure 4-5 a-d). The P-MLC relocalizaion after uniform FSS with 4-HAP treatment was more obvious when comparing the P-MLC cortex/cytoplasm ratio (Figure 4-5 e). The enhanced ratio indicated the relocalizaion of P-MLC from cytoplasm to the cortex. In view of this, we further quantified the FTE after the uniform FSS with 4-HAP. The results showed that 4-HAP treatment restored FTE under high uniform FSS, including both 2 dyne/cm^2 and 4 dyne/cm^2 (Figure 4-5 f-h). Considering the effect of 4-HAP on myosin II subcellular localization under high uniform FSS, these results suggested that there was a causal relationship between myosin II subcellular localization and FTE.

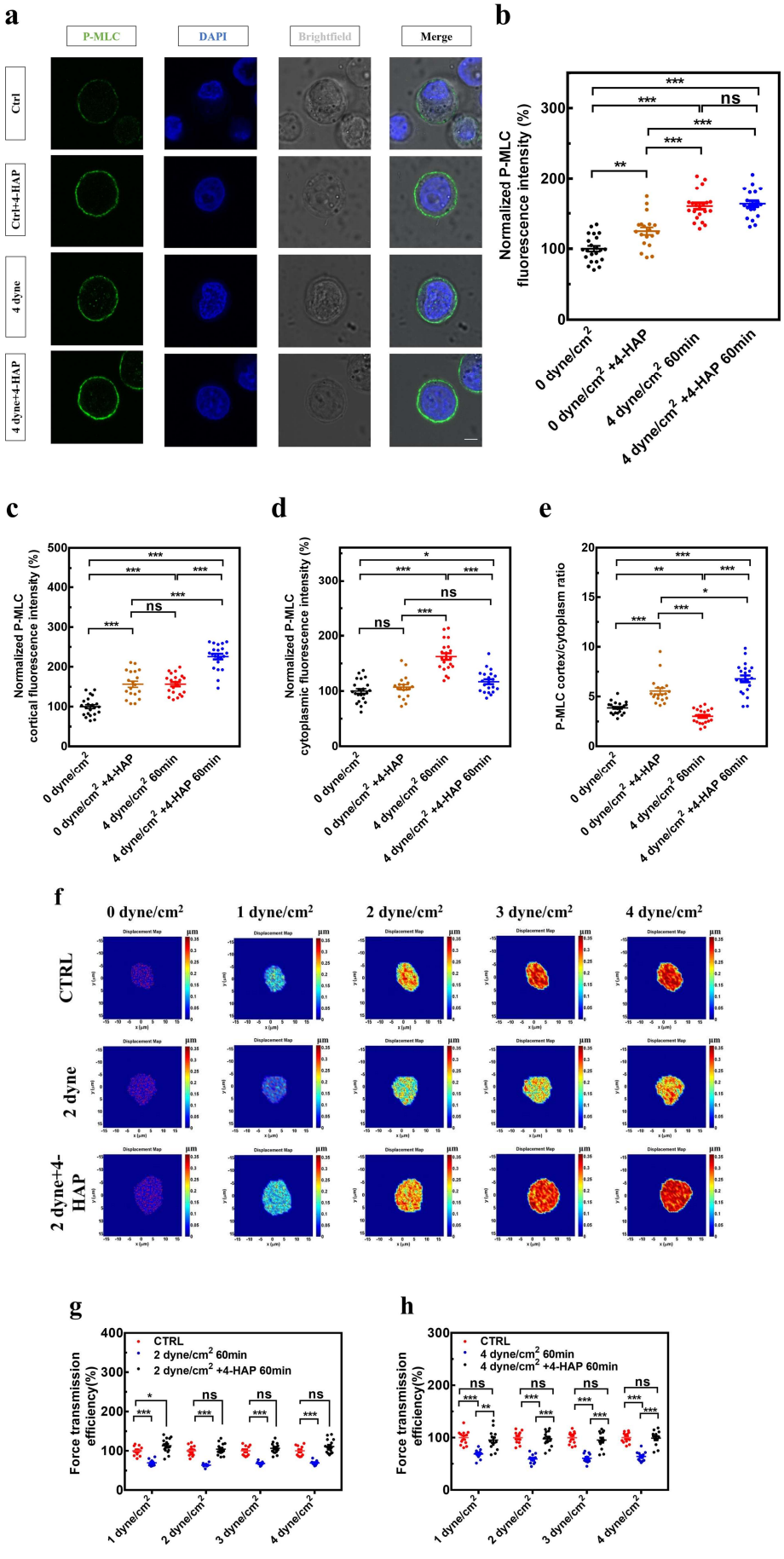
a
P-MLC
DAPI
Brightfield
Merge
Ctrl
Ctrl+4-HAP
4 dyne
4 dyne+4-HAP
b
Normalized P-MLC fluorescence intensity (%)
0 dyne/cm2
0 dyne/cm2 +4-HAP
4 dyne/cm2 60min
4 dyne/cm2 +4-HAP 60min
c
Normalized P-MLC cortical fluorescence intensity (%)
d
Normalized P-MLC cytoplasmic fluorescence intensity (%)
e
P-MLC cortex/cytoplasm ratio
f
0 dyne/cm2
1 dyne/cm2
2 dyne/cm2
3 dyne/cm2
4 dyne/cm2
CTRL
2 dyne
2 dyne+4-HAP
g
Force transmission efficiency(%)
CTRL
2 dyne/cm2 60min
2 dyne/cm2 +4-HAP 60min
h
Force transmission efficiency(%)
CTRL
4 dyne/cm2 60min
4 dyne/cm2 +4-HAP 60min

Figure 4-5 FTE is determined by P-MLC subcellular localization. (a-d) Representative immunofluorescence images **(a)** and quantitative data of P-MLC total **(b)**, cortical **(c)** and cytoplasmic **(d)** fluorescence intensity after an hour 4 dyne/cm^2 uniform FSS with or without 4-HAP treatment. **(e)** P-MLC cortex/cytoplasm ratio after an hour 4 dyne/cm^2 uniform FSS with or without 4-HAP treatment. **(f)** Representative H2B displacement maps after one hour 2 dyne/cm^2 uniform FSS with or without 4-HAP treatment. **(g-h)** FTE after one hour 2 dyne/cm^2 uniform FSS (**g**) or 4 dyne/cm^2 uniform FSS (**h**) treatment with 4-HAP. Scale bar=5 μm; N = 3 independent experiments; mean ± SEM; *, p <0.05; **, p < 0.01; and ***, p < 0.001

Then, we wanted to further determine cortical or cytoplasmic P-MLC, which one contributed to the deceased FTE under high uniform FSS. To do that, we treated SBTCs with Bleb, a myosin II specific ATPase inhibitor, to downregulate myosin II activity[261]. We first tested the inhibitory effects of Bleb on STBCs under static status (that is, no shear stress pre-treatment). In the absence of uniform FSS, Bleb treatment inhibited myosin II activity both in cortex and cytoplasm. To our surprise, in the presence of uniform FSS, Bleb treatment decreased myosin II activity mainly in the cell cortex, while had little inhibitory effect in cytoplasmic myosin II activity (Figure 4-6 a-e). According to this, we further specifically modulate cortical myosin II activity and measured FTE under uniform FSS by Bleb. As it was shown in Figure 4-6 f, Bleb treatment failed to restore FTE under high uniform FSS, suggesting cortical myosin II activity was dispensable to FTE of SBTCs under high uniform FSS.

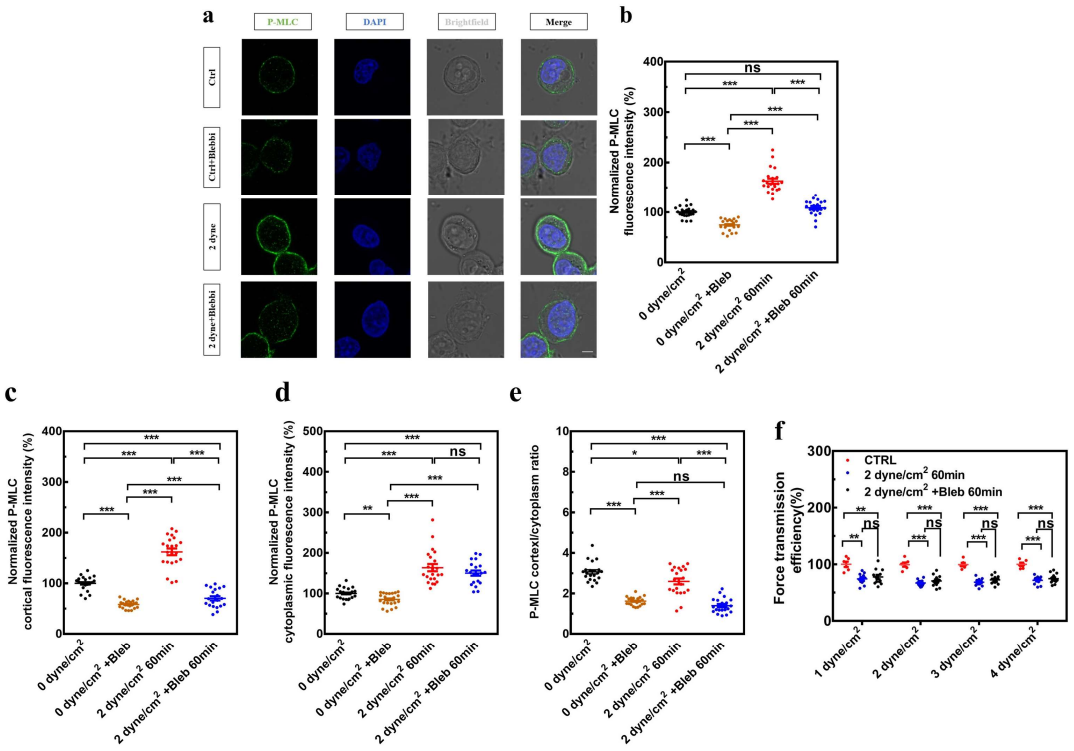

Figure 4-6 Cortical myosin II activity is dispensable for FTE in SBTCs. (a-d) Representative immunofluorescence images **(a)** and quantitative data of P-MLC total **(b)**, cortical **(c)** and cytoplasmic **(d)** fluorescence intensity after an hour 2 dyne/cm^2 uniform FSS in the presence or absence of Bleb. **(e)** P-MLC cortex/cytoplasm ratio after an hour 2 dyne/cm^2 uniform FSS in the presence or absence of Bleb. **(f)** FTE after an hour 2 dyne/cm^2 uniform FSS treatment in the presence or absence of Bleb. Scale bar=5 μm; N = 3 independent experiments; mean ± SEM; *, p <0.05; **, p < 0.01; and ***, p < 0.001

In view of 4-HAP rescued FTE under uniform FSS while Bleb failed to do so, we therefore speculated that cytoplasmic myosin II activity was the determinate factor that regulated FTE under high uniform FSS. To test this hypothesis, we treated SBTCs with Y27, a selective Rho kinase inhibitor to decrease myosin II activity through RhoA/ROCK pathway[262]. Intriguingly, 20 μM and ten minutes Y27 treatment after shear stress specifically inhibited cytoplasmic P-MLC of SBTCs while had little effect on cortical P-MLC. This conclusion was valid by Figure 4-7 a-e.

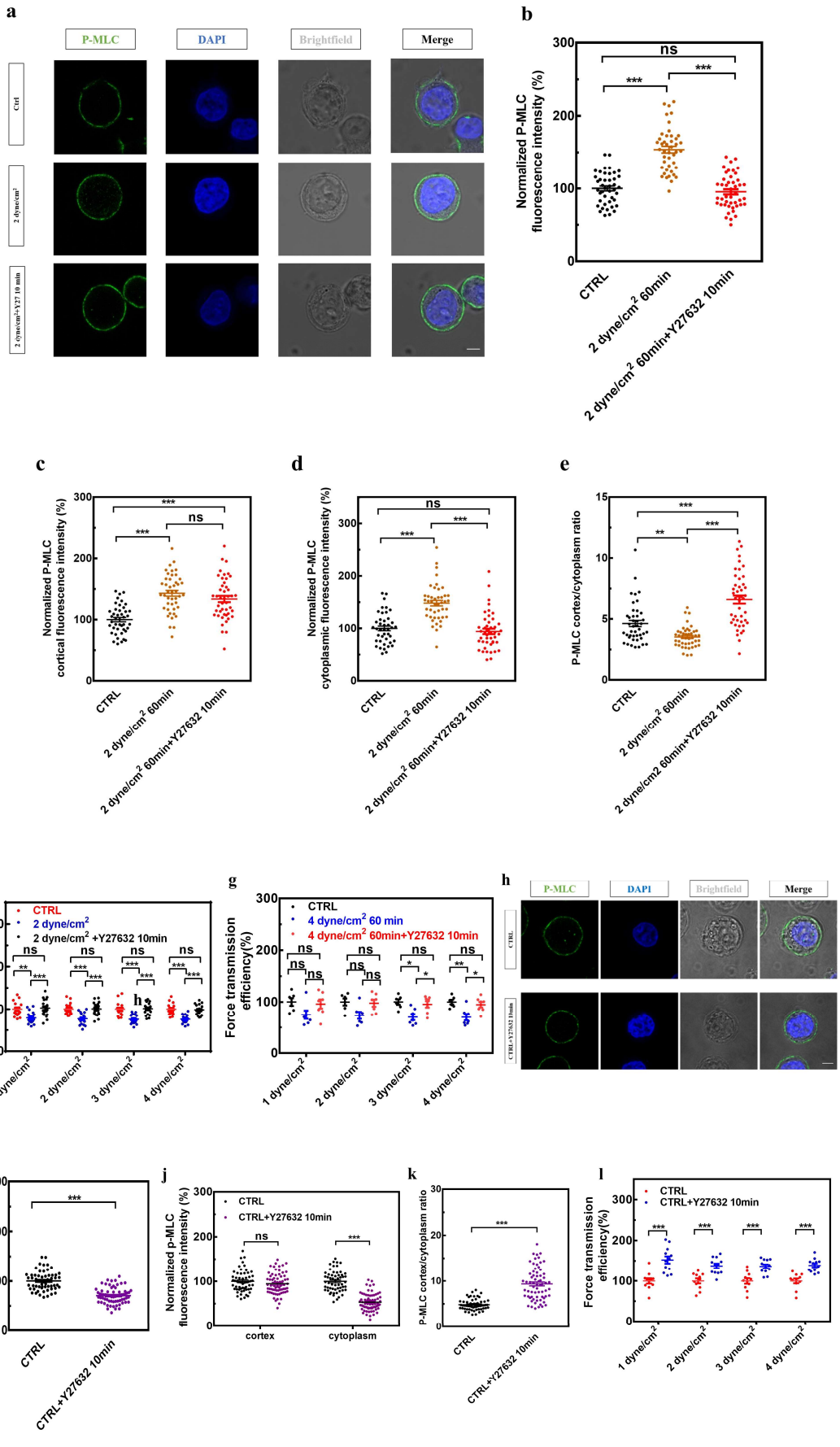
a
P-MLC
DAPI
Brightfield
Merge
Ctrl
2 dyne/cm²
2 dyne/cm²+Y27 10 min
b
Normalized P-MLC fluorescence intensity (%)
ns
***
CTRL
2 dyne/cm² 60min
2 dyne/cm² 60min+Y27632 10min
c
Normalized P-MLC cortical fluorescence intensity (%)
d
Normalized P-MLC cytoplasmic fluorescence intensity (%)
e
P-MLC cortex/cytoplasm ratio
**
2 dyne/cm2 60min+Y27632 10min
f
Force transmission efficiency(%)
CTRL
2 dyne/cm²
2 dyne/cm² +Y27632 10min
1 dyne/cm²
2 dyne/cm²
3 dyne/cm²
4 dyne/cm²
g
4 dyne/cm² 60 min
4 dyne/cm² 60min+Y27632 10min
h
CTRL+Y27632 1hrs
i
Normalized p-MLC fluorescence intensity (%)
CTRL+Y27632 10min
j
cortex
cytoplasm
k
l

Figure 4-7 Cytoplasmic myosin II activity determines FTE in SBTCs. (a-d) Representative immunofluorescence images **(a)** and quantitative data of P-MLC total **(b)**, cortical **(c)** and cytoplasmic **(d)** fluorescence intensity after short-term Y27 treatment following 2 dyne/cm^2 uniform FSS. **(e)** P-MLC cortex/cytoplasm ratio after short-term Y27 treatment following 2 dyne/cm^2 uniform FSS. **(f-g)** FTE after short-term Y27 treatment following 2 dyne/cm^2 **(f)** and 4 dyne /cm^2 **(g)** high uniform FSS. **(h-i)** Representative immunofluorescence images **(h)** and quantitative data of P-MLC total **(i)**, cortical and cytoplasmic **(j)** fluorescence intensity after short-term Y27 treatment in SBTCs without shear stress pretreatment. **(k)** P-MLC cortex/cytoplasm ratio after short-term Y27 treatment in SBTCs without shear stress pretreatment. **(l)** FTE after short-term Y27 treatment. Scale bar=5 μm; N = 3 independent experiments; mean ± SEM; *, p <0.05; **, p < 0.01; and ***, p < 0.001

Based on this finding, we used Y27 to determine whether targeting cytoplasmic myosin II activity could rescue FTE under high uniform FSS. After high uniform FSS, we treated SBTCs with 20 μM Y27 for ten minutes and quantified the FTE as soon as possible. As it can be seen in Figure 4-7 f-g, FTE under both 2 dyne/cm^2 and 4 dyne/cm^2 high uniform FSS were fully restored by Y27 in short time. To further confirm the role of cytoplasmic myosin II activity, we treated SBTCs with short-term Y27 without shear stress pretreatment. Consistently, 10 minutes Y27 treatment specifically regulated myosin II cytoplasmic localization, while leaving myosin II cortical activity almost the same (Figure 4-7 h-k). The P-MLC cortical/cytoplasmic ratio thus increased. Strikingly, FTE was substantially raised up to about 150 % after short-term Y27 treatment (Figure 4-7 l). Given that cortical myosin II activity was dispensable for the FTE (Figure 4-6), our results collectively suggested that cytoplasmic myosin II activity, but not cortical, was necessary to regulate FTE under high uniform FSS.

To make the usage of Y27 more clinically relevant, we further analyzed long-term effects of Y27 treatment during high uniform FSS application. Noted that when Y27 was added to SBTCs during high uniform FSS, although Y27 decreased total myosin II activity in dose-dependent manner, high concentration (20 μM) of Y27, but not low (2 μM), diminished cytoplasmic myosin II activity (Figure 4-8 a-d), suggesting different

concentrations of Y27 played distinct roles in SBTCs under high uniform FSS. Strikingly, 20 μM of Y27 treatment during high uniform FSS application diminished both cortical and cytoplasmic myosin II activity (Figure 4-8 e-h). Consistent with previous result, cytoplasmic myosin II inhibition enhanced FTE of SBTCs under high uniform FSS, even to the level higher than no shear stress pretreatment (Figure 4-8 i).

In short summary, cytoplasmic myosin II localization, instead of cortical myosin II activity, negatively regulated FTE of SBTCs under FSS.

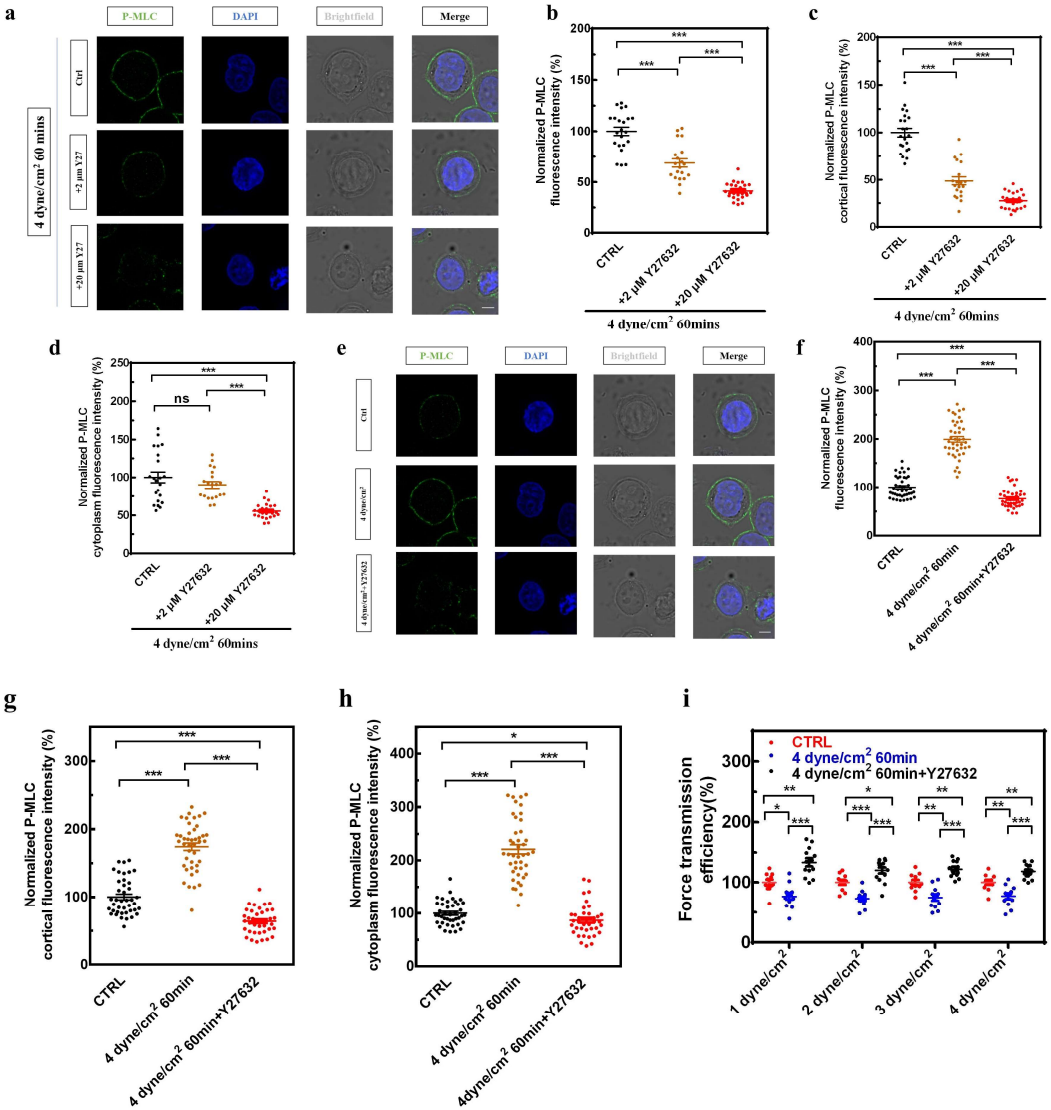

Figure 4-8 Myosin II activity and FTE after long-term Y27 treatment under high uniform FSS. **(a-d)** Representative immunofluorescence images **(a)** and quantitative data of P-MLC total **(b)**, cortical **(c)** and cytoplasmic **(d)** fluorescence intensity with long-term, different concentrations of Y27 treatment under high uniform FSS. **(e-h)** Representative immunofluorescence images **(e)** and

quantitative data of P-MLC total **(f)**, cortical **(g)** and cytoplasmic **(h)** fluorescence intensity with 20 μM Y27 treatment in SBTCs after high uniform FSS for an hour. **(i)** FTE with 20 μM Y27 treatment in SBTCs after high uniform FSS for an hour. Scale bar=5 μm; N = 3 independent experiments; mean ± SEM; *, p <0.05; **, p < 0.01; and ***, p < 0.001

4.4 Specific modulation of myosin II activity influences FTE in SBTCs

Given that Y27 is a RhoA/ROCK inhibitor that not only act on myosin II [263], the inhibitory effects of Y27 on other proteins or signaling pathways may interfere our conclusion. Therefore, to solidify the role of myosin II in force transmission of SBTCs, we further interfered myosin II activity through siRNA. At first, we stained both myosin IIA and myosin IIB in SBTCs and found they all distributed in both cortex and cytoplasm (Figure 4-9 a). To keep the cell viability after knocking down myosin II, we knocked down Myosin IIB which was encoded by *MYH10*. Both sets of immunofluorescence and quantitative RT-PCR data suggested that si*MYH10*-2 had the best knockdown efficiency (Figure 4-9 b-f). We thus used si*MYH10* sequence 2 to knockdown myosin IIB and further quantified FTE in SBTCs.

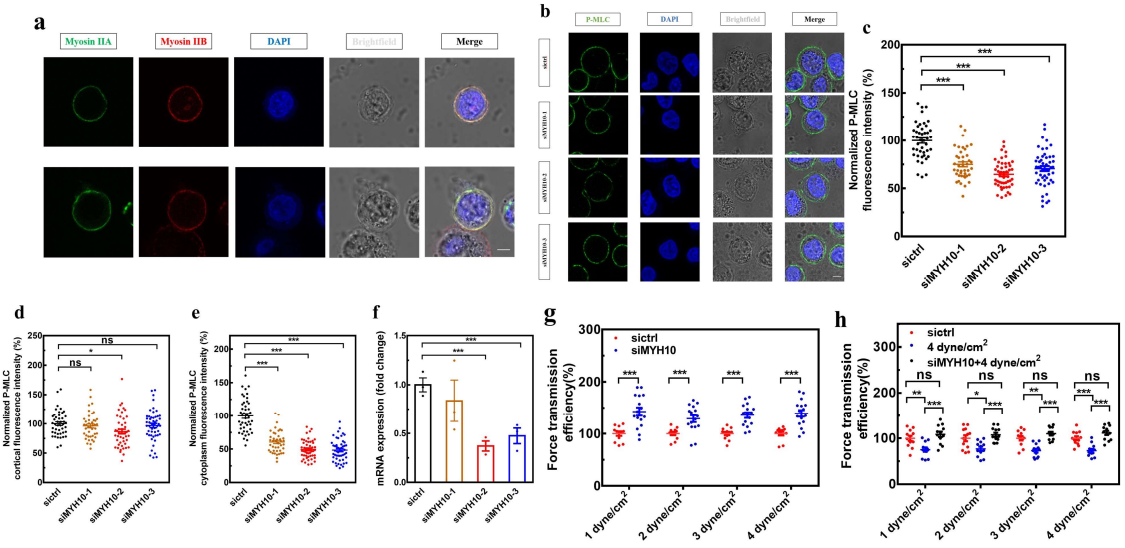

Figure 4-9 Specifically interfering myosin II activity through siRNA elevates FTE. (a) Immunofluorescence images of myosin IIA (green) and myosin IIB (red) in two SBTCs **(b-e)** Representative immunofluorescence images **(b)** and quantitative data of P-MLC total **(c)**, cortical **(d)** and cytoplasmic **(e)** fluorescence intensity after knockdown *MYH10* **(f)** RT-PCR results of

knockdown efficiency of *MYH10*. **(g)** FTE of SBTCs after knocking down *MYH10* without FSS. **(h)** FTE of STBCs after knocking down *MYH10* under 4 dyne/cm^2 uniform FSS. Scale bar=5 μm; N = 3 independent experiments; mean ± SEM; *, p <0.05; **, p < 0.01; and ***, p < 0.001

The results showed that knocking down *MYH10* substantially enhanced FTE of SBTCs without uniform FSS pretreatment (Figure 4-9 g), indicating myosin II activity decreased FTE in SBTCs. To further validated this conclusion, we first knocked down *MYH10* gene in SBTCs and then applied high uniform FSS. Similar with Y27 treatment (Figure 4-8 i), knocking down *MYH10* rescued high uniform FSS induced decreased FTE (Figure 4-9 h). All the results showed above suggested that myosin II activity in cell cytoplasm reduced FTE of SBTCs.

4.5 Cytoplasmic myosin II activity is sufficient to decrease FTE

So far, we revealed that myosin II cytoplasmic inhibition restored decreased FTE in SBTCs under high shear stress, indicating cytoplasmic myosin II activity was necessary for SBTCs to decline FTE. However, whether increased myosin II activity was sufficient to decrease FTE in SBTCs was still unclear. To answer this question, we used calyculin A to activate myosin II through MLCP inhibition[264]. Indeed, 20 nM calyculin A treated for thirty minutes significantly increased myosin II activity (Figure 4-10 a-b). To our surprise, while myosin II activity substantially enhanced in cytoplasm after calyculin treatment, cortical myosin II activity remained nearly the same and SBTCs exhibited significantly decreased P-MLC cortical/cytoplasmic ratio, indicating calyculin A predominantly activated cytoplasmic myosin II in SBTCs (Figure 4-10 c-d). Further, we quantified FTE after calyculin A treatment. The data showed in Figure 4-10 e demonstrated that after calyculin A treatment, FTE was substantially dropped in SBTCs without shear stress treatment. These data suggested that myosin II cytoplasmic activation was sufficient to decrease FTE in SBTCs. In light of the above saying, cytoplasmic myosin II activity was both necessary and sufficient to decrease FTE of SBTCs under high uniform FSS.

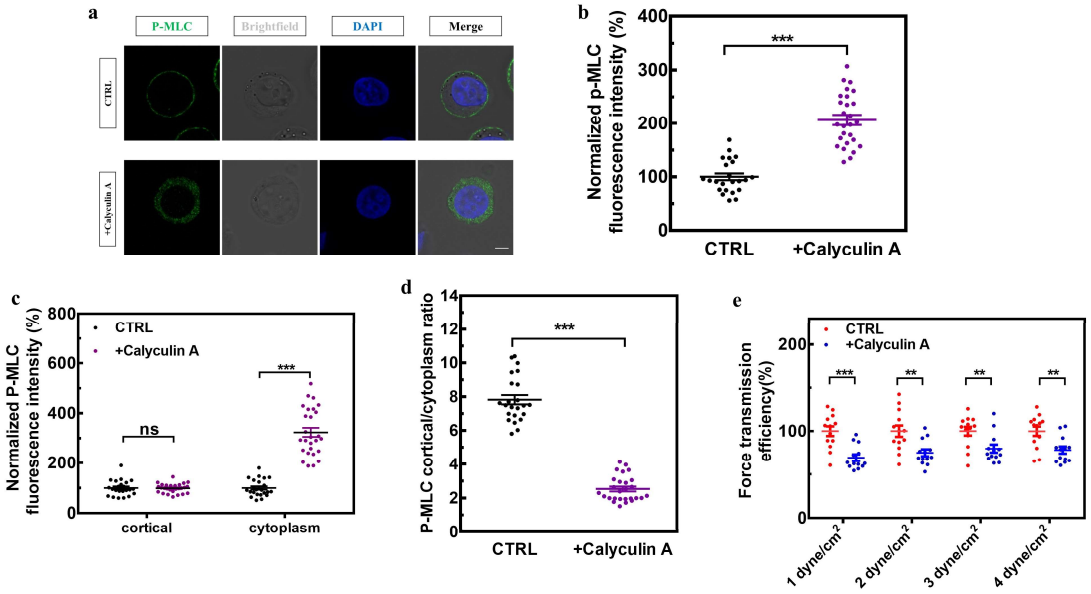

Figure 4-10 Myosin II cytoplasmic activity is sufficient to regulates FTE of SBTCs. (a-d) Representative immunofluorescence images **(a)** and quantitative data of P-MLC total **(b)**, cortical and cytoplasmic **(c)** fluorescence intensity after calyculin A treatment. **(d)** P-MLC cortical/cytoplasm ratio after calyculin A treatment **(e)** FTE after calyculin A treatment. Scale bar=5 μm; N = 3 independent experiments; mean ± SEM; *, p <0.05; **, p < 0.01; and ***, p < 0.001

4.6 Interfering myosin II activity diminishes force transmission into nucleus

We previously revealed that cytoplasmic myosin II activity decreased FTE in SBTCs. However, as FTE was calculated through H2B displacement and the nuclear strain was determined by both force and nuclear stiffness, one may be concerned that the decreased or increased FTE through myosin II modulation were through the variation in nuclear stiffness but not the force transmitted to cell nucleus. To verified that the change in FTE induced by myosin II inhibition definitely induce different force transmitted to cell nucleus, we used the strength of Nesprin-based tension sensor to directly measure the force across the LINC complex[122]. This Nesprin-based tension sensor had been shown that it can respond to cytoskeletal prestress generated by actomyosin and external mechanical stimuli such as biaxial strain[247]. Consistently, we found that inhibition of myosin II ATPase activity through Bleb increased FRET index of Nesprin-based tension

sensor in adherent breast cancer cells, indicating attenuated tension within Nesprin-based tension sensor, providing a justification of this sensor (Figure 4-11 a-b). Furthermore, we measured the FRET index of Nesprin-based tension sensor under different levels of uniform FSS treatment (see Materials and Methods). The results in Figure 4-11 c demonstrated that the tension within Nesprin-based tension sensor was increased under shear stress. More importantly, when comparing FRET index under different levels of shear stress, we found larger shear stress applied on cell surface elicited lower FRET index, indicating higher force transmitted to LINC complex. Thus, Nesprin-based tension sensor correctly reflected the tension transmitted across cytoskeleton to LINC complex of SBTCs under shear stress.

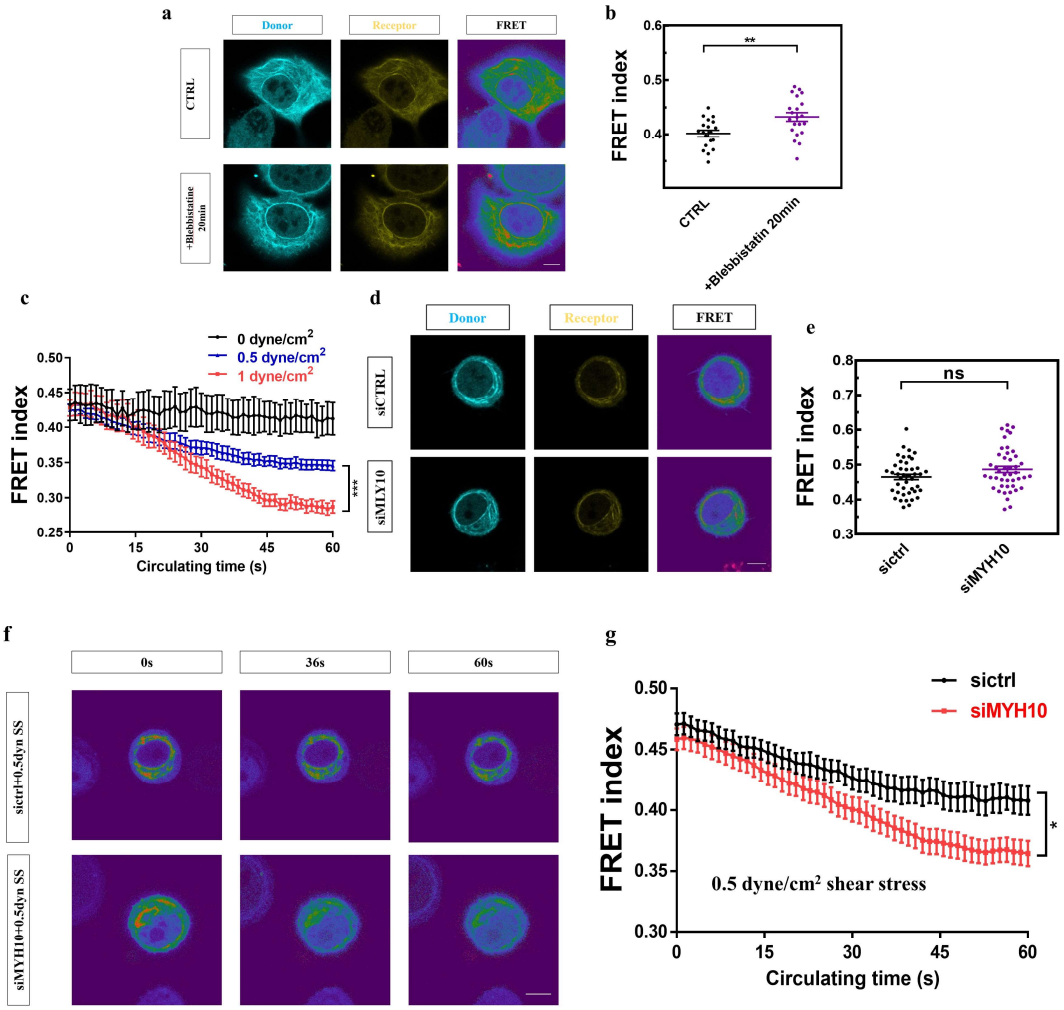

Figure 4-11 Measuring the shear force across cytoskeleton to LINC complex through Nesprin-based tension sensor. (a-b) Representative FRET images **(a)** and FRET index **(b)** after bleb treatment in adherent breast cancer cell. **(c)** FRET index under 0, 0.5 and 1 dyne/cm^2 uniform FSS. **(d-e)** Representative FRET images **(d)** and FRET index **(e)** of SBTCs after knockdown *MYH10*. **(f-g)** Representative FRET images **(f)** and FRET index **(g)** of SBTCs under 0.5 dyne/cm^2 uniform FSS. Scale bar=5 μm; N = 4 independent experiments; mean ± SEM; *, p <0.05; **, p < 0.01; and ***, p < 0.001

Based on this, we wanted to further explore the role of myosin II activity in shear force transmitted to LINC complex through Nesprin-based tension sensor. At first, we compared FRET index between si*ctrl* and si*MYH10* in SBTCs without shear stress pretreatment. Unlike adherent cells in which myosin II activity regulates tension across LINC complex[122, 247], SBTCs exhibited almost same FRET index after *MYH10* knockdown (Figure 4-11 d-e), indicating myosin IIB activity was dispensable for tension between cytoskeleton and LINC complex in suspended cells. Intriguingly, when we measured FRET index during shear stress application, we saw that for *MYH10* knockdown group, the FRET index decreased more sharply and quickly. As a result, after 60 seconds shear stress application, the FRET index was smaller in *MYH10* knockdown group than CTRL group (Figure 4-11 f-g). As FRET index inversely correlates with its tension, this result indicated that even though the shear force applied on cell surface was the same, knockdown *MYH10*, or inhibits myosin II activity, increased the force transmission across cytoskeleton to LINC complex in SBTCs.

In summary, our results indicated that myosin II activity reduced force transmission across cytoskeleton to cell nucleus in SBTCs.

Chapter 5. Targeting cytoplasmic myosin II promotes shear-induced DNA damage and cell apoptosis

5.1 Decreased FTE enhances SBTCs' survival under shear stress *in vitro*

We revealed that cytoplasmic P-MLC was indispensable for decreased FTE under high uniform FSS. Nevertheless, the biological functions of decreased FTE under high uniform FSS were still elusive. As the FTE determined how much proportion of shear stress was transmitted to the cell nucleus as well as nuclear deformation elicited by shear stress, we therefore focused on the evens in the cell nucleus.

Given that high nuclear deformation could trigger DNA damage because of mechanical distortions[68, 144, 215], we therefore determined whether decreased FTE protected SBTCs from DNA damage under high shear stress. We first tested whether treatment of 4-HAP, which redistributed cytoplasmic myosin II into cell cortex and rescued FTE (Figure 4-5 a-h), could elevate DNA damage under shear stress. As it was shown in Figure 5-1 a-b, shear stress applied to SBTCs for an hour induced more DNA damage represented by γ-H2AX positive cells/total compared with static control, indicating force transmitted to cell nucleus indeed triggered mechanical distortions and DNA damage as the consequence. More importantly, whereas 4-HAP treatment itself did not trigger DNA damage, 4-HAP treatment combined with 2 dyne/cm^2 uniform FSS enhanced DNA damage (Figure 5-1 a-b). This result strongly suggested that, while same external force was applied on the cell surface, enhanced FTE induced more force transmitted across cell cytoskeleton to nucleus and elicited more mechanical distortions, finally resulted in more DNA damage in cell nucleus.

To exclude the possibility that 4-HAP could activate other signaling pathways that may induce DNA damage under shear stress, we repeated similar experiments under Y27 treatment. Consistently, 20 μM Y27, which inhibited cytoplasmic myosin II activity and increased FTE (Figure 4-8 e-i), triggered more DNA damage under high shear stress,

whereas Y27 treatment itself did not trigger more DNA damage (Figure 5-1 a-b). As accumulated DNA damage may induce cell apoptosis[265], we therefore speculated that SBTCs mechanically adapted to high uniform FSS through decreased FTE, which influenced their survival under shear stress. To test this idea, we attached SBTCs to PLL coated microfluidic chip and treated the cells with 20 μM Y27 during high uniform FSS application. As some of SBTCs may not form stable attachment with PLL coated microfluidic chip and shed from PLL, we first quantified cell viability through propidium Iodide (PI) staining in cell supernatant.

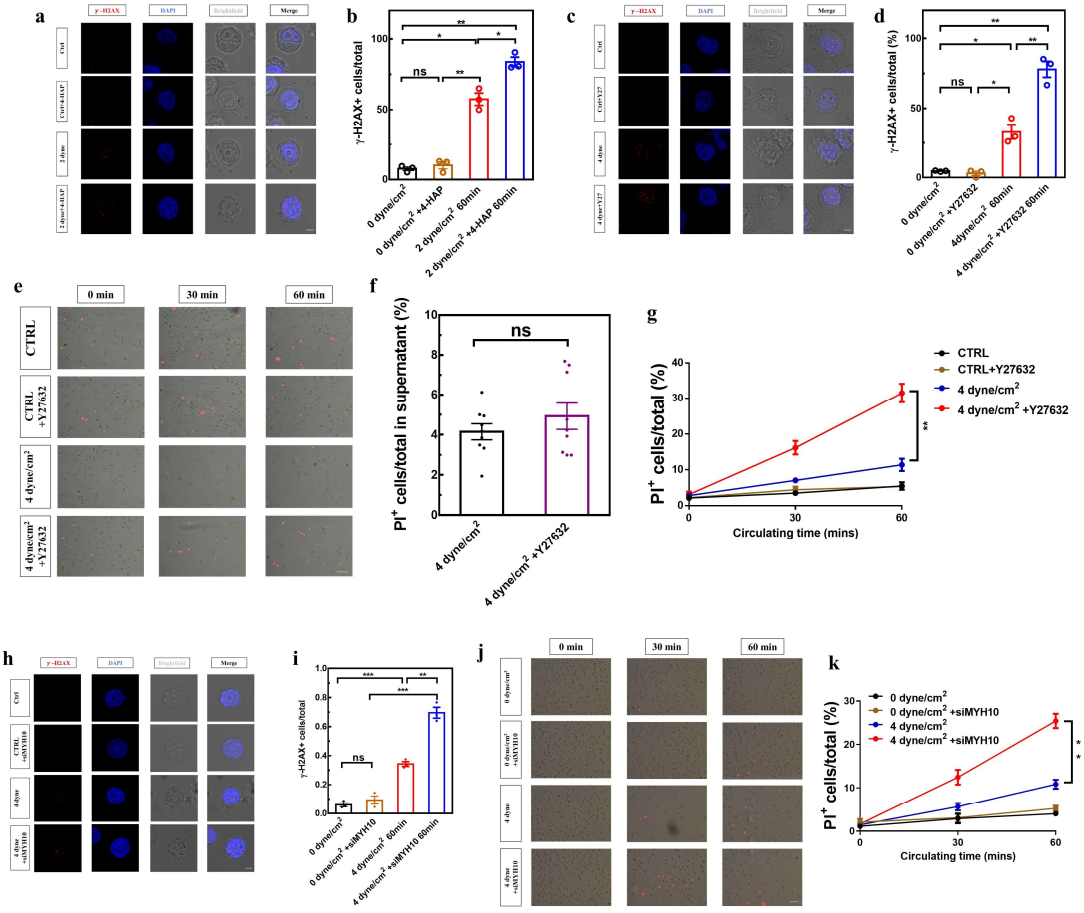

Figure 5-1 Targeting FTE through myosin II inhibition enhances DNA damage and cell apoptosis under uniform FSS. (a-b) Representative immunofluorescence images **(a)** and quantitative result **(b)** of γ-H2AX positive cells/total after 4-HAP treatment under 2 dyne/cm^2 uniform FSS. **(c-d)** Representative immunofluorescence images **(c)** and quantitative result **(d)** of γ-H2AX positive cells/total after 20 μM Y27 treatment under 4 dyne/cm^2 uniform FSS. **(e-g)** Representative images **(e)** and quantitative result of PI positive cell/total in supernatant **(f)** and still

attached to PLL coated microfluidic chip **(g)**. **(h-i)** Representative immunofluorescence images **(h)** and quantitative result **(i)** of γ-H2AX positive cells/total after knocking down *MYH10* under 4 dyne/cm^2 uniform FSS. **(j-k)** Representative images **(j)** and quantitative result **(k)** of PI positive cell/total after knocking down *MYH10* under 4 dyne/cm^2 uniform FSS. Scale bar=5 μm for **(a), (c), (h)**; 100 μm for **(e), (j).** N = 3 independent experiments; mean ± SEM; *, p <0.05; **, p < 0.01; and ***, p < 0.001

The results in Figure 5-1 e-f showed that SBTCs detached from PLL did not show difference in cell viability after Y27 treatment under shear stress, likely due to insufficient shear stress duration. In contrast, for these SBTCs that still attached to PLL, cell apoptosis significantly enhanced after an hour high uniform FSS under Y27 treatment, while Y27 itself did not impact cell viability (Figure 5-1 g). This result hinted that elevated FTE through myosin II cytoplasmic inhibition attenuated mechanoadaptation ability of SBTCs and enhanced cell apoptosis under high uniform FSS. To further corroborated this conclusion, we implemented siRNA to specifically interfered myosin II activity and quantified cell viability under high uniform FSS. Consistent with previous finding, knocking down *MYH10* in SBTCs substantially increased cell apoptosis after one-hour high uniform FSS application. All these aforementioned results suggested that inhibition of myosin II activity decreased mechanoadaptation ability of SBTCs toward high uniform FSS and increased SBTCs' apoptosis.

The experiments we performed above were based on PLL coated microfluidic chips which lack physiological relevance. To make the conclusions more relevant to physiological context where CTCs flowed in blood circulation and suffered from FSS, we conducted similar experiments in *in-vitro* circulatory pump system. At first, we treated the SBTCs with 20 μM Y27 and let them circulate under 30 dyne/cm^2 high FSS for four hours. The results from Figure 5-2 a-b showed that while high FSS could trigger DNA damage, increasing FTE through myosin II inhibition further enhanced DNA damage of SBTCs under high FSS. Moreover, Y27 treatment also increased cell apoptosis after high FSS treatment for 4 hours (Figure 5-2 c-d), similar with high

uniform FSS (Figure 5-1 e-f, j-k).

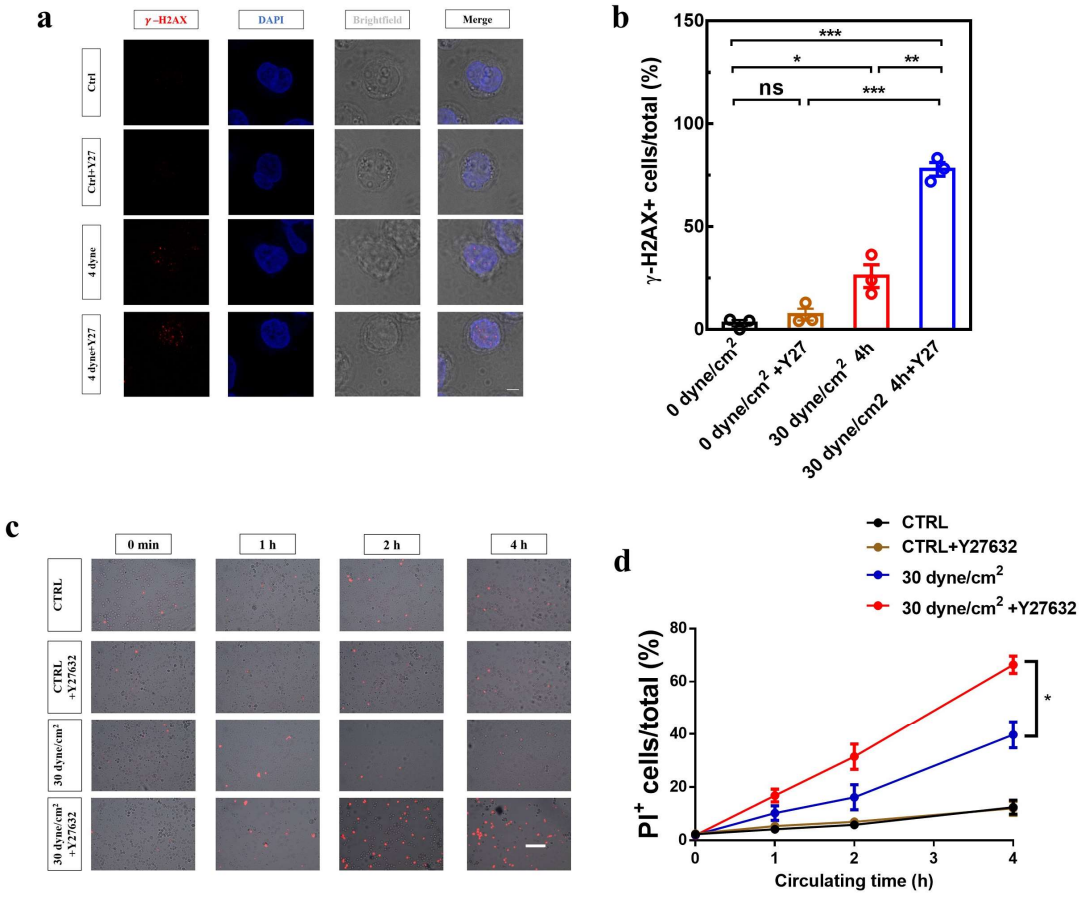

Figure 5-2 Targeting FTE through myosin II inhibition increases DNA damage and cell apoptosis under FSS. (a-b) Representative immunofluorescence images **(a)** and quantitative result **(b)** of γ-H2AX positive cells/total after 20 μM Y27 treatment under 30 dyne/cm^2 FSS for four hours. **(c-d)** Representative images **(c)** and quantitative result **(d)** of PI positive cell/total after 20 μM Y27 treatment under 30 dyne/cm^2 FSS for four hours. Scale bar=5 μm for **(a)** and 100 μm for **(c);** N = 3 independent experiments; mean ± SEM; *, p <0.05; **, p < 0.01; and ***, p < 0.001

All the data presented above suggested that SBTCs benefit from decreased FTE to avoid from accumulated DNA damage and enhance their survival under shear stress. Improving FTE through myosin II inhibition re-sensitizes SBTCs to shear force, elevates their DNA damage and decreases their survival under shear stress.

5.2 Targeting cytoplasmic myosin II-mediated mechanoadaptation decreases the survival of CTCs *in vivo*

To further study the therapeutically role of myosin II-mediated mechanoadaptation, we utilized *in vivo* mice model to test whether targeting myosin II activity in cytoplasm killed more SBTCs during blood circulation. To do so, we used the strength of pNLuc plasmid to detect cell apoptosis *in vivo*[251]. After pNLuc transfection, cell death triggers luciferase release that reacts with coelenterazine and emits bioluminescence. The bioluminescence emitted after cell death can last for more than 12 hours and can be further detected by Bioluminescence Imaging (BLI). Thus, pNLuc transfected cells can be used to estimate cell death.

We first tested the feasibility of pNLuc-based cell death measurement *in vitro*. We transfected MDA-MB-231 cells with pNLuc and seeded $5*10^4$, $1*10^5$ and $1.5*10^5$ cells per well, then used Triton X-100 to induce cell death. Further, we added 20 μM coelenterazine to each well of the plate with different number of cells. The results in Figure 5-3 a showed that the radiant efficient increased linearly with the number of dead cells, indicating that the bioluminescence signal can be utilized to represent cell death. Based on this, we further used pNLuc to measure cell apoptosis *in vivo*. MDA-MB-231 cells were treated with DMSO as negative control or 20 μM Y27632 to inhibit myosin II activity. Further, $1*10^6$ cells were injected. After 12 hours *in vivo* circulation, the whole blood of mice was collected and reacted with coelenterazine and the bioluminescence signal was detected. Our results showed that Y27632 treatment group exhibited significantly higher bioluminescence signal, suggesting that the inhibition of cytoplasmic myosin II activity increased CTCs apoptosis *in vivo* (Figure 5-3 b-d), consistent with our *in vitro* results (Figure 5-2).

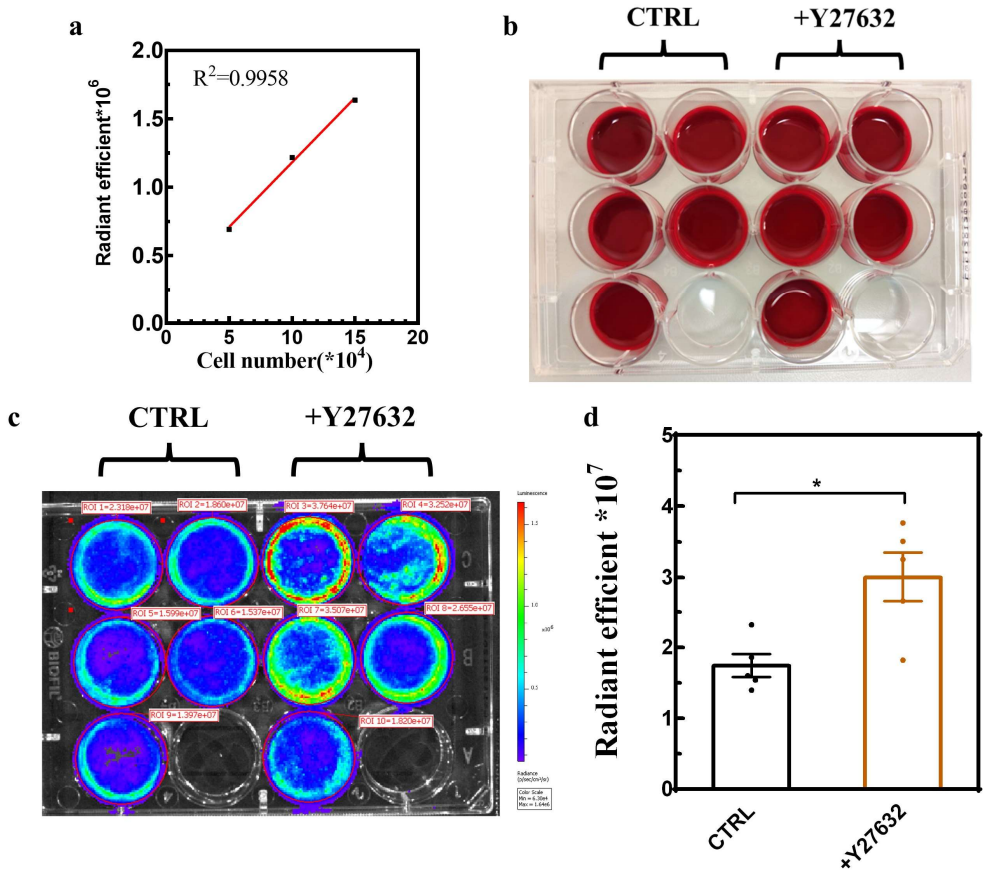

Figure 5-3 *In vivo* study of myosin II-mediated mechanoadaptation during blood circulation. **(a)** *In vitro* test of pNLuc transfected MDA-MB-231 cells with different cell number. **(b)** Whole blood collected from nude mice after injection. **(c)** Bioluminescence of mice blood from **(b)**. **(d)** Quantitative result of bioluminescence signal from **(c)**.

5.3 Low FTE of CSCs protects them from mechanical damage

Previous studies suggest that fibrin selected CSCs have higher metastatic potential and compacity to survive under shear force[56, 250, 266], while the underlying mechanisms are far from understood. We thus investigated whether and how CSCs benefit from myosin II-mediated mechanoadaptation under shear stress. To this end, we first compared myosin II activity between non selected CSCs (non-CSCs) and fibrin selected CSCs. Intriguingly, compared with non-CSCs, CSCs showed higher myosin II activation in both cortex and cell cytoplasm (Figure 5-4 a-d). Moreover, CSCs exhibited low FTE (~60%) as compared to non-CSCs (Figure 5-4 e), indicating when identical level of force was applied on CSCs' surface, the force transmitted across the cytoskeleton and

elicited nuclear deformation was relatively lower, which may render CSCs escape from shear force-induced cell damage.

To test this assumption, we treated CSCs with 20 μM Y27 for ten minutes and found that similar with SBTCs (Figure 4-7 i-l), short-term treatment of Y27 restored FTE in CSCs to same extent with non-CSCs (Figure 5-4 f), suggesting similar characteristic of cytoplasmic myosin II in regulating FTE in CSCs. Further, we treated CSCs and non-CSCs with same level of high uniform FSS for an hour on PLL coated chip and found that non-CSCs elevated DNA damage as just proved. Intriguingly, for CSCs, DNA damage remained nearly constant after high uniform FSS application for one hour (Figure 5-4 g-h), implying higher shear stress-resistance in CSC. To further investigated the role of myosin II-mediated FTE in CSCs during shear flow, we treated CSCs with 20 μM Y27 during high uniform FSS. The results clearly showed that while Y27 itself did not impact DNA damage, Y27 treatment combined with high uniform FSS significantly enhanced DNA damage of CSC (Figure 5-4 i-j). More importantly, while 30 dyne/cm^2 high FSS destroyed only a small population of CSCs, treatment of high dose Y27 to CSCs substantially increased CSCs' apoptosis after four hours circulation (Figure 5-4 k-l). These findings demonstrated that CSCs utilized low FTE to mechanically adapt to high FSS, as inhibition of myosin II activity re-sensitized CSCs to mechanical destructions under shear stress during circulation.

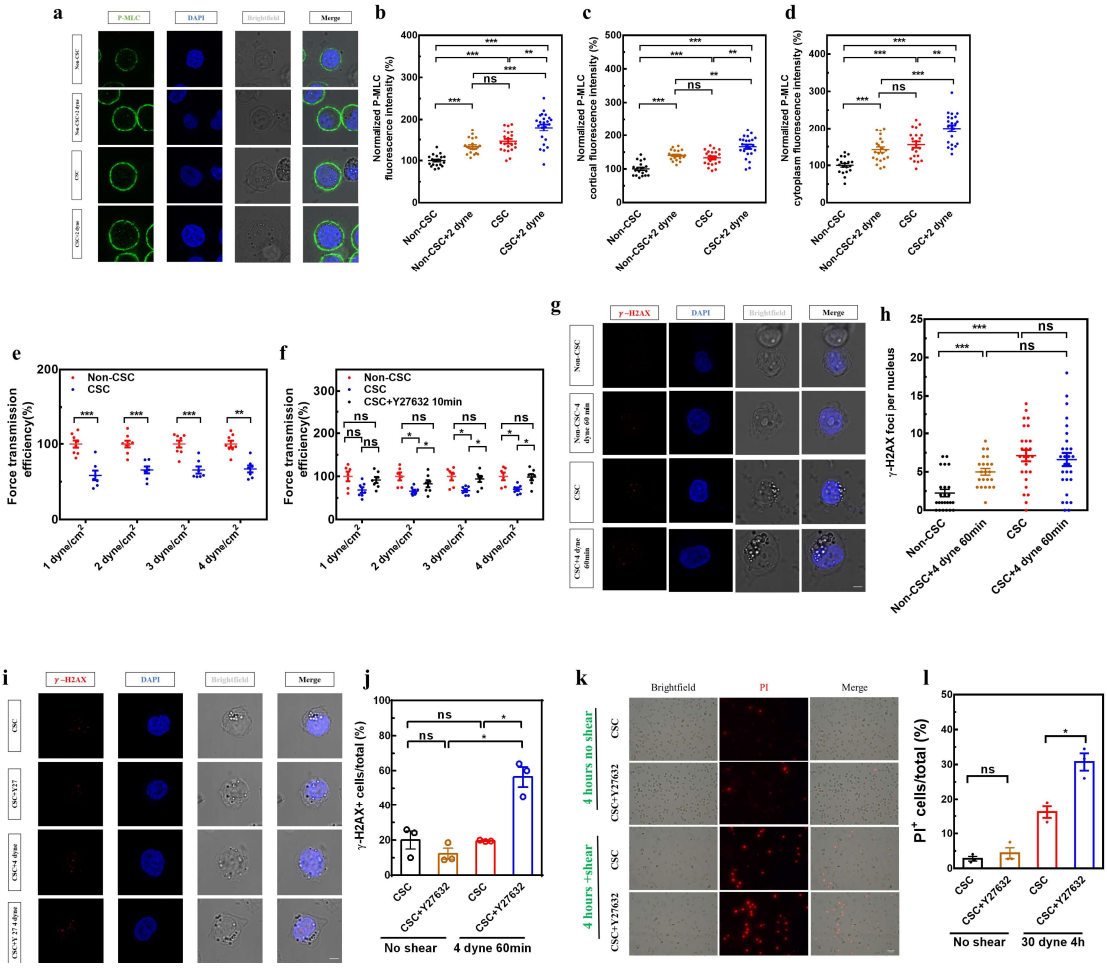

Figure 5-4 Targeting FTE re-sensitizes CSCs to mechanical destructions caused by shear stress. **(a-d)** Representative immunofluorescence images **(a)** and quantitative data of P-MLC total **(b)**, cortical **(c)** and cytoplasmic **(d)** fluorescence intensity in CSCs and non-CSCs. **(e)** FTE of CSCs compared with non-CSCs. **(f)** FTE of CSCs after short-term Y27 treatment. **(g-h)** Representative immunofluorescence images **(g)** and quantitative result **(h)** of γ-H2AX positive cells/total in CSCs and non-CSCs under high uniform FSS. **(i-j)** Representative immunofluorescence images **(i)** and quantitative result **(j)** of γ-H2AX positive cells/total in CSCs after 20 μM Y27 treatment under high uniform FSS. **(k-l)** Representative images **(k)** and quantitative data **(l)** of PI positive cell/total after 20 μM Y27 treatment in CSCs under high FSS. Scale bar=5 μm for **(a), (g), (i)** and 100 μm for **(k)**; N = 3 independent experiments; mean ± SEM; *, p <0.05; **, p < 0.01; and ***, p < 0.001

5.4 Low FTE of jurkat cells facilities their survival under FSS

To further explore the generality of myosin II-mediated FTE in mechanoadaptation of suspended cell toward shear flow, we focused on jurkat cells. Recent study reveals that leukemic cells, which had similar phenotype with blood cells, have higher resistance to fluid flow[54], while the mechanism that endowed leukemic cells this unique property is still elusive. To solve this problem, we investigated whether and how leukemic cells, jurkat cells in particular, benefit from cytoplasmic myosin II activity mediated FTE under shear stress.

Firstly, we compared myosin II activity between MCF-7 breast cancer cell line and jurkat E6.1 cell line. To our surprise, jurkat cells showed higher myosin II activity in cell cytoplasm (Figure 5-5 a-c) and exhibited lower (~65%) FTE (Figure 5-5 f). Similar with CSCs, inhibition of cytoplasmic myosin II activity through 20 μM Y27 restored FTE in jurkat cells to same level with SBTCs (Figure 5-5 d-f). Moreover, increasing mechanosensitivity through myosin II inhibition via 20 μM Y27 increased jurkat cells' apoptosis under 30 dyne/cm^2 high FSS (Figure 5-5 g-j). The comparable trends have been observed after 6 hours and 12 hours circulation. All these results suggested that jurkat cell also utilized high cytoplasmic myosin II activity to decrease FTE, thus afforded protection of cell nucleus and facilitated their survival under high FSS.

Based on the saying above, low FTE endowed by cytoplasmic myosin II activity protects SBTCs from accumulated DNA damage and facilitates their survival under high shear stress. Furthermore, CSCs and jurkat cells also benefit from their low FTE to help their survival during blood circulation.

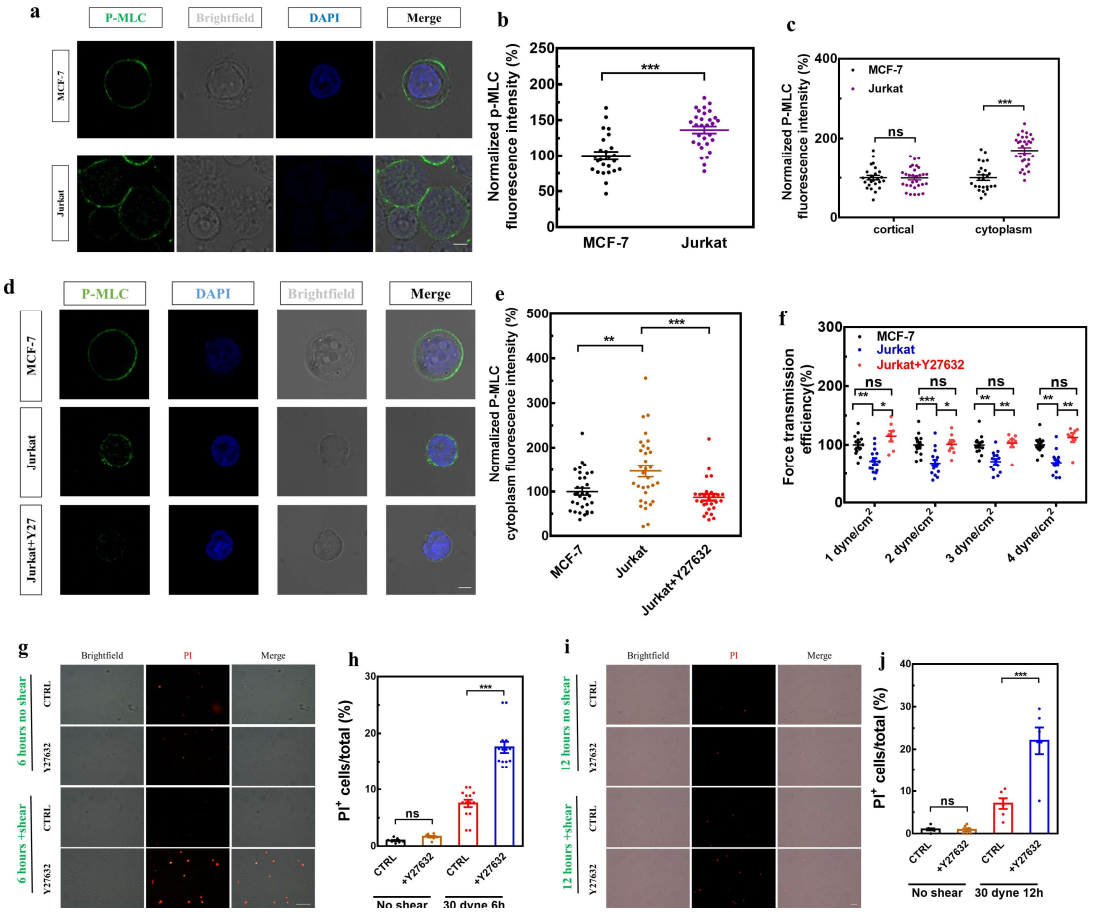

Figure 5-5 Targeting FTE re-sensitizes jurkat cells to mechanical destructions caused by shear stress. (a-c) Representative immunofluorescence images **(a)** and quantitative data of P-MLC total **(b)**, cortical and cytoplasmic **(c)** fluorescence intensity in MCF-7 and jurkat cells. **(d-e)** Representative immunofluorescence images **(d)** and quantitative result **(e)** of P-MLC fluorescence intensity after short-term Y27 treatment in MCF-7 and jurkat cells. **(f)** FTE of MCF-7 and jurkat cells after short-term Y27 treatment. **(g-h)** Representative images **(g)** and quantitative data **(h)** of PI positive cell/total after 20 μM Y27 treatment in jurkat cells under 30 dyne/cm^2 high FSS for six hours. **(i-j)** Representative images **(i)** and quantitative data **(j)** of PI positive cell/total after 20 μM Y27 treatment in jurkat cells under 30 dyne/cm^2 high FSS for twelve hours. Scale bar=5 μm for **(a), (d)** and 100 μm for **(g), (i)**; N = 3 independent experiments; mean ± SEM; *, p <0.05; **, p < 0.01; and ***, p < 0.001

5.5 DNA damage does not feedback to myosin II activity and FTE

Our previous results suggested that high shear stress triggered DNA damage. Improving FTE through myosin II cytoplasmic inhibition further enhanced DNA damage under shear stress. Recent studies disclose that DNA damage response could influence nuclear mechanics[267, 268]. To investigate whether DNA damage feedback to myosin II activity and FTE in SBTCs, we first used doxycycline (Dox) to induce DNA damage deliberately[269]. The results showed that 10 μg/ml Dox induction for 30 or 60 minutes substantially increased DNA damage of SBTCs, while Dox induction did not impact cell viability (Figure 5-6 a-d). Based on this, we further tested whether DNA damage feedback to myosin II activity and FTE in SBTCs. The results from Figure 5-6 e-h showed that DNA damage influenced neither myosin II activity nor FTE. As Dox treatment for both thirty minutes and sixty minutes showed consistent results, we thus concluded that DNA damage response of SBTCs did not feedback to myosin II activity or FTE under shear stress.

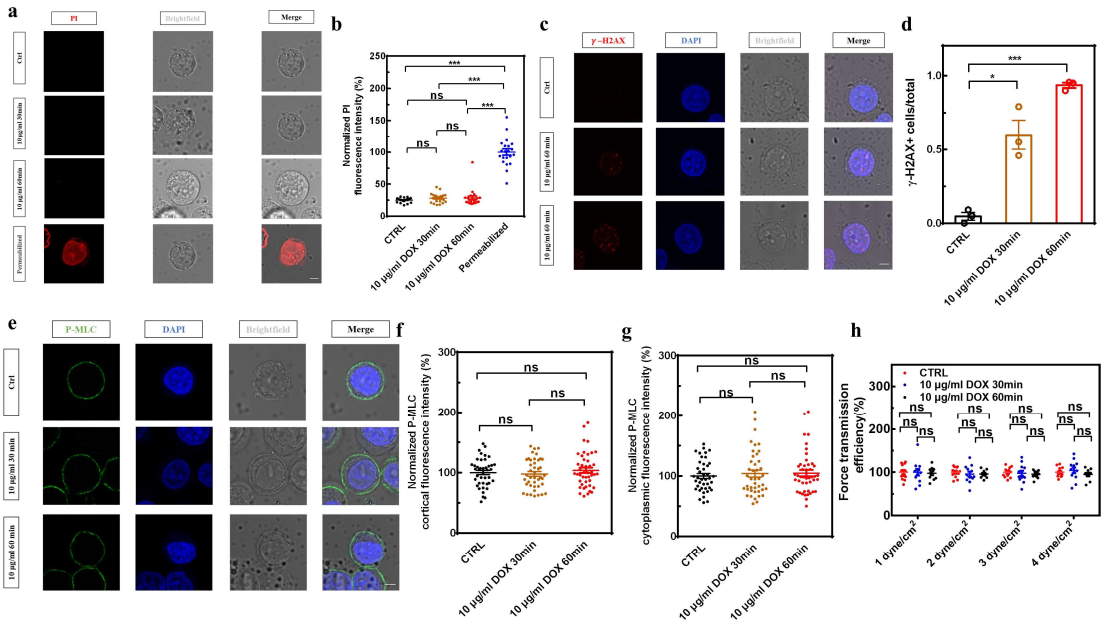

Figure 5-6 DNA damage does not feedback to myosin II activity and FTE. (a-b) Representative images **(a)** and quantitative data **(b)** of PI staining in SBTCs after Dox treatment. **(c-d)** Representative immunofluorescence images **(c)** and quantitative data **(d)** of γ-H2AX positive cells/total in SBTCs after Dox treatment. **(e-g)** Representative images **(e)** and quantitative data of

P-MLC cortical **(f)** and cytoplasmic **(g)** florescence intensity after Dox treatment in SBTCs. **(h)** FTE of SBTCs after Dox treatment. Scale bar=5 μm; N = 3 independent experiments; mean ± SEM; *, $p < 0.05$; **, $p < 0.01$; and ***, $p < 0.001$

Chapter 6. Nuclear mechanosensing orchestrates SBTCs' responses to shear stress

6.1 Lamin A/C and NE tension respond to shear stress prior to myosin II subcellular localization

Up to now, we have found that cytoplasmic myosin II localization reduces FTE of SBTCs under high shear stress, while the potential mechanism that initiating myosin II subcellular distribution was still unknown. Previous studies suggest that nuclear itself works as a mechanosensor that directly senses and responds to external mechanical stimuli[204, 207, 212]. Indeed, our group recently found nuclear expansion of suspended tumor cells under FSS, suggesting nucleus may play important roles in the mechano-responses of SBTCs to FSS[77]. We hereby explored the roles of nuclear mechanosensing in the perception of FSS for SBTCs. As nuclear mechanosensing strongly depended on the nucleoskeleton Lamin A/C, we thus investigated the influence of Lamin A/C on this mechanotransduction process[127, 270].

First, we quantified Lamin A/C protein expression under shear stress through immunofluorescence. The results disclosed that Lamin A/C in SBTCs gradually increased under uniform FSS in a force-dependent manner (Figure 6-1 a-b). Recent studies suggest that Lamin A/C serves as nucleoskeleton and contributes to NE tension[212, 271]. We thus tested whether Lamin A/C expression changed NE tension. Therefore, we utilized EOP_{NE} (see Materials and Methods) to represent NE tension and quantified it in SBTCs under shear stress[212]. Lower EOP_{NE} indicates less nuclear wrinkle and higher NE tension. Interestingly, after the treatment of 1 dyne/cm^2 uniform FSS for an hour, EOP_{NE} decreased, indicating increased NE tension. Under 4 dyne/cm^2 uniform FSS, EOP_{NE} and Lamin A/C further decreased and increased, respectively, suggesting a strong correlation between Lamin A/C expression and NE tension (Figure 6-1 b-c). In order to confirm this result, we used western blot to measure Lamin A/C expression and myosin II activity of SBTCs after shear treatment in the circulatory

pump system. Consistently, after high FSS treatment for thirty minutes, both Lamin A/C expression and P-MLC were substantially enhanced (Figure 6-1 d). It is noteworthy that Lamin protein has relatively long turnover time in mammalian cells[272]. Therefore, the detailed molecular mechanism of quick Lamin A/C response under shear stress needs further investigation. These data suggested that Lamin A/C in SBTCs responded to shear stress in a force-dependent manner.

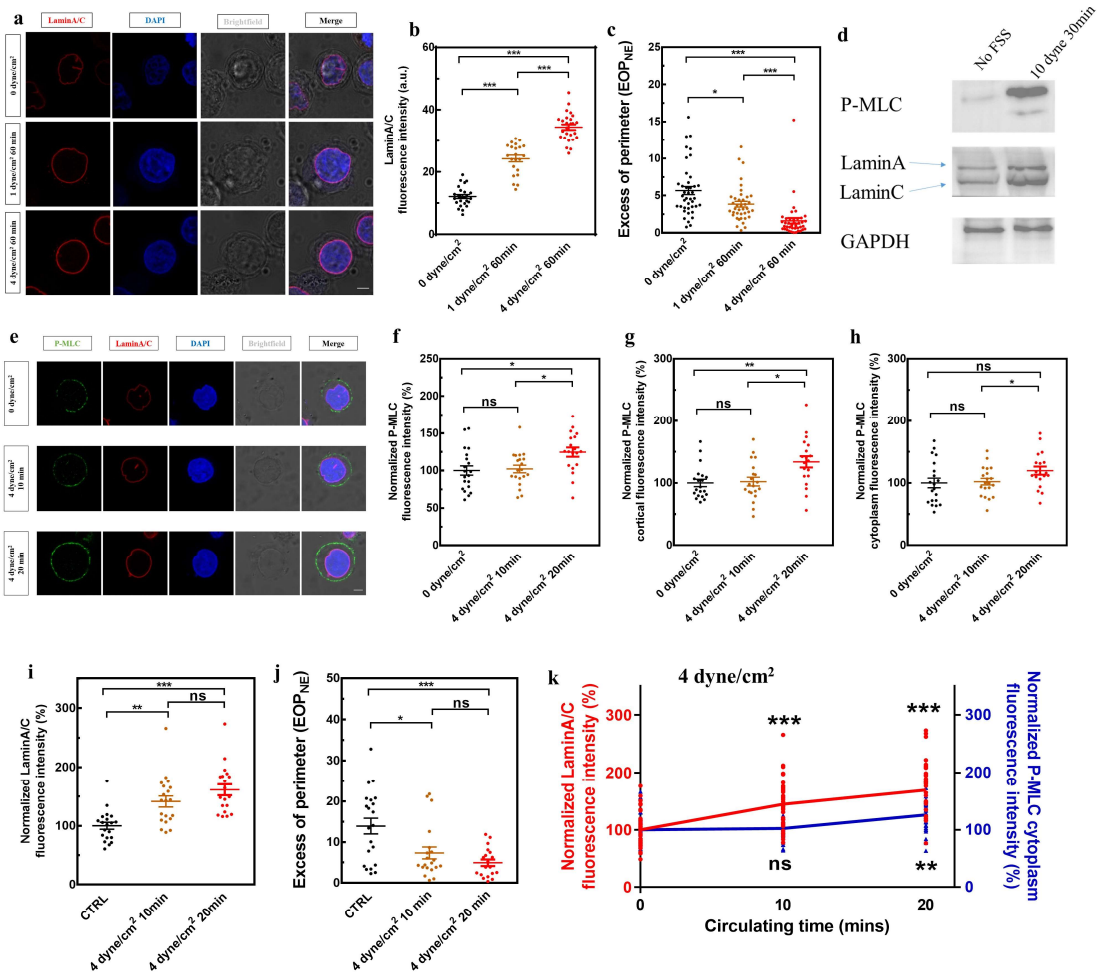

Figure 6-1 Lamin A/C responds to shear stress prior to myosin II activity. (a-b) Representative images **(a)** and quantitative data **(b)** of Lamin A/C fluorescence intensity in SBTCs under different levels of uniform FSS. **(c)** EOP_{NE} of SBTCs under different levels of uniform FSS. **(d)** Western blot of Lamin A/C as well as P-MLC of SBTCs under FSS. **(e-i)** Representative images **(e)** and P-MLC (green) total **(f),** cortical **(g),** cytoplasmic **(h)** fluorescence intensity, as well as Lamin A/C (red**, i)** fluorescence intensity of SBTCs under high uniform FSS. **(j)** EOP_{NE} of SBTCs under different time points of high uniform FSS. **(k)** Dynamic change of Lamin A/C and P-MLC under high uniform

FSS with time. Scale bar=5 μm; N = 3 independent experiments; mean ± SEM; *, p <0.05; **, p < 0.01; and ***, p < 0.001

Next, we explored whether there was any correlation between Lamin A/C expression and myosin II activation under shear stress. Towards this goal, we co-stained P-MLC and Lamin A/C in the same cells and quantified their responses in different time points under shear force. Intriguingly, while myosin II activity in both cortex and cytoplasm began to increase at 20 minutes under high uniform FSS (Figure 6-1 e-h), Lamin A/C and EOP_{NE} changed as early as 10 minutes after shear treatment (Figure 6-1 i-j). The data presented in Figure 6-1 k showed that Lamin A/C responded to high uniform FSS prior to myosin II, indicating Lamin A/C may serve as the upstream of myosin II subcellular distribution of SBTCs under shear stress.

6.2 Lamin A/C-mediated nuclear mechanosensing regulates myosin II subcellular localization of SBTCs

Then, we wanted to further investigate whether Lamin A/C controlled myosin II subcellular localization under shear stress. Hereby, we inhibited Lamin A/C expression through selective siRNA to knockdown *LMNA* gene. Interestingly, knockdown *LMNA* did not influence myosin II activity of SBTCs without shear stress. Nevertheless, it compromised myosin II distributions in both cortex and cytoplasm under high uniform FSS (Figure 6-2 a-d). Of note, inhibiting Lamin A/C expression rescued shear stress-induced decreased FTE, while did not influence FTE of SBTCs under static status (Figure 6-2 e-f). These results suggested that myosin II subcellular localization and FTE of SBTCs under high uniform FSS were regulated by Lamin A/C expression.

To further confirm the role of Lamin A/C in myosin II localization, we quantified myosin II subcellular localization after Lamin A/C inhibition under low uniform FSS. Similar with high uniform FSS, *LMNA* selectively knockdown restored low uniform FSS induced myosin II activation (Figure 6-2 g-h). Of note, while cortical myosin II activity can be rescued by *LMNA* knockdown, cytoplasmic myosin II activity remained

nearly constant irrespective of low uniform FSS treatment (Figure 6-2 i-j). Combined with Figure 6-2 b-d showing that knockdown *LMNA* did not influence myosin II subcellular distribution under static status, these findings indicated that the regulation of Lamin A/C in myosin II was highly selective to shear stress. Moreover, knockdown *LMNA* did not impact FTE under low uniform FSS (Figure 6-2 k), consistent with previous conclusion that cytoplasmic, instead of cortical myosin II localization regulates of FTE of SBTCs.

Based on the saying above, Lamin A/C-mediated nuclear mechanosensing was indispensable for myosin II subcellular activation and FTE under shear stress.

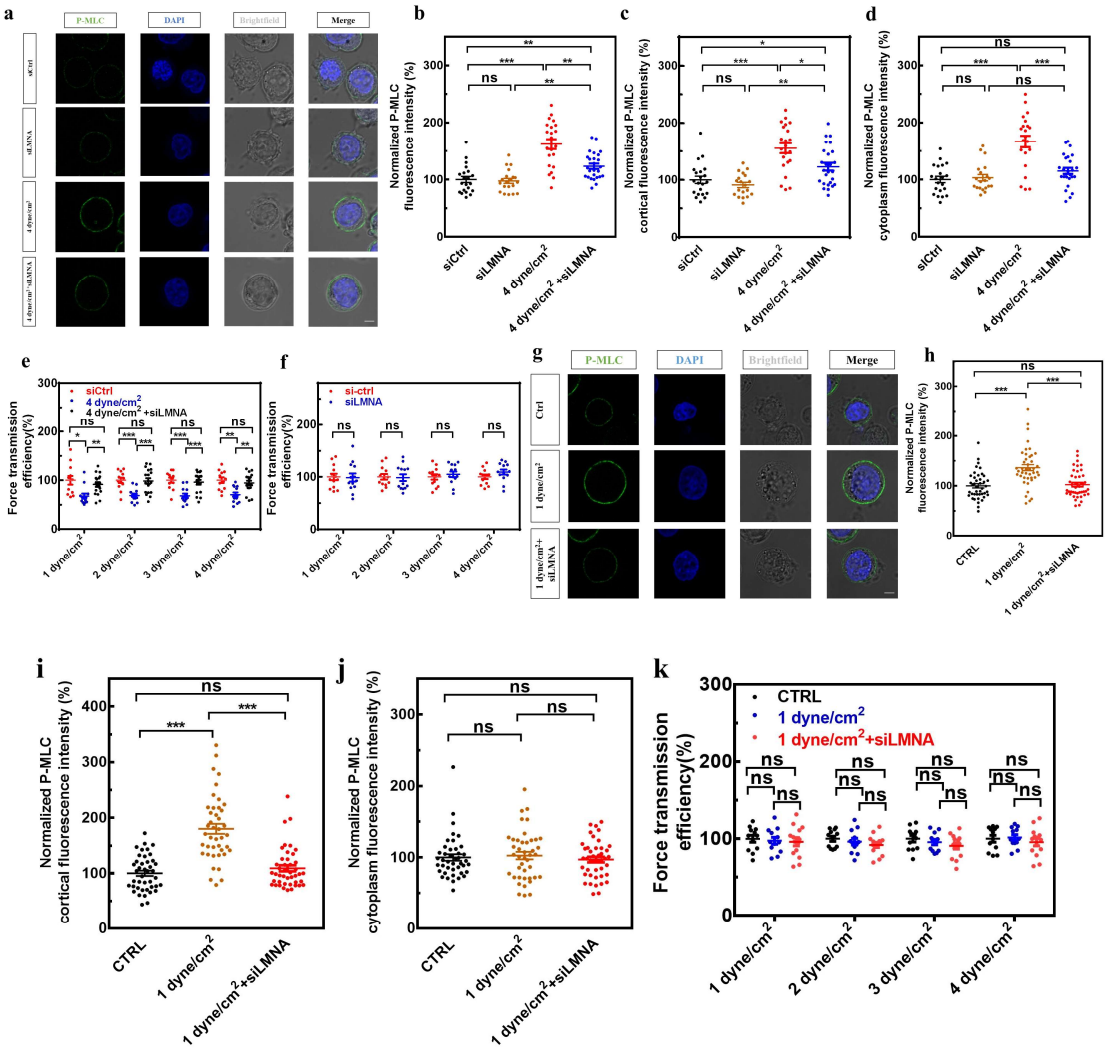

Figure 6-2 Lamin A/C is indispensable for myosin II subcellular localization and FTE under shear stress. (a-d) Representative images **(a)** and quantitative data of total **(b)**, cortical **(c)** or cytoplasmic **(d)** P-MLC fluorescence intensity after knockdown *LMNA* under high uniform FSS. **(e)**

FTE of SBTCs after knockdown *LMNA* under high uniform FSS. **(f)** FTE of SBTCs after knockdown *LMNA* in static status. **(g-j)** Representative image **(g)** and quantitative data of total **(h)**, cortical **(i)** or cytoplasmic **(j)** P-MLC fluorescence intensity after knockdown *LMNA* under low uniform FSS. **(k)** FTE of SBTCs after knockdown *LMNA* under low uniform FSS. Scale bar=5 μm; N = 3 independent experiments; mean ± SEM; *, p <0.05; **, p < 0.01; and ***, p < 0.001

6.3 Lamin A/C overexpression is sufficient to actives myosin II and regulates FTE of SBTCs

So far, we have found that Lamin A/C-mediated nuclear mechanosensing was required for myosin II activation and decreased FTE under shear stress. However, whether Lamin A/C expression was sufficient to activate myosin II of SBTCs was still elusive. To answer this question, we overexpressed Lamin A/C through transfecting active form of Lamin A/C. Strikingly, Lamin A/C overexpression directly triggered myosin II activation even without shear stress (Figure 6-3 a-b), while it had minor effect under high uniform FSS, suggesting Lamin A/C was already in high level under high uniform FSS. The cortical as well as cytoplasmic myosin II showed consistently improved trends (Figure 6-3 c-d). In accordance with previous findings, cytoplasmic myosin II activation through Lamin A/C overexpression decreased FTE even without shear stress pretreatment (Figure 6-3 e). These results provided a notion that Lamin A/C expression was not only required but also sufficient to activate myosin II and further diminished FTE in SBTCs.

Further, in order to test potential possible feedbacks of myosin II activity to Lamin A/C expression, we knocked down *MYH10* and used immunofluorescence to measure Lamin A/C expression as well as NE tension represented by EOP_{NE}. The results in Figure 6-3 f-g demonstrated distinct roles of *MYH10* in regulating Lamin A/C expression with or without shear stress. Under static status, myosin II inhibition decreased Lamin A/C expression, possibly due to decreased prestress applied to cell nucleus[237]. However, under shear stress, decreased myosin II activity further enhanced Lamin A/C expression. This result was in accordance with foregoing findings that

decreased myosin II activity enhanced FTE of SBTCs (Figure 4-9). In that way, knockdown *MYH10* increased external force transmitted to cell nucleus in SBTCs, which led to higher Lamin A/C expression. Moreover, we again found the correlation between Lamin A/C expression and NE tension represented by EOP_{NE}, where knockdown *MYH10* led to further enhanced Lamin A/C expression and NE tension under high uniform FSS (Figure 6-3 h).

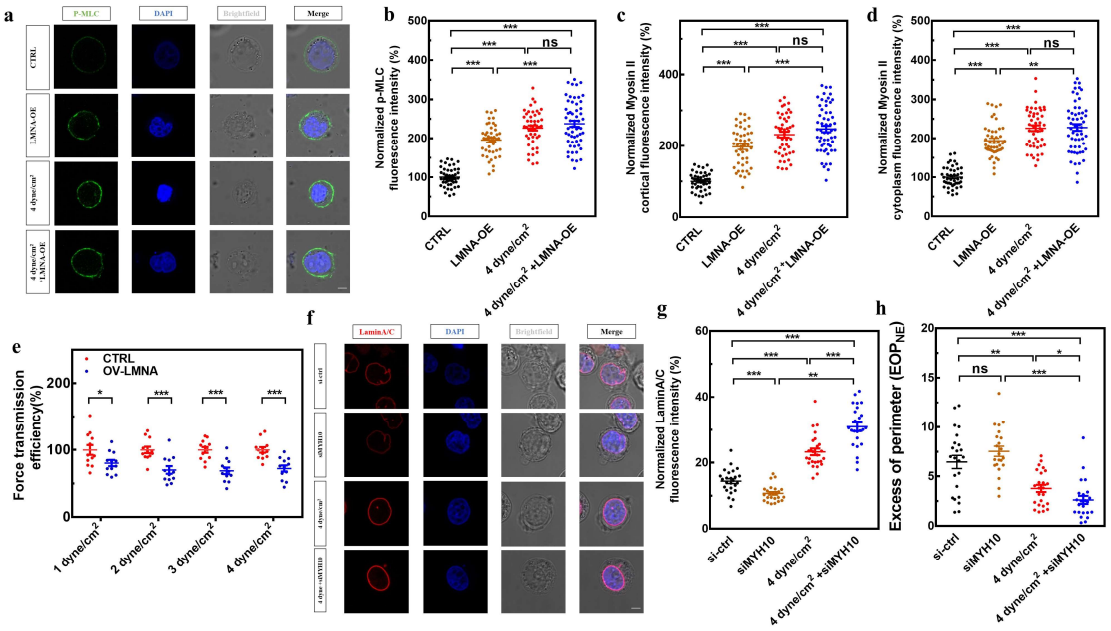

Figure 6-3 Lamin A/C expression is sufficient for myosin II activation of SBTCs. (a-d) Representative images **(a)** and quantitative data of total **(b)**, cortical **(c)** or cytoplasmic **(d)** P-MLC fluorescence intensity after Lamin A/C overexpression (LMNA-OE) under high uniform FSS. **(e)** FTE of SBTCs after LMNA-OE without FSS. **(f-g)** Representative images **(f)** and quantitative data **(g)** of Lamin A/C fluorescence intensity after knocking down *MYH10* under high uniform FSS. **(h)** EOP_{NE} of SBTCs after knocking down *MYH10* under high uniform FSS. Scale bar=5 μm; N = 3 independent experiments; mean ± SEM; *, p <0.05; **, p < 0.01; and ***, p < 0.001

6.4 Lamin A/C-mediated NE tension triggers calcium release from endoplasmic reticulum in SBTCs under shear stress

Then, we would like to further investigate how Lamin A/C-mediated nuclear mechanosensing triggered myosin II subcellular distribution under shear stress. As aforementioned, there was a positive correlation between Lamin A/C expression and NE tension (Figure 6-1 b-c, i-j and 4-25g-h). Recent study discovers that increased NE tension triggers calcium release from ER[212]. We thus wanted to investigate whether calcium played important role in SBTCs' responses to FSS.

At first, we compared intracellular calcium level before and after shear stress. To achieve this goal, we utilized GCaMP6 calcium sensor which has been used to measure calcium response of endothelial cell under shear stress[85]. At first, we verified the performance of this calcium sensor in SBTCs. As it can be seen in Figure 6-4 a-b, the florescence intensity of GCaMP6 calcium sensor was significantly enhanced after treating SBTCs with Yoda 1, a mechanosensitive ion channel agonist[273], indicating enhanced intracellular calcium level. Thus, this calcium sensor worked well in our system.

Based on this, we further analyzed calcium response of SBTCs under shear stress stimulation. Intriguingly, after high uniform FSS treatment for 60 minutes, intracellular calcium level of SBTCs was strikingly enhanced (Figure 6-4 c-d). Furthermore, we tracked the dynamic changes of calcium level in SBTCs during high uniform FSS application. The statistical results unambiguously demonstrated that calcium level indeed increased during shear stress application (Figure 6-4 e).

In order to link Lamin A/C-mediated nuclear mechanosensing to calcium response of SBTCs under shear stress, we knocked down *LMNA* and tracked dynamic change of intracellular calcium level through GCaMP6. The results in Figure 6-4 e disclosed that inhibition of Lamin A/C abolished shear-induced calcium response, indicating that Lamin A/C-mediated nuclear mechanosensing regulated intracellular calcium

responses of SBTCs under shear stress.

Although we had observed a clear calcium response of SBTCs mediated by Lamin A/C, it remained a question that how Lamin A/C triggered intracellular calcium response of SBTCs under shear stress. Previous research discloses that high NE tension could trigger calcium release from ER[212]. We thus speculated that FSS upregulated Lamin A/C expression and NE tension, leading to the release of calcium from ER. To test this possibility, we pre-treated cancer cells with Thapsigargin (Tg) two days before the experiments to empty calcium stored in ER. The data in Figure 6-4 e disclosed that inhibiting calcium release from ER abolished shear-triggered calcium response. On the contrary, chelation of calcium ion with EGTA inhibited extracellular calcium influx but did not influence calcium response of SBTCs under shear stress, suggesting that the calcium response was from calcium stored in ER, but not extracellular environment. It was noteworthy that ER calcium release of SBTCs under shear stress persisted for more than thirty minutes, which was different from the short-lived and oscillatory calcium response of human mesenchymal stem cells under magnetic bead induced complex force[274]. The constant calcium response may be caused by continuous and high mechanical stimulation we applied. Future study should focus on the detailed mechanism underlying this persistent calcium response.

Altogether, our data indicated that Lamin A/C-mediated nuclear mechanosensing triggers calcium release form ER and increases intracellular calcium concentration under shear stress.

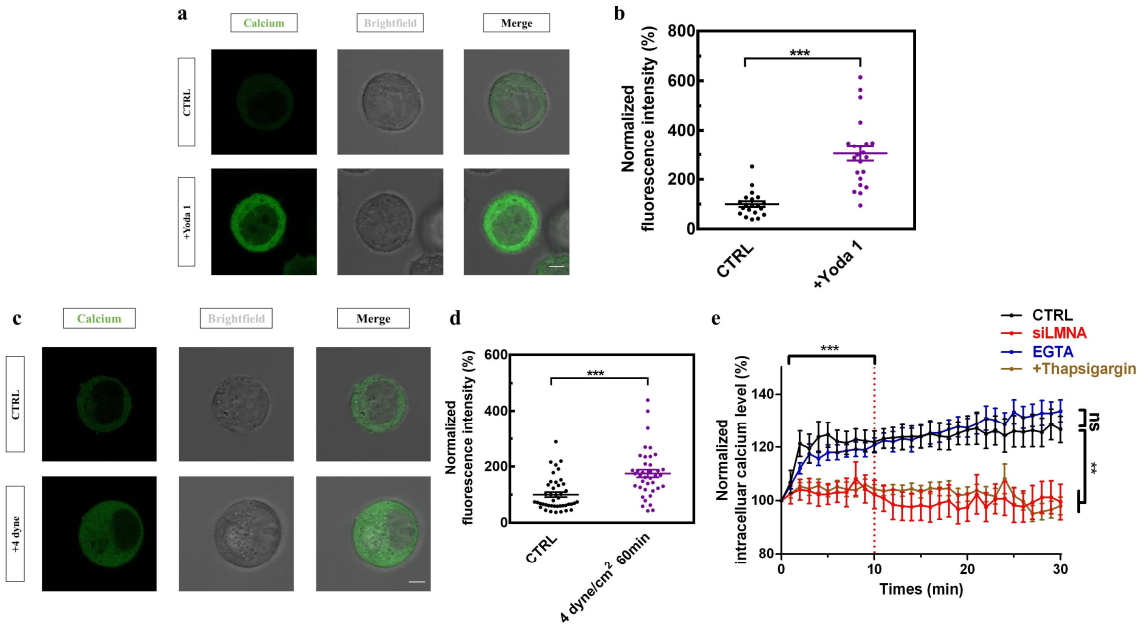

Figure 6-4 Lamin A/C-mediated nuclear mechanosensing triggers calcium release from ER. **(a-b)** Representative images **(a)** and quantitative data **(b)** of GCaMP6 fluorescence intensity after Yoda 1 treatment in SBTCs. **(c-d)** Representative images **(c)** and quantitative data **(d)** of GCaMP6 fluorescence intensity of SBTCs under high uniform FSS. **(e)** Dynamic change of GCaMP6 fluorescence intensity after si*LMNA* (red), treating with Tg (brown) or treating medium with EGTA (blue) in SBTCs during high uniform FSS. Scale bar=5 μm; N = 3 independent experiments; mean ± SEM; *, p <0.05; **, p < 0.01; and ***, p < 0.001

6.5 Lamin A/C dephosphorylation mediates quick response of nucleus toward shear stress

Figure 6-4 e showed that intracellular calcium concentration increased at two minutes under high uniform FSS. Nevertheless, our previous data showed that Lamin A/C protein expression enhanced at ten minutes under high uniform FSS (Figure 6-1 i), while whether Lamin A/C-mediated nuclear mechanosensing happed prior to calcium response was unclear. Thus, to further investigated quick response of Lamin A/C to shear stress, we quantified Lamin A/C protein expression within 10 minutes. Unfortunately, Lamin A/C expression did not show significant change within two

minutes under high uniform FSS. In fact, Lamin A/C protein expression began to increase at about five minutes under high uniform FSS (Figure 6-5 a-b). Intriguingly, while protein expression of Lamin A/C remained unchanged, the EOP_{NE} significantly decreased within two minutes under high uniform FSS, indicating NE tension increased within short period (Figure 6-5 c). The inconsistency between Lamin A/C protein expression and NE tension triggered use to further study whether and how Lamin A/C activity, instead of protein expression, responded to shear stress.

Previous studies demonstrate that Lamin A/C post-transcriptional modifications, especially phosphorylation, regulates Lamin A/C activity through protein degradation[231, 275]. Specifically, Lamin A/C phosphorylation at Ser22 facilitates Lamin A/C degradation and decrease Lamin A/C activity during nuclear deformation[220]. We thus investigated whether Lamin A/C phosphorylation played the important role in quick response of cell nucleus under shear stress. Hereby, we quantified pSer/LMNA ratio as previously mentioned under high uniform FSS in SBTCs[220]. To our surprise, pSer/LMNA ratio was substantially decreased within two minutes under high uniform FSS treatment, indicating Lamin A/C activity increased within two minutes under shear stress (Figure 6-5 d-e), in line with calcium response we found before (Figure 6-4 e).

Based on the results above, Lamin A/C dephosphorylation establishes immediate response of nucleus toward shear stress, which leads to high NE tension and further calcium release.

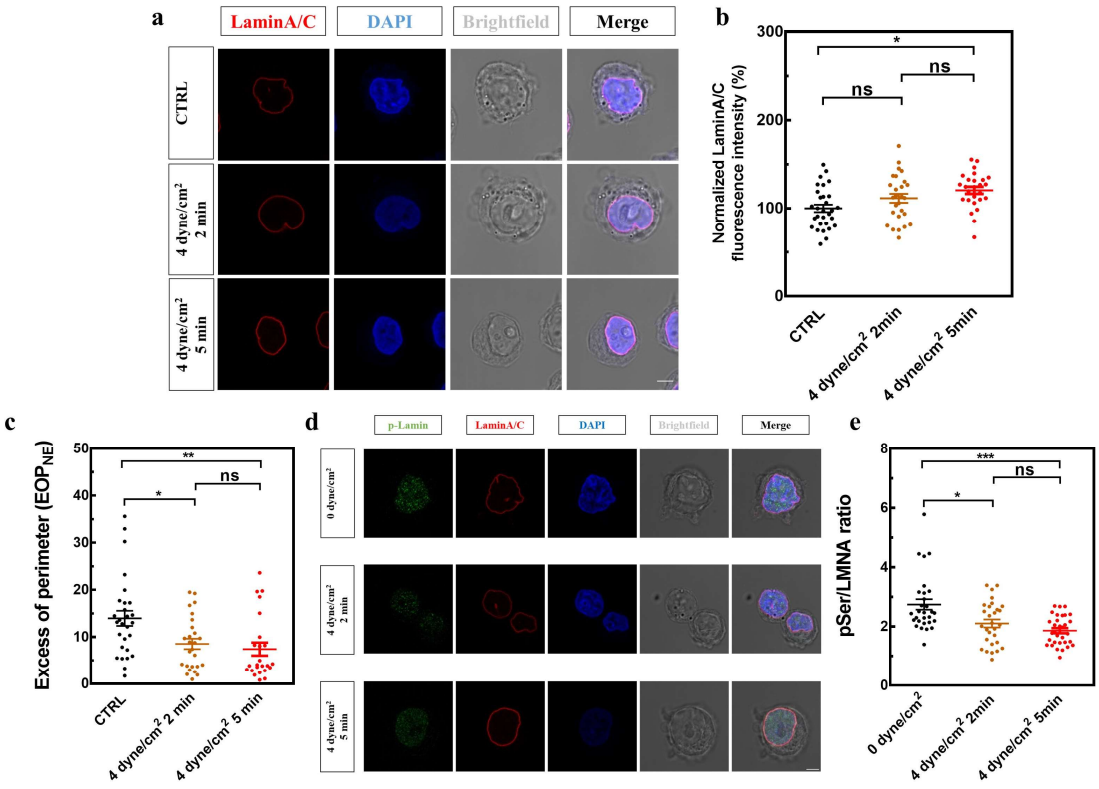

Figure 6-5 Lamin A/C activity increased within two minutes under high uniform FSS. (a-b) Representative images **(a)** and quantitative data **(b)** of Lamin A/C fluorescence intensity under high uniform FSS within five minutes. **(c)** EOP_{NE} of SBTCs under high uniform FSS within five minutes. **(d-e)** Representative images of phosphorylated Lamin A/C (green), Lamin A/C (red) **(d)** and quantitative data **(e)** of pSer/LMNA ratio under high uniform FSS within five minutes. Scale bar=5 μm; N = 3 independent experiments; mean ± SEM; *, p <0.05; **, p < 0.01; and ***, p < 0.001

6.6 Calcium release from ER, but not calcium influx, regulates myosin II subcellular localization and FTE of SBTCs under shear stress

Our data suggested that Lamin A/C-mediated nuclear mechanosensing triggered calcium release from ER and further increased intracellular calcium concentration. However, whether calcium could further activate myosin II and influence FTE were still unclear. We thus treated SBTCs with either Tg or treated medium with EGTA to test potential role of calcium. The results from Figure 6-6 a-c showed that treated SBTCs with Tg to empty ER calcium rescued shear stress-induced myosin II

subcellular activation in both cortex and cell cytoplasm. Consistently, Tg treatment restored FTE under high uniform FSS (Figure 6-6 d). In contrast with Tg, EGTA failed to rescue shear stress-induced cortical as well as cytoplasmic myosin II activation and incapable to influence FTE of SBTCs under shear stress (Figure 6-6 e-h). Based on the finding above, calcium release from ER mediated by Lamin A/C and nuclear mechanosensing was indispensable for both myosin II subcellular distribution and FTE of SBTCs under shear stress.

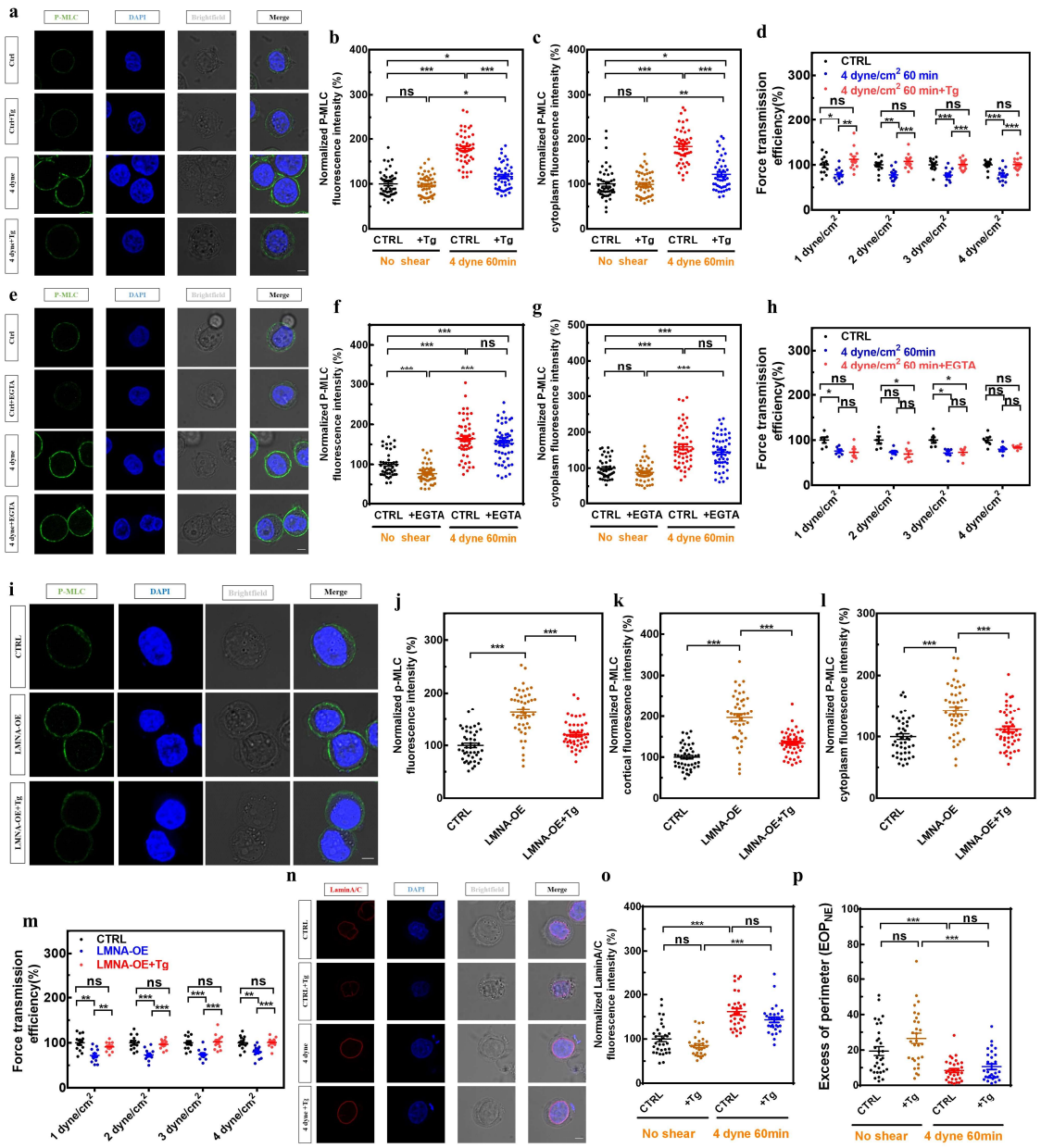

Figure 6-6 Calcium release from ER, but not from extracellular medium, triggers myosin II activation and decrease FTE of SBTCs under FSS. (a-c) Representative images **(a)** and quantitative data of cortical **(b)** or cytoplasmic **(c)** P-MLC fluorescence intensity after Tg treatment under high uniform FSS. **(d)** FTE of SBTCs after Tg treatment under high uniform FSS. **(e-g)** Representative images **(e)** and quantitative data of cortical **(f)** or cytoplasmic **(g)** P-MLC fluorescence intensity after EGTA treatment under high uniform FSS. **(h)** FTE of SBTCs after EGTA treatment under high uniform FSS. **(i-l)** Representative images **(i)** and quantitative data of total **(j)**, cortical **(k)** or cytoplasmic **(l)** P-MLC fluorescence intensity after Tg treatment under Lamin A/C overexpression. **(m)** FTE after Tg treatment under Lamin A/C overexpression. **(n-o)** Representative images **(n)** and quantitative data **(o)** of Lamin A/C fluorescence intensity after Tg treatment under high uniform FSS. **(p)** EOP_{NE} of SBTCs after Tg treatment under high uniform FSS. Scale bar=5 μm; N = 3 independent experiments; mean ± SEM; *, p <0.05; **, p < 0.01; and ***, p < 0.001

Our previous data showed that Lamin A/C overexpression was sufficient to activate myosin II (Figure 6-3 a-d) and decreased FTE (Figure 6-3 e), while whether it through calcium release from ER was still unclear. To further explore the potential role of nuclear mechanosensing mediated calcium release from ER in SBTCs after Lamin A/C overexpression, we overexpressed Lamin A/C with Tg treatment simultaneously. As it can be seen in Figure 6-6 i-m, Tg addition rescued Lamin A/C overexpression triggered myosin II subcellular distribution and declined FTE, indicating Lamin A/C overexpression induced myosin II localization was through calcium release from ER, similar with shear stress application.

Until now, we have found indispensable roles of calcium released from ER by Lamin A/C-mediated nuclear mechanosensing in SBTCs under shear stress. However, whether calcium could feedback to Lamin A/C expression and NE tension were still unknown. To test it, we quantified Lamin A/C protein expression after Tg treatment. The results reflected that inhibition of calcium from ER did not impact Lamin A/C expression and NE tension. Thus, the regulation of Lamin A/C-mediated nuclear mechanosensing to calcium was unidirectional (Figure 6-6 n-p).

Based on the saying above, Lamin A/C dephosphorylation increases Lamin A/C activity, which further enhances NE tension and triggers calcium release from ER, finally leads to myosin II subcellular distribution and decreased FTE.

Chapter 7. MLCK and ROCK regionally activate myosin II and differentially regulates FTE and survival of SBTCs under shear stress

7.1 Nuclear mechanosensing regulates MLCK expression and ROCK activation under shear stress

Thus far, we have discovered that Lamin A/C-mediated nuclear mechanosensing increased NE tension that further triggered calcium release from ER. Then, we investigated how intracellular calcium signaling induced myosin II subcellular distribution. It had been found that calcium activates myosin II mainly through interacting with MLCK or ROCK, thus increasing its kinase activity and binding affinity with myosin motors[26, 176]. We thus wanted to investigate whether calcium activated myosin II through MLCK and ROCK in SBTCs under shear stress.

At first, we measured MLCK protein expression under high uniform FSS. The results showed that MLCK expression substantially increased under high uniform FSS. However, MLCK seems to be regionally distributed under high uniform FSS: while cortical MLCK significantly enhanced, cytoplasmic MLCK remained almost the same. In that way, MLCK cortical/cytoplasm ratio was significantly increased, indicating MLCK was more localized in cell cortex under high uniform FSS. Interfering *LMNA* through siRNA recued shear stress-induced MLCK expression (Figure 7-1 a-e). Further, we quantified ROCK activity under high uniform FSS through phosphorylated ROCK in Ser 1366 site [180]. The result from Figure 7-1 f-j showed that, phospho-ROCK was increased both in cell cortex and cell cytoplasm under high uniform FSS. Compared with MLCK which exhibit higher cortical/cytoplasm ratio, phospho-ROCK showed lower cortical/cytoplasm ratio under high uniform FSS, indicating distinct distribution patterns between MLCK and phospho-ROCK. Similar with MLCK, phospho-ROCK can be rescued by Lamin A/C inhibition. Thus, MLCK protein expression and ROCK activation were controlled by Lamin A/C-mediated nuclear mechanosensing under

shear stress.

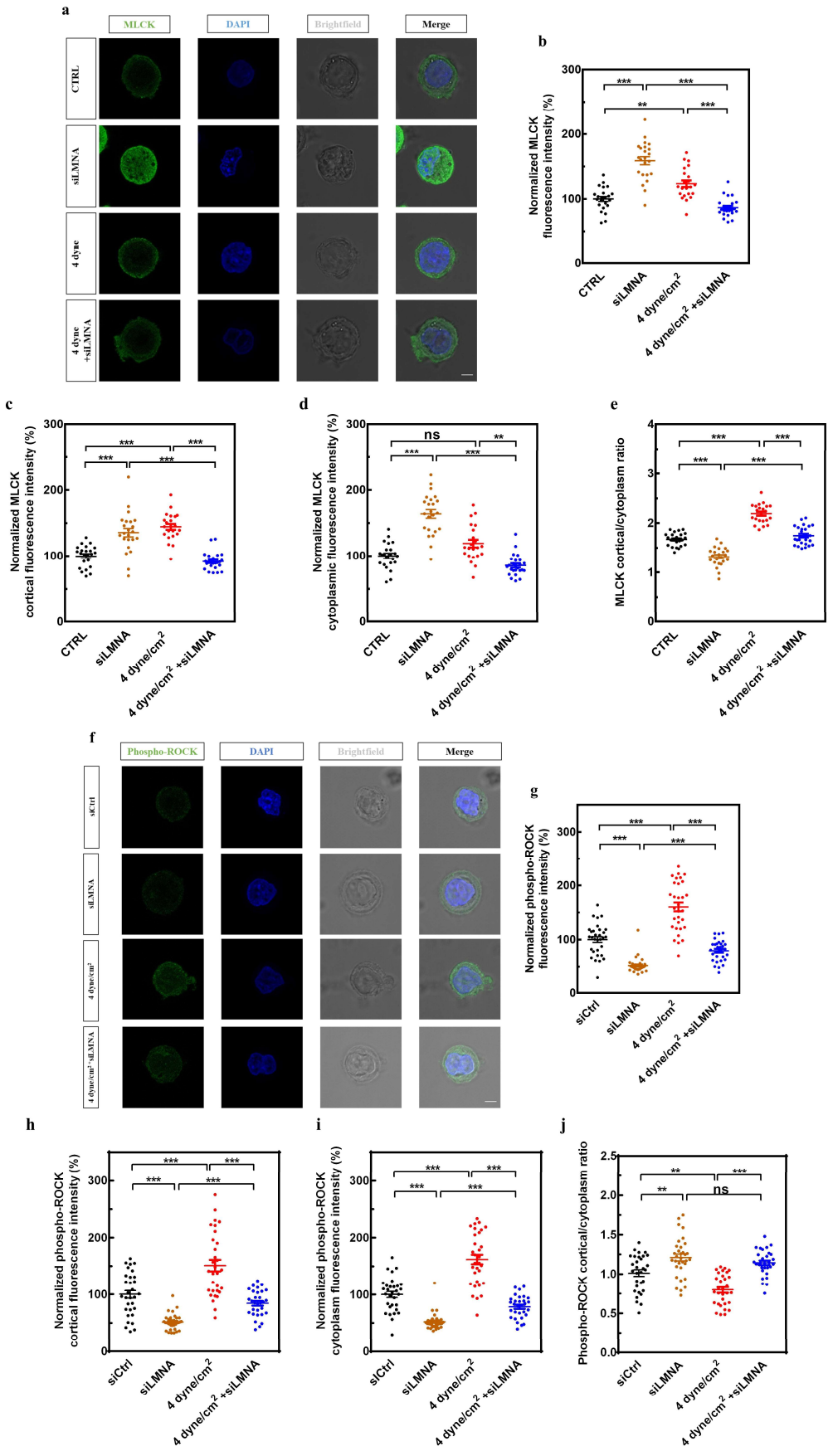

Figure 7-1 MLCK expression and ROCK activation are controlled by Lamin A/C-mediated nuclear mechanosensing. (a-d) Representative images **(a)** and quantitative data of total **(b)**, cortical **(c)** or cytoplasmic **(d)** MLCK fluorescence intensity after knocking down *LMNA* under high uniform FSS. **(e)** MLCK cortical/cytoplasm ratio after knocking down *LMNA* under high uniform FSS. **(f-i)** Representative images **(f)** and quantitative data of total **(g)**, cortical **(h)** or cytoplasmic **(i)** phospho-ROCK fluorescence intensity after knocking down *LMNA* under high uniform FSS **(j)** phospho-ROCK cortical/cytoplasm ratio after knocking down *LMNA* under high uniform FSS. Scale bar=5 μm; N = 3 independent experiments; mean ± SEM; *, p <0.05; **, p < 0.01; and ***, p < 0.001

We previously found that Lamin A/C-mediated nuclear mechanosensing triggered calcium release from ER and further activated myosin II. To further investigate whether this calcium response activated myosin II through MLCK and ROCK, we treated SBTCs with Tg to inhibit calcium release under shear stress and measured MLCK or phosphorylated ROCK under high uniform FSS. Interestingly, inhibition of calcium signaling diminished ROCK activation both in cell cortex and cytoplasm (Figure 7-2 a-d), suggesting that ROCK activation was caused by calcium release from ER. Instead, Tg treatment failed to inhibit MLCK expression (Figure 7-2 e-h). Future study should focus on investigating the potential upstream that initiate MLCK expression, such us the transcriptional co-activator YAP[213].

In summary, Lamin A/C-mediated nuclear mechanosensing of SBTCs regulates MLCK expression and ROCK activation under shear stress.

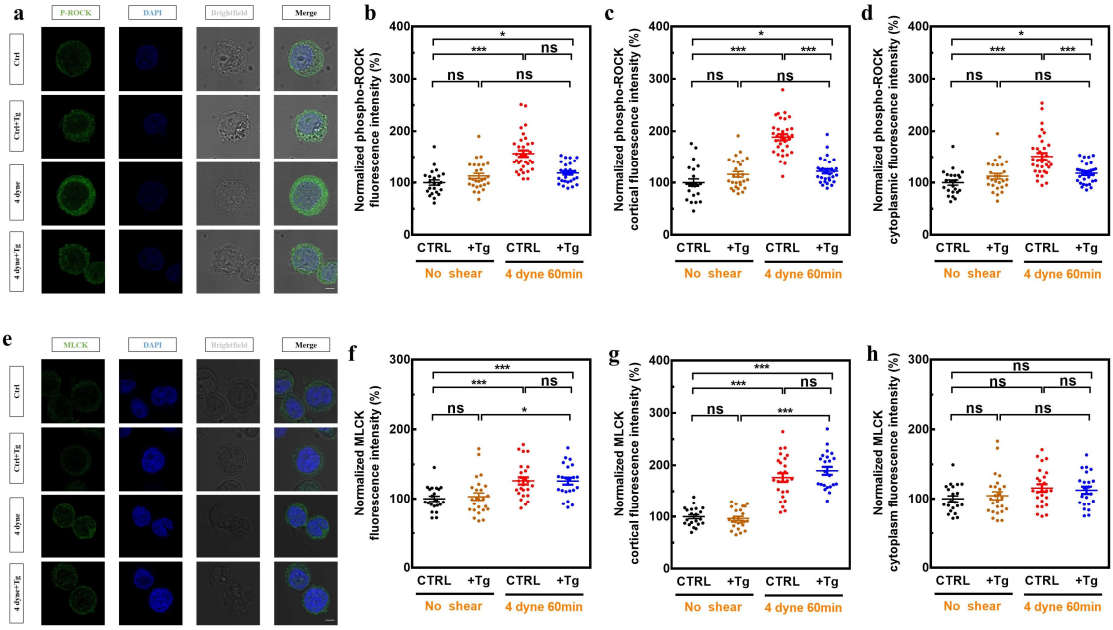

Figure 7-2 ROCK activation is controlled by calcium release from ER. (a-d) Representative images **(a)** and quantitative data of total **(b)**, cortical **(c)** or cytoplasmic **(d)** phospho-ROCK fluorescence intensity after Tg treatment under high uniform FSS. **(e-h)** Representative images **(e)** and quantitative data of total **(f)**, cortical **(g)** or cytoplasmic **(h)** MLCK fluorescence intensity after Tg treatment under high uniform FSS. Scale bar=5 μm; N = 3 independent experiments; mean ± SEM; *, p <0.05; **, p < 0.01; and ***, p < 0.001

7.2 MLCK and ROCK show distinct responses to varying levels of FSS

The works have done so far showed that nuclear mechanosensing triggered MLCK expression and ROCK activation. Previous studies suggest that MLCK and ROCK have different functions in myosin II activation[186, 187]. Therefore, we further investigated whether MLCK and ROCK showed distinct responses to shear stress and whether they differentially regulated myosin II subcellular localization.

At first, we investigated whether MLCK and ROCK in SBTCs differentially responded to shear stress. Here, we applied low uniform FSS or high uniform FSS to SBTCs and quantified MLCK expression and ROCK activation by immunofluorescence. To our surprise, MLCK and ROCK exhibited distinct responses to different level of shear stress. Under low uniform FSS, MLCK expression was increased but not further

enhanced under high uniform FSS, indicating MLCK reached a plateau already under low uniform FSS (Figure 7-3 a-b). In contrast, ROCK activation remained unchanged under low uniform FSS but substantially increased under high uniform FSS, suggesting ROCK activation was specific to high uniform FSS instead of low uniform FSS (Figure 7-3 f-g). More importantly, MLCK expression under shear stress was not uniformly distributed in SBTCs. While most of MLCK was localized in cell cortex, cytoplasmic MLCK had minor response under shear stress (Figure 7-3 c-d), which led to higher MLCK cortical/cytoplasm ratio (Figure 7-3 e). Compared with MLCK expression, ROCK activation was both increased in cell cortex and cytoplasm (Figure 7-3 f-i). Intriguingly, when comparing ROCK cortical/cytoplasm ratio under high uniform FSS, we observed a declined trend (Figure 7-3 j), indicating ROCK was more localized in cytoplasm, in sharp contrast with MLCK (Figure 7-3 e).

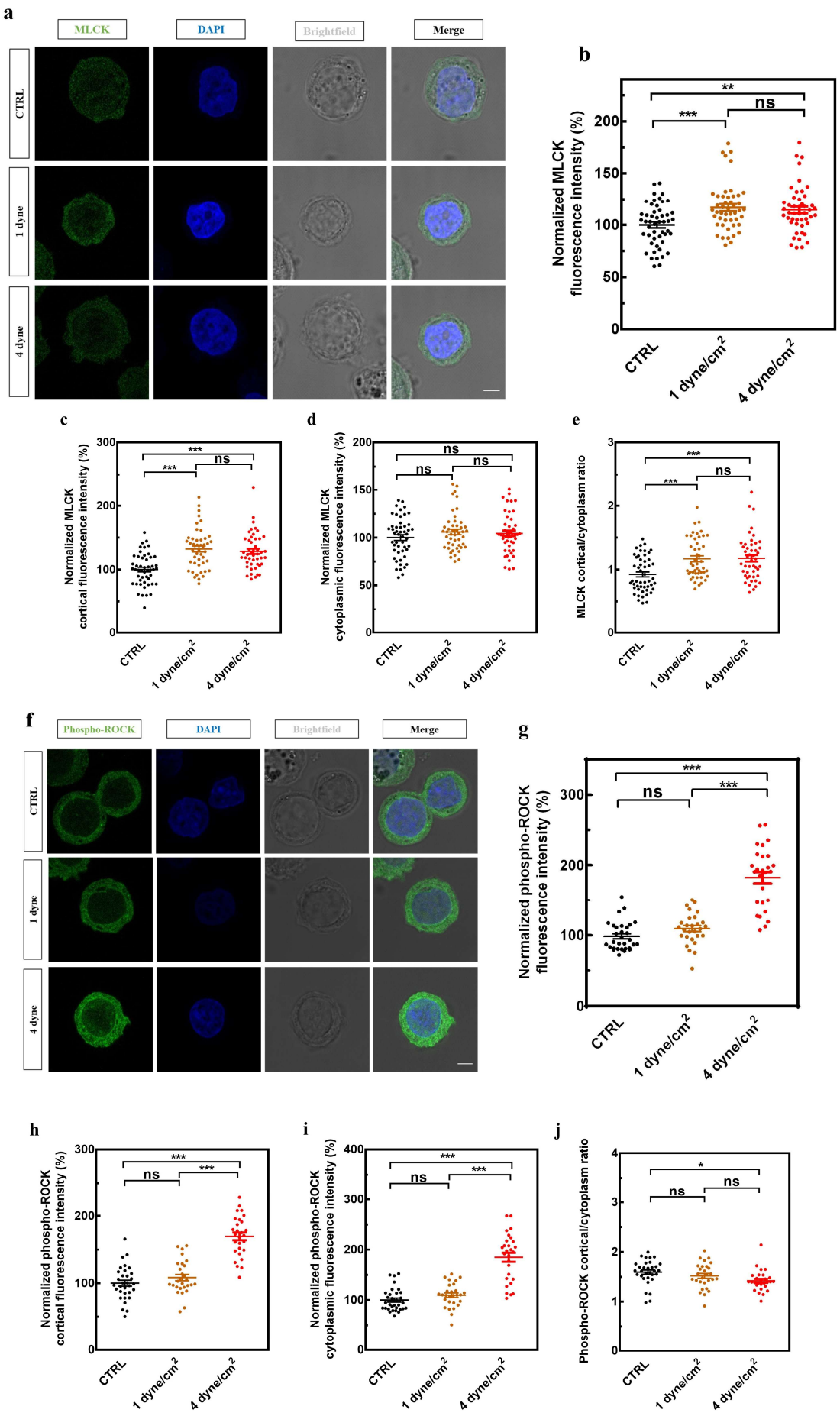
a
MLCK
DAPI
Brightfield
Merge
CTRL
1 dyne
4 dyne
b
Normalized MLCK fluorescence intensity (%)
c
Normalized MLCK cortical fluorescence intensity (%)
d
Normalized MLCK cytoplasmic fluorescence intensity (%)
e
MLCK cortical/cytoplasm ratio
f
Phospho-ROCK
g
Normalized phospho-ROCK fluorescence intensity (%)
h
Normalized phospho-ROCK cortical fluorescence intensity (%)
i
Normalized phospho-ROCK cytoplasmic fluorescence intensity (%)
j
Phospho-ROCK cortical/cytoplasm ratio
ns
CTRL
1 dyne/cm2
4 dyne/cm2

Figure 7-3 MLCK expression and ROCK activation show distinct responses to low uniform FSS or high uniform FSS. (a-d) Representative images **(a)** and quantitative data of total **(b)**, cortical **(c)** or cytoplasmic **(d)** MLCK fluorescence intensity under different levels of uniform FSS. **(e)** MLCK cortical/cytoplasm ratio under different levels of uniform FSS. **(f-i)** Representative images **(f)** and quantitative data of total **(g)**, cortical **(h)** or cytoplasmic **(i)** phospho-ROCK fluorescence intensity under different levels of uniform FSS. **(j)** Phospho-ROCK cortical/cytoplasm ratio under different levels of uniform FSS. Scale bar=5 μm; N = 3 independent experiments; mean ± SEM; *, p <0.05; **, p < 0.01; and ***, p < 0.001

7.3 MLCK controls myosin II cortical localization under shear stress

Our previous findings suggested distinct responses of MLCK or ROCK under shear stress. The distinct subcellular localization and activation of MLCK and ROCK rendered us to reminiscent of myosin II subcellular distribution under shear stress. Indeed, there was a strong correlation between myosin II subcellular distribution and MLCK and ROCK activity. Under low uniform FSS, myosin II was activated in cell cortex but not cytoplasm (Figure 4-6). Intriguingly, MLCK, instead of ROCK, was distributed in cell cortex. Under high uniform FSS, myosin II was localized in cell cytoplasm and ROCK was activated also. These coincidences triggered use to speculate that MLCK controlled cortical myosin II localization in cell cortex under low uniform FSS, while ROCK was responsible for cytoplasmic myosin II activation under high uniform FSS.

To test our assumption, we first treated SBTCs with ML-7, a MLCK ATP-competitive inhibitor under uniform FSS[276]. Interestingly, under low uniform FSS, ML-7 treatment fully rescued shear stress-induced myosin II cortical activation. Instead, ML-7 treatment showed almost no effects on cytoplasmic myosin II activity (Figure 7-4 a-d). Consistent with previous findings, ML-7 treatment under low uniform FSS did not change FTE (Figure 7-4 e). These results suggested that MLCK mainly controlled myosin II activation and localization in cell cortex.

To further confirm the role of MLCK in cortical myosin II localization, we treated

SBTCs with ML-7 under high uniform FSS. The results showed that treatment of ML-7 under high uniform FSS rescued high uniform FSS-induced cortical myosin II activation, while ML-7 had little influence in cytoplasmic myosin II localization (Figure 7-4 f-i). Furthermore, ML-7 treatment failed to rescue high uniform FSS-induced decreased FTE, confirming the conclusion that cytoplasmic, but not cortical myosin II localization control FTE od SBTCs (Figure 7-4 j).

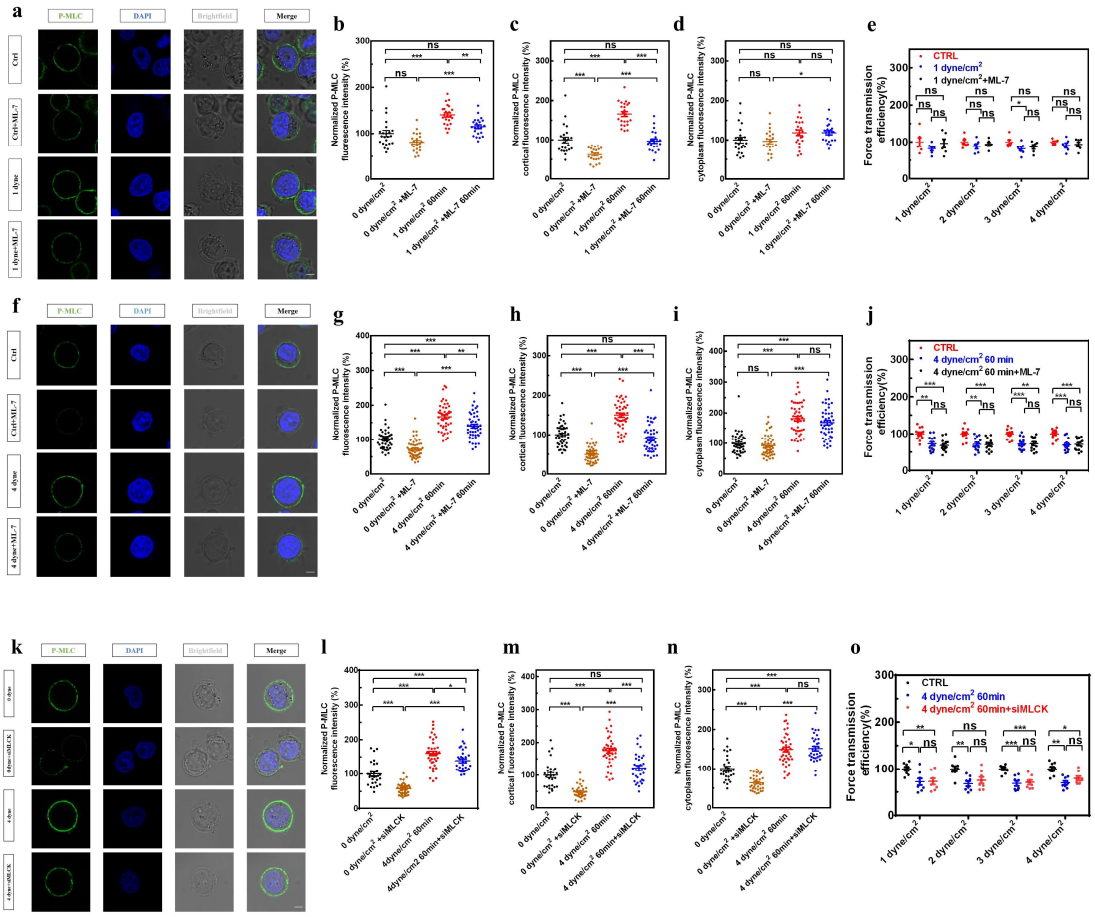

Figure 7-4 MLCK expression controls cortical myosin II localization under shear stress. (a-d) Representative images **(a)** and quantitative data of total **(b)**, cortical **(c)** or cytoplasmic **(d)** P-MLC fluorescence intensity after ML-7 treatment under low uniform FSS. **(e)** FTE of SBTCs after ML-7 treatment under low uniform FSS. **(f-i)** Representative images **(f)** and quantitative data of total **(g)**, cortical **(h)** or cytoplasmic **(i)** P-MLC fluorescence intensity after ML-7 treatment under high uniform FSS. **(j)** FTE of SBTCs after ML-7 treatment under high uniform FSS. **(k-n)** Representative images **(k)** and quantitative data of total **(l)**, cortical **(m)** or cytoplasmic **(n)** P-MLC fluorescence

intensity after knocking down *MLCK* under high uniform FSS. **(o)** FTE of SBTCs after knocking down *MLCK* under high uniform FSS. Scale bar=5 μm; N = 3 independent experiments; mean ± SEM; *, p <0.05; **, p < 0.01; and ***, p < 0.001

As ML-7 was not a MLCK specific inhibitor, it also influenced other kinases activity such cAMP-dependent protein kinase A that may confuse the conclusions[277]. We thus confirmed the role of MLCK through specifically interfere *MLCK* gene. To this end, we knocked down *MLCK* and then quantified myosin II subcellular distribution and FTE of SBTCs under high uniform FSS. The results from Figure 7-4 k-n showed that knocking down *MLCK* decreased myosin II localization specifically in cell cortex, while leaving cytoplasmic myosin II activity almost the same (Figure 7-4 k-n). Consistent with ML-7, *MLCK* knockdown failed to rescue decreased FTE under high uniform FSS (Figure 7-4 o).

In summary, MLCK expression was responsible for myosin II cortical localization and did not contribute to FTE in SBTCs under shear stress.

7.4 ROCK controls cytoplasmic myosin II localization and FTE

Thus far, we have unveiled the role of MLCK in cortical myosin II localization under shear stress. As mentioned before, MLCK and ROCK had distinct reactions under FSS (Figure 7-3). Our previous results suggested that ROCK activation was specific to high uniform FSS (Figure 7-3 f-g), as cytoplasmic myosin II localization and FTE also exhibited specific changes under high uniform FSS but not low uniform FSS (Figure 4-8), the coincidence suggested that ROCK was responsible for myosin II cytoplasmic localization and control FTE under high uniform FSS. Indeed, via inhibiting ROCK activity through Y27, we successfully decreased myosin II cytoplasmic activity and restored FTE under high uniform FSS (Figure 4-7). Although Y27 is a highly selective ROCK inhibitor, it may also influence cell cycle and cell proliferation that interfere with our conclusion[278]. Thus, to further confirm the role of ROCK, we decided to specifically inhibit ROCK activity via siRNA.

Here, we designed a doxycycline inducible si*ROCK* to knockdown *ROCK2* in drug-dependent manner. The data showed in Figure 7-5 a-b demonstrated that after 100 µg/ml doxycycline induction for 48 hours, the ROCK activity represented by phosphor-ROCK was significantly decreased to about 50%. Furthermore, myosin II activity, which was downstream of ROCK, substantially dropped to nearly 60% compared with DMSO group (Figure 7-5 c-d). In line with previous findings where 20 µM Y27 treatment enhanced FTE in SBTCs (Figure 4-7 h-l), specifically inhibited ROCK activity through siRNA decreased myosin II cytoplasmic localization and elevated FTE without shear stress pre-treatment (Figure 7-5 e-f). Hence, ROCK controlled cytoplasmic myosin II localization and FTE of SBTCs.

In summary, our data collectively suggested that while MLCK controlled myosin II cortical localization, ROCK was responsible for cytoplasmic myosin II activation and further controlled FTE under high shear stress.

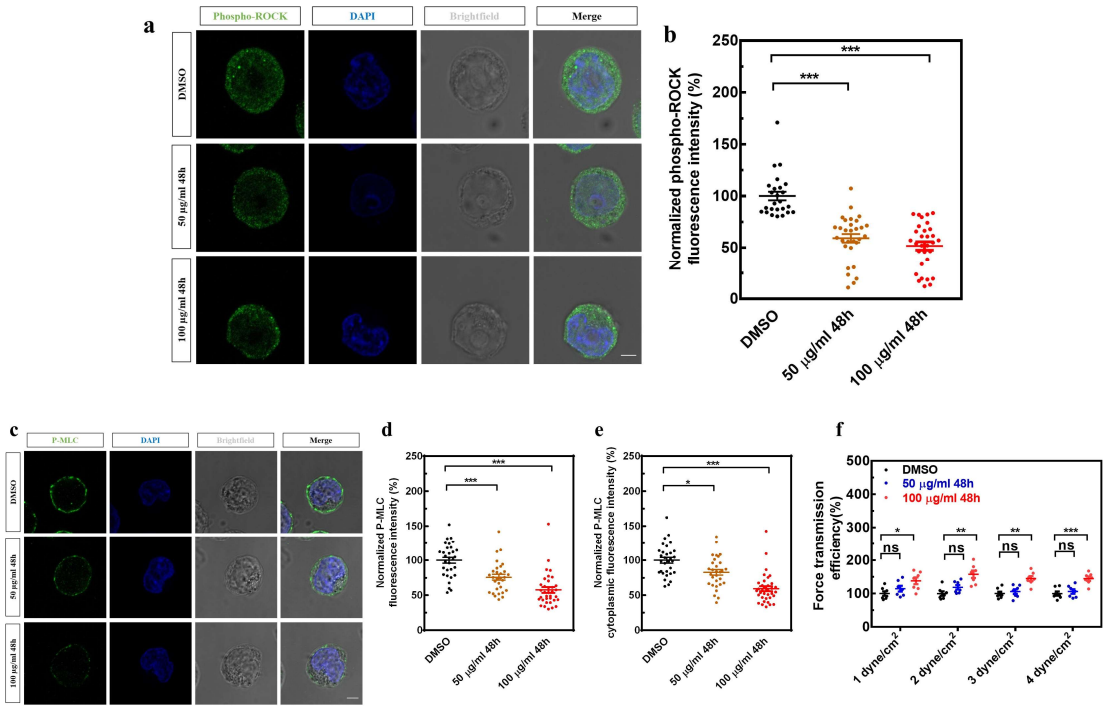

Figure 7-5 ROCK activity controls cytoplasmic myosin II localization and FTE of SBTCs. (a-b) Representative images **(a)** and quantitative data of **(b)** phospho-ROCK after doxycycline induction in SBTCs. **(c-e)** Representative images **(c)** and quantitative data of total **(d)** and cytoplasmic **(e)** myosin II activity after doxycycline induction in SBTCs. **(f)** FTE of SBTCs after

doxycycline induction. Scale bar=5 μm; N = 3 independent experiments; mean ± SEM; *, p <0.05; **, p < 0.01; and ***, p < 0.001

7.5 Targeting ROCK activity, but not MLCK, enhances SBTCs apoptosis under shear stress

Now, we have found distinct roles of MLCK and ROCK in myosin II subcellular localization and FTE. To further investigated the contributions of MLCK or ROCK in SBTCs survival and explored potential therapeutic targets, we first treated SBTCs with ML-7 to inhibit MLCK activity then quantified DNA damage as well as cell viability under high uniform FSS. The results in Figure 7-6 a-b disclosed that ML-7 cannot enhance DNA damage of SBTCs under FSS. Furthermore, inhibition of MLCK through ML-7 cannot increase cell apoptosis under high uniform FSS (Figure 7-6 c-d), indicating MLCK mediated cortical myosin II localization did not influence SBTCs survival under high shear stress.

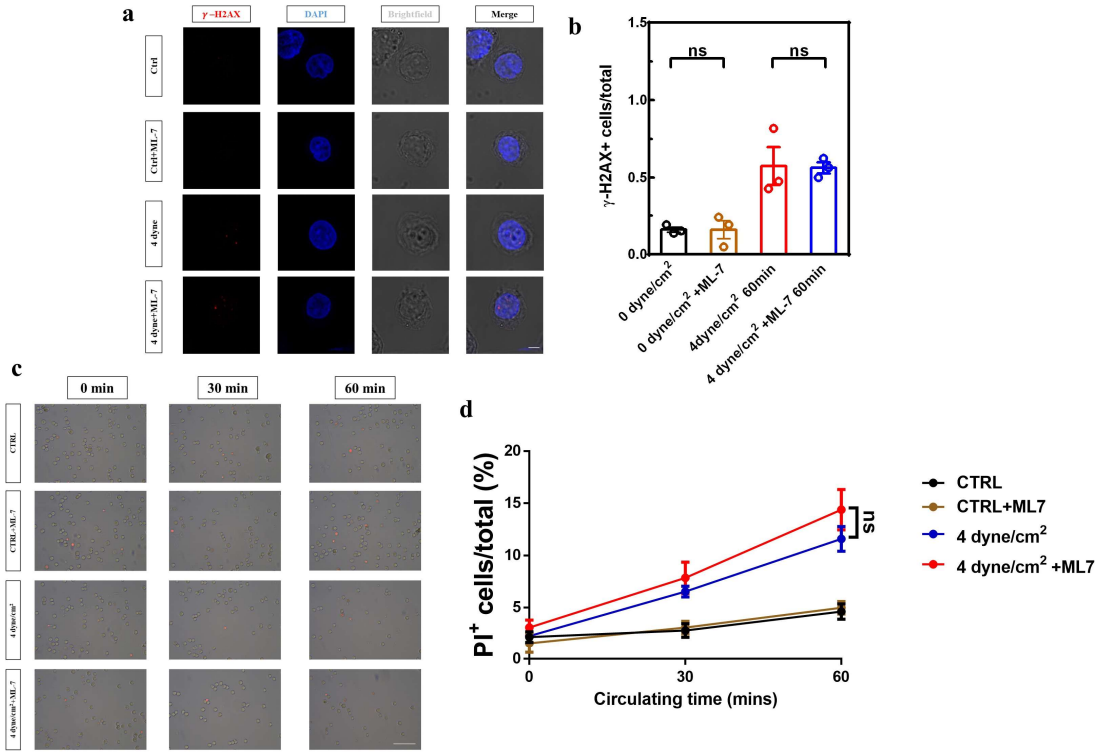

Figure 7-6 MLCK mediated cortical myosin II localization does not contribute to SBTCs survival under high uniform FSS. (a-b) Representative images **(a)** and quantitative data of **(b)** of

γ-H2AX positive cells/total after ML-7 treatment under high uniform FSS. **(c-d)** Representative images **(c)** and quantitative result **(d)** of PI positive cell/total after ML-7 treatment under high uniform FSS. Scale bar=5 μm for **(a)** and 100 μm for **(c)**; N = 3 independent experiments; mean ± SEM; *, p <0.05; **, p < 0.01; and ***, p < 0.001

As ML-7 did not influence FTE as well as cell survival under high uniform FSS, we further wanted to test whether specially targeting ROCK through siRNA enhanced SBTCs apoptosis under shear stress. To this end, we quantified PI^+ cells/total of SBTCs under high uniform FSS after knockdown *ROCK2*. Similar with the effect of Y27, knockdown *ROCK2* decreased SBTCs survival under high uniform FSS (Figure 7-7 a-b). To further confirm the role of ROCK mediated cytoplasmic myosin II localization in SBTCs survival under FSS, we used *in vitro* circulatory pump system to apply high FSS to SBTCs after knockdown *ROCK2*. The results in Figure 7-7 c-d revealed that knockdown *ROCK2* similarly enhanced SBTCs' apoptosis under high FSS.

Based on the saying above, our data suggested that ROCK, but not MLCK, mediated cytoplasmic myosin II localization helped SBTCs survival under high shear stress. Targeting ROCK activity, but not MLCK, enhances SBTCs apoptosis under shear stress *in vitro*.

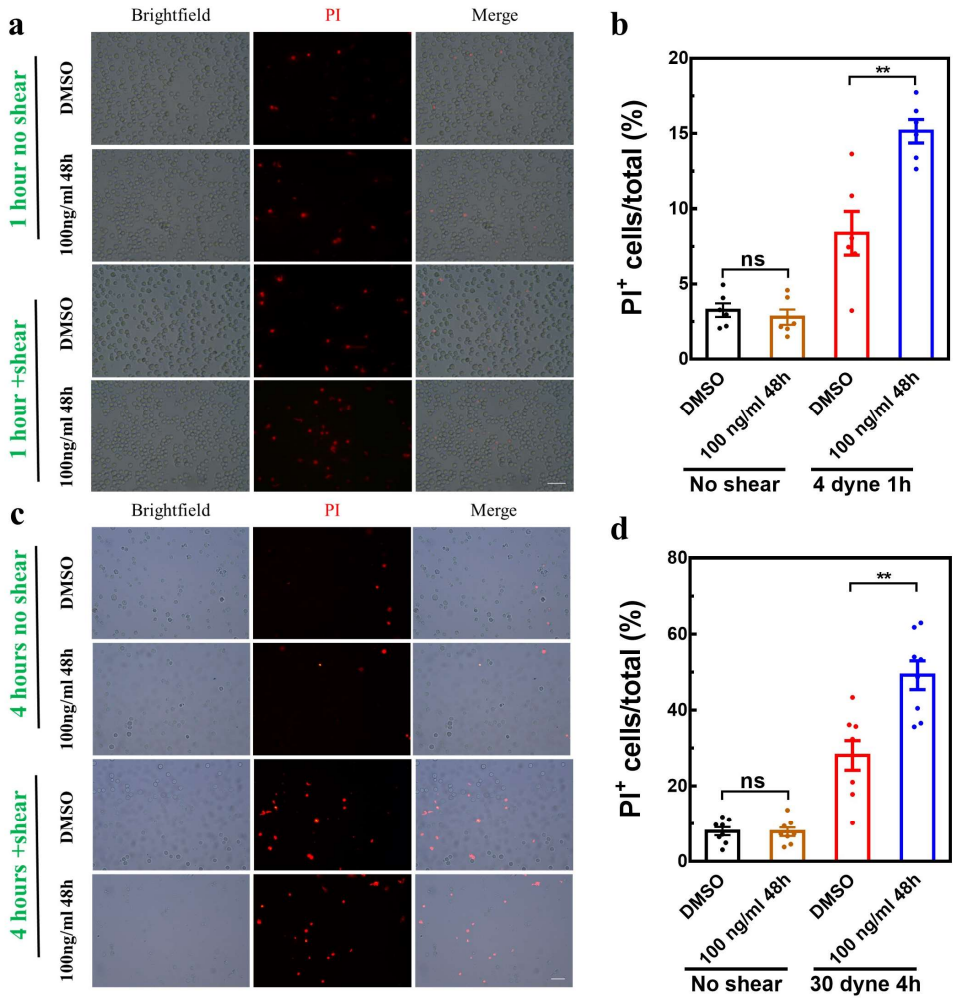

Figure 7-7 ROCK activity controls SBTCs survival under high uniform FSS. (a-b) Representative images **(a)** and quantitative data of **(b)** of PI positive cell/total after knocking down *ROCK2* through doxycycline under high uniform FSS. **(c-d)** Representative images **(c)** and quantitative data of **(d)** of PI positive cell/total after knocking down *ROCK2* through doxycycline under high FSS. Scale bar= 100 μm; N = 3 independent experiments; mean ± SEM; *, p <0.05; **, p < 0.01; and ***, p < 0.001

7.6 Mechanotransduction to cell nucleus is required for SBTCs responses under shear stress

Up to now, we have found that Lamin A/C-mediated nuclear mechanosensing orchestrated downstream cell responses including calcium release from ER (Figure 6-4), MLCK expression induced cortical myosin II localization and ROCK activation

triggered decreased FTE (Figure 7-4 and Figure 7-5). However, whether the nuclear mechanosensing need force transmission across cytoskeleton to the LINC complex and whether mechanotransduction to cell nucleus was required to elicit SBTCs responses were still unclear.

It has been well demonstrated that KASH domain of Nesprin played a crucial role in the physical linkage between cell cytoskeleton and nucleus and that DN-KASH abolishes force transmission into cell nucleus and prevents nuclear mechanosensing[125]. We thus employed DN-KASH to test whether nuclear mechanosensing of SBTCs under shear stress required the force transmission through LINC complex.

First, we transfected DN-KASH to SBTCs to prevent force transmission through LINC complex and measured FTE without shear stress pretreatment. Here, ΔPPPL was used as negative control. The result in Figure 7-8 a showed that impeding force transmission through LINC complex significantly decreased FTE, indicating mechanotransduction from cytoskeleton to LINC complex was required for nuclear deformation of SBTCs under shear stress.

As DN-KASH impeded force transmission to SBTCs nucleus, we further used this method to confirm the role of nuclear mechanosensing in our project. Consistent with previous data, DN-KASH partially rescued shear-induced Lamin A/C expression and EOP_{NE} (Figure 7-8 b-d), suggesting the important role of nuclear mechanotransduction in SBTCs under shear stress. Intriguingly, without shear treatment, DN-KASH itself decreased Lamin A/C expression and increased EOP_{NE}, suggesting that prestress applied to nucleus was required to sustain nuclear envelop tension[279, 280]. Moreover, DN-KASH abolished shear stress triggered cellular responses such as calcium release from ER (Figure 7-8 e). In line with previous findings, hampering calcium release from ER through DN-KASH inhibited myosin II cortical and cytoplasmic localization (Figure 7-8 f-i).

Based on the results shown above, mechanotransduction from cytoskeleton to cell nucleus is required for responses of SBTCs under shear stress, highlighting the

importance of nuclear mechanosensing in sensing and responding to shear stress.

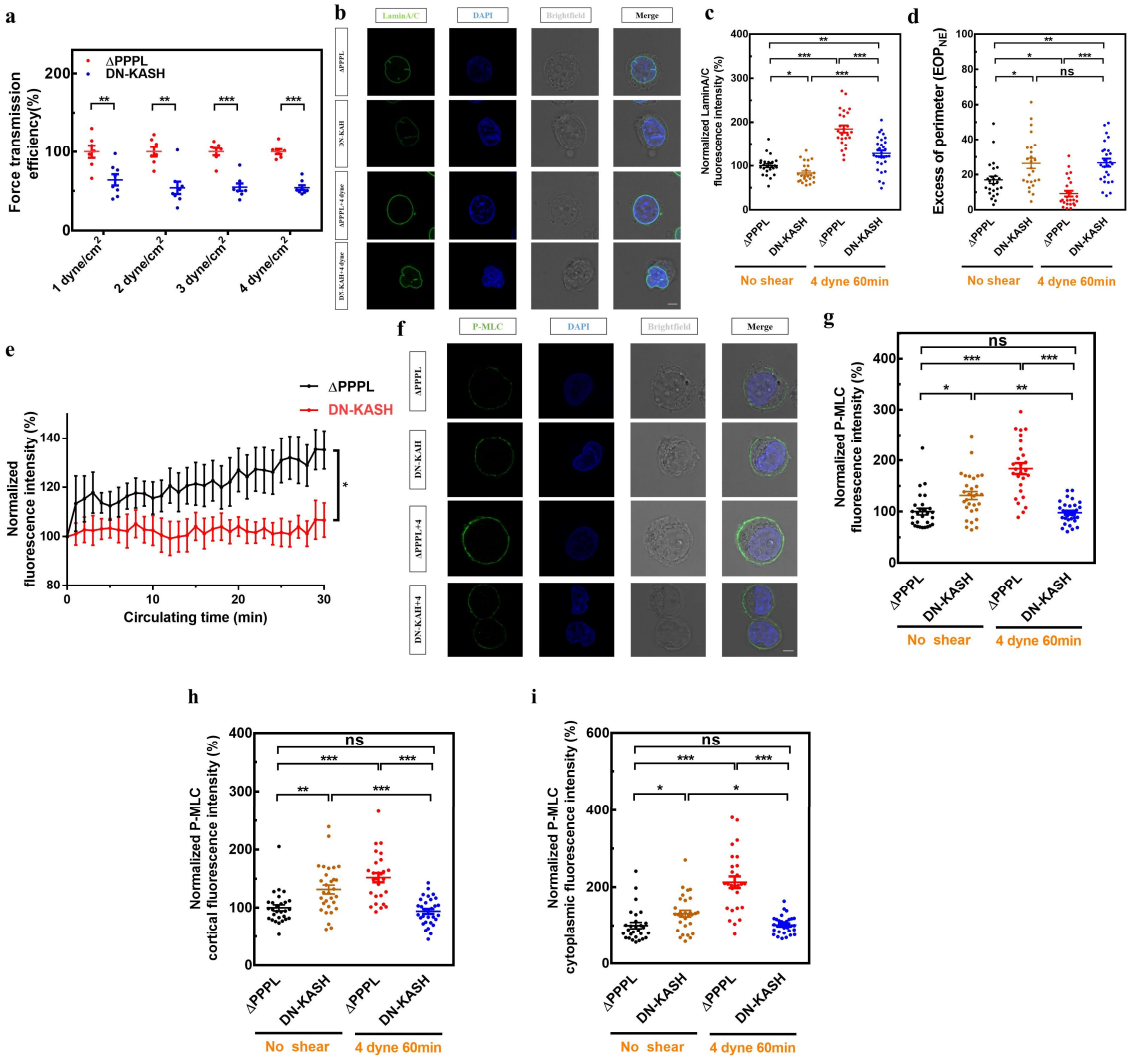

Figure 7-8 Mechanotransduction across LINC complex to nucleus is required for SBTCs responses under FSS. (a) FTE of SBTCs after transfecting DN-KASH. **(b-c)** Representative images **(b)** and quantitative data of **(c)** of Lamin A/C after transfecting DN-KASH under high uniform FSS. **(d)** EOP_{NE} of SBTCs after transfecting DN-KASH under high uniform FSS. **(e)** Dynamic change of GCaMP6 fluorescence intensity after transfecting DN-KASH under high uniform FSS. **(f-i)** Representative images **(f)** and quantitative data of total **(g)**, cortical **(h)** or cytoplasmic **(i)** P-MLC fluorescence intensity after transfecting DN-KASH under high uniform FSS. Scale bar= 5 μm; N = 3 independent experiments; mean ± SEM; *, p <0.05; **, p < 0.01; and ***, p < 0.001

Chapter 8. Conclusion

In summary, our data collectively suggested that (1) Distinct mechanosensitivity and responses of SBTCs to low or high shear stress. (2) A new mechanism by which myosin II cytoplasmic localization mediated mechanoadaptation of SBTCs affords protection of cell nucleus from mechanical distortions under shear stress. (3) Novel insights of how nuclear mechanosensing orchestrates cellular responses of SBTCs toward shear stress. (4) Distinct roles of MLCK and ROCK in myosin II subcellular distributions in SBTCs. (5) Targeting myosin II-mediated mechanoadaptation increases apoptosis of SBTCs *in vivo*.

As it was shown in Figure 5-1, under shear stress, Lamin A/C would dephosphorylate within two minutes. The dephosphorylated Lamin A/C further increases its activity and enhances NE tension. The increased NE tension then triggers calcium release from ER and increases intracellular calcium concentration. Under low shear stress, calcium release from ER induces myosin II cortical localization through binding with MLCK, whereas under high shear stress, calcium release from ER further induces myosin II cytoplasmic localization through activating ROCK. (Figure 9-1 a). The cytoplasmic myosin II localization, but not cortex, decreases FTE of SBTCs under high FSS. In this scenario, when same level of shear stress is applied on cell surface, the force transmitted to cell nucleus and induced nuclear deformation are relatively lower (Figure 9-1 b). Thus, decreased FTE affords protection of nucleus from accumulated DNA damage and thereby enhancing cell survival under shear stress. Targeting FTE through ROCK inhibition enhances the vulnerability of SBTCs under FSS both *in vitro* and *in vivo*. Our study disclosed a new mechanotransduction pathway that SBTCs utilized to respond and mechanically adapt to fluid shear flow.

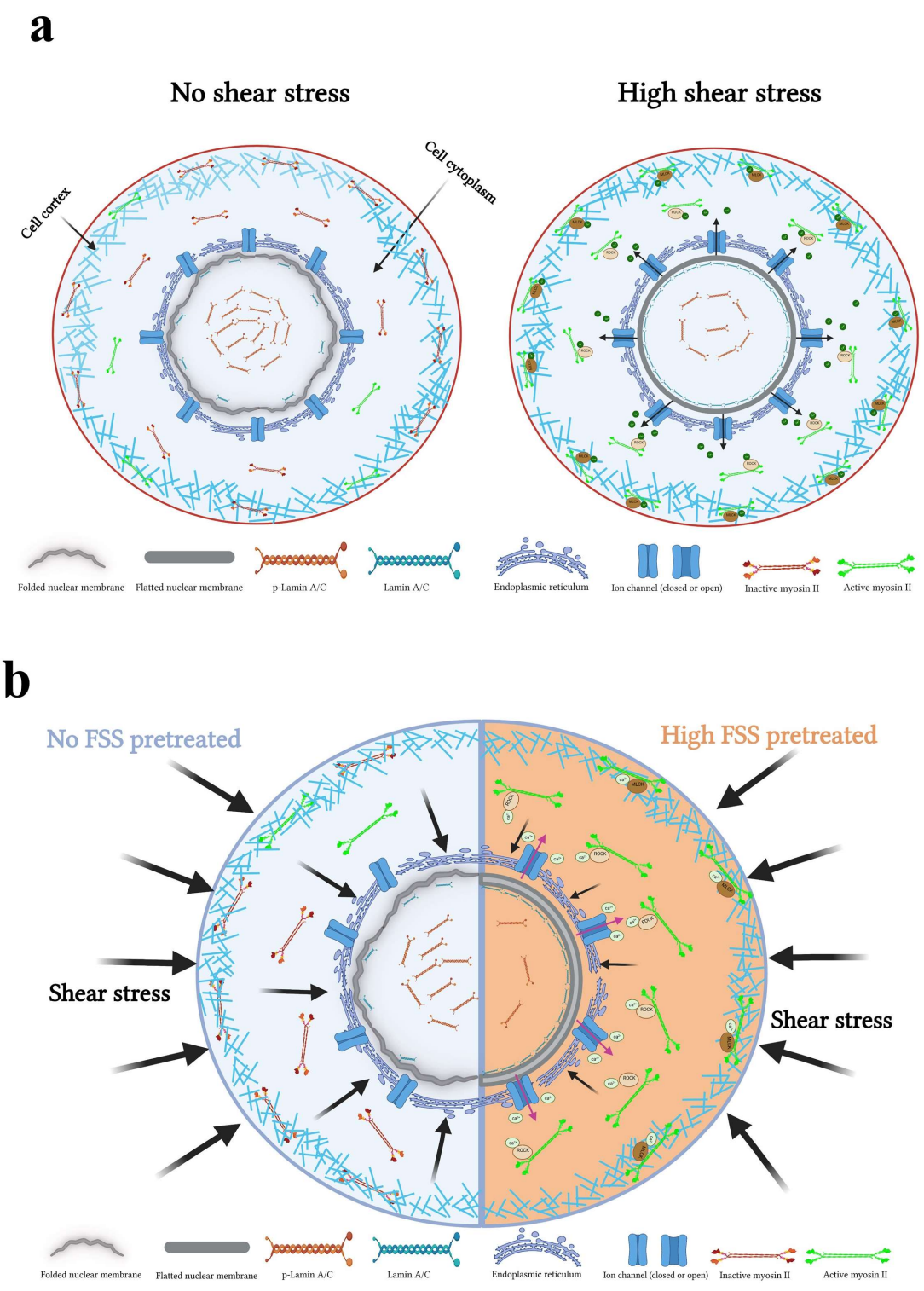

Figure 8-1 Schematic of how SBTCs sense and respond to FSS through myosin II-mediated mechanoadaptation. (a) Illustration of SBTCs responses under high FSS. **(b)** Illustration of decreased FTE under high FSS.

Chapter 9. Discussion and limitations

9.1 Discussion and future works

Cancer cells metastasis to distant organs mainly through hematogenous dissemination during which CTCs experience varying magnitudes of shear stress from 1 to 30 dyne/cm[253]. The majority of CTCs become apoptosis within vasculature, while a small subpopulation (<0.1%) can survive and grow into metastatic tumors[72], which account for over 90% of cancer deaths and become a grand challenge in cancer therapy[8]. While previous studies have enlarged our knowledge of how CTCs survive under shear stress[56, 75, 79], whether CTCs exhibit distinct responses to different levels of shear stress and how CTCs mechanically adapt to high level of shear stress were still unclear.

To solve these questions, we began to investigate whether SBTCs exhibited distinct mechanosensitivity to different magnitudes of shear stress. Here, we applied FSS in the rage from 0.5 dyne/cm^2 to 20 dyne /cm^2 to mimic shear stress level in veins, capillaries, and arteries [50]. The duration of FSS we applied was one hour. In fact, the time that CTCs travel within the blood vessel was elusive. One study using colon cancer rat model discovered that the CTCs could be blocked within the lung for four days before extravasate[66]. Based on the modeling of breast cancer after surgery, researchers found that the half-time of breast cancer CTCs was about 1-2.4 hours[254]. In line with this idea, other studies demonstrated that the time that CTCs spent during circulation was 25-30 minutes[64]. More recently, through exchanging the blood of two tumor-bearing mice and measuring the kinetics and counts of lung cancer CTCs, it was estimated that the CTCs' half-time was 40 to 260 seconds[281]. The discrepancy between the half-time of CTCs in different studies may origin from the cell types and measuring methods the researchers used. Intriguingly, CTCs may re-intravasate into blood circulation after their extravasation, indicating travel of CTCs during blood circulation was a long journey[282]. As we chose breast cancer CTCs as a model to study CTCs responses, we thus treated SBTCs for one hour and explore potential mechanism of SBTCs' mechanoadaptation under shear stress[254].

Our data suggested that SBTCs showed weaker increase rate of apoptosis under high shear stress, indicating SBTCs exhibited lower mechanosensitivity under high shear stress. To explore the potential mechanism, we focused on myosin motors which was important for mechanotransduction and mechanosensing[153]. Intriguingly, myosin II showed distinct subcellular distributions under low and high shear stress. While myosin II mainly localized at cell cortex under low shear stress, myosin II redistributed and activated in cytoplasm only under high shear stress. The different myosin II subcellular distributions suggested that SBTCs had distinct mechanotransduction machinery under low and high shear stress, which may help them to tackle physical complexities during blood circulation.

Indeed, we further found that cytoplasmic myosin II localization decreased FTE of SBTCs under high uniform FSS. The decreased FTE means that when the same level of force was applied on cell surface, the force that transmitted to nucleus and trigged nuclear deformation were relatively lower. We acknowledged that the decreased FTE we measured here may not absolutely originates from the force transmitted to cell nucleus, as nuclear stiffness also contributes to nuclear deformability and further FTE[283]. To dispel this suspicion, we used Nesprin-based tension sensor to directly measure the force across cytoskeleton to LINC complex. Our results unambiguously showed that after myosin II inhibition, the force transmitted to LINC complex indeed increased, indicating myosin II activity negatively regulates force transmitted to LINC complex in SBTCs. However, although tension-sensing modules of Nesprin-based tension sensor was design to exhibits linear response to external force magnitudes[284, 285], we cannot gauge whether this tension sensor linearly response to force when it was transfected to living cells. Thus, we cannot get the specific numerical value of how much force was transmitted to LINC complex through FRET index of Nesprin-based tension sensor. Future development and calibration of tension sensor in living cells may help us to quantify how much force was transmitted to cell nucleus.

Second, through pharmacological inhibition, our data suggested that cytoplasmic myosin II localization, but not cortical, decreased FTE of SBTCs. This finding was in

line with the role of myosin II in adherent cells, where cytoskeletal contractility was mainly responsible for mechanotransduction from cell surface to cell nucleus[120]. The significance of cytoplasmic myosin II activity in force transmission did not meaning that cortical myosin II localization we found here was dispensable for SBTCs function under shear stress, as previous study had already found that myosin II activity facilitated CTCs survival through membrane repair[79]. Further functional analysis of myosin II cortical localization will improve our understanding of regionally activated myosin II in SBTCs during shear flow.

The finding that cytoplasmic myosin II activity negatively regulates FTE in SBTCs seems contradictory to our common understanding of force transduction, in which actomyosin contractility was indispensable for mechanotransduction in adherent cells[103, 225]. However, recent study suggested enhanced myosin II activity soften suspended cell, which was in great contrast to the role of actomyosin in adherent cells, where inhibition of myosin II activity decrease cell stiffness[183]. Thus, our study, combined with former one, strongly suggested that myosin II had distinct functions in suspended cells compared with adherent cells.

So, what is the underlying mechanism of decreased FTE of SBTCs? Our data showed that myosin II cytoplasmic localization was both required and sufficient to regulate FTE of SBTCs. As mentioned before, mechanotransduction across the cytoskeleton required certain level of actomyosin contractility[120]. The generation of cell contractility was mainly through myosin motors bind and interact with actin filaments. Thus, it was possible that myosin II showed weaker interaction with actin filaments that further decreased FTE in SBTCs. Another potential explanation of decreased FTE was due to physical properties of cell cytoplasm. Cells were widely regarded as viscoelastic materials, meaning that it exhibited both elasticity and viscosity under certain scenario[202]. In term of mechanotransduction, while cell elasticity facilitated force transmission, viscosity led to energy dissipation and impeded force transduction[286]. Recent investigation in how contractility transmitted from SFs to ECM found that low α-actinin level induced slippage between F-actin and F-actin, leading to more friction

during contractility transfer, finally resulted in less efficient force transmission[287]. Strikingly, recent studies have found that activated myosin II could endow the network softer[173] and more liquid-like[288]. Thus, combined with previous finding that myosin II activity softened suspended cells[173], it was likely that cytoplasmic myosin II localization in SBTCs triggered fluidization of cytoplasm, thus increasing energy dissipation during force transmission and leading to decreased FTE. Further study needs to focus on whether and how cytoplasmic viscosity influences force transmission process in suspended cells.

It has been found that DNA damage could influence nuclear mechanics in adherent cells [267, 268]. In contrast, out result indicated that DNA damage did not feedback to myosin II activation and mechanotransduction in suspended tumor cells. This may be caused by the higher resistance of suspended cells to DNA damage compared with adherent cells[289]. Further research is needed to decipher the underlying molecular mechanisms.

During last decades, emerging findings have suggested that nucleus itself works as a mechanosensor[207]. Our group also discovered nuclear expansion via histone acetylation of SBTCs under shear stress[77]. Here, our data suggest that nuclear mechanosensing orchestrates downstream cellular responses, including myosin II subcellular distribution and FTE. As one part of nucleoskeleton, Lamin A/C expression changed at five to ten minutes after shear treatment. Intriguingly, Lamin A/C was rapidly dephosphorylated within two minutes under high shear stress, indicating post-transcriptional modifications, instead of protein synthesis, which served as an immediate response of SBTCs toward external mechanical stimuli[290]. It was noteworthy that while Lamin A/C expression was altered under shear stress, it may not contribute to nuclear stiffness, as previous study found that Lamin A/C contributed to nuclear stiffness only under large strain (>3 μm)[291, 292]. Thus, in our scenario, Lamin A/C upregulation itself may not influence nuclear stiffness and FTE, as SBTCs exhibited relatively lower nuclear deformation (< 1 μm) under shear stress.

Nuclear mechanosensing strongly depends on NE tension, which triggers NPC

expansion[208, 210], NE rapture[216, 217] and calcium release from ER[212]. Our data strongly suggested that Lamin A/C expression regulates NE tension. This assumption was valid as Lamin A/C served as nucleoskeleton and sustained nuclear structure[270]. However, direct evidence that Lamin A/C governs NE tension was still lacking, as there was no NE tension sensor nowadays to directly measuring and comparing NE tension. Future development of NE tension sensor will undoubtedly enhance our understanding of how NE tension is established and regulated.

To further deciphered how Lamin A/C-mediated nuclear mechanosensing induce myosin II subcellular distribution, we focused on calcium ions, whose importance has been shown in endothelial cells responses to shear flow[85]. Intriguingly, we found calcium release from ER was synchronized with Lamin A/C activity, suggesting NE tension control calcium release. Indeed, interfering with Lamin A/C expression abolished shear stress-induced calcium response. As calcium activated both MLCK and ROCK[26, 176], we further systematically investigated MLCK and ROCK activation under shear stress. Although both MLCK and ROCK can be regulated by nuclear mechanosensing mediated by Lamin A/C, only ROCK activity can be rescued by Tg treatment. This may attribute to MLCK we measured here was protein expression, which depended on nuclear mechanosensing but not calcium ion. Instead, ROCK activation through phosphorylation can be stimulated by high calcium concentration[293].

It has been found that MLCK and ROCK differentially regulated myosin II subcellular localization in adherent cells[187]. Intriguingly, our results suggested that MLCK and ROCK also showed distinct responses to shear stress, which led to different myosin II subcellular localization. While low shear stress was sufficient to trigger MLCK expression, only high shear stress induced ROCK phosphorylation and further myosin II cytoplasmic localization. The distinct responses of MLCK and ROCK to shear stress may because of the competition between[188]. Moreover, our results proved that MLCK regulated cortical myosin II localization while ROCK regulated cytoplasmic myosin II activity. Notably, recent study found that MLCK induces monophosphorylation of RLC in peripheral SFs, while ROCK triggers dephosphorylation of RLC in central SFs. Thus,

it was plausible that monophosphorylation of RLC mainly happened in cell cortex while dephosphorylation of RLC predominantly happened in cell cytoplasm in SBTCs. Future researches are needed to ascertain whether and how RLC monophosphorylation or dephosphorylation regulates myosin II subcellular localization, particularly regarding the functions of MLCK and ROCK.

Finally, our data showed that inhibition of ROCK, but not MLCK, enhanced DNA damage and cell apoptosis of SBTCs under shear stress *in vitro*. Targeting myosin II activity through pharmacological inhibition for short-term (12h) elevated SBTCs apoptosis during blood circulation *in vivo*. These unforeseen findings highlight the role of cytoplasmic myosin II localization mediated FTE in SBTCs survival under high shear stress. As survival of CTCs during blood circulation was prerequisite for seeding metastasis, our results indicated that myosin II activity was a potential clinical target for preventing cancer metastasis. Furthermore, our results provided a promising insight in clinical usage of ROCK inhibitors, which has been widely tested in phase 1 to phase 4 clinical trial[294]. Now, we are preparing mice model to systematically study long-term effects of myosin II inhibition during circulation, which may give us comprehensive understanding of myosin II-mediated mechanoadaptation in cancer metastasis.

9.2 Limitations

Although we have disclosed a previously unappreciated role of cytoplasmic myosin II localization in mechanoadaptation of SBTCs under FSS, there were still some limitations in our study. At first, the suspended tumor cells we used in this study were come from cell line cultured in laboratory but not CTCs separated from cancer patients, which may hinder the clinical application of our study. Second, the FTE we measured here was based on resultant nuclear strain under shear stress. As nuclear strain was determined by both stress and nuclear stiffness, we cannot fully exclude the possibility that nuclear stiffness was changed under shear stress that further contributed to FTE we measured here. Last but not least, although we have proved that on PLL coated substrate, SBTCs show similar responses to different levels of shear stress compared with real

suspended status, the effective deformation of SBTCs attached to PLL coated substrate was quite different from CTCs *in vivo*, as CTCs *in vivo* were flowed with shear stress and spin. Further theoretical modeling of SBTCs attached to PLL coated substrate could help us to better understand the force profile that cell sensed.

Reference

1. Siegel, R.L., Miller, K.D., Fuchs, H.E. & Jemal, A. Cancer Statistics, 2021. *CA Cancer J Clin* **71**, 7-33 (2021).
2. Sung, H. *et al.* Global Cancer Statistics 2020: GLOBOCAN Estimates of Incidence and Mortality Worldwide for 36 Cancers in 185 Countries. *CA Cancer J Clin* **71**, 209-249 (2021).
3. Siegel, R.L., Miller, K.D., Wagle, N.S. & Jemal, A. Cancer statistics, 2023. *CA Cancer J Clin* **73**, 17-48 (2023).
4. Nolan, E., Lindeman, G.J. & Visvader, J.E. Deciphering breast cancer: from biology to the clinic. *Cell* **186**, 1708-1728 (2023).
5. Wang, H. & Mao, X. Evaluation of the Efficacy of Neoadjuvant Chemotherapy for Breast Cancer. *Drug Des Devel Ther* **14**, 2423-2433 (2020).
6. Abbott, M. & Ustoyev, Y. Cancer and the Immune System: The History and Background of Immunotherapy. *Semin Oncol Nurs* **35**, 150923 (2019).
7. Ferlay, J. *et al.* Cancer statistics for the year 2020: An overview. *Int J Cancer* (2021).
8. Jonckheere, S. *et al.* Epithelial-Mesenchymal Transition (EMT) as a Therapeutic Target. *Cells Tissues Organs* **211**, 157-182 (2022).
9. Liang, Y., Zhang, H., Song, X. & Yang, Q. Metastatic heterogeneity of breast cancer: Molecular mechanism and potential therapeutic targets. *Semin Cancer Biol* **60**, 14-27 (2020).
10. Welch, D.R. & Hurst, D.R. Defining the Hallmarks of Metastasis. *Cancer Res* **79**, 3011-3027 (2019).
11. Gerstberger, S., Jiang, Q. & Ganesh, K. Metastasis. *Cell* **186**, 1564-1579 (2023).
12. van Neerven, S.M. *et al.* Apc-mutant cells act as supercompetitors in intestinal tumour initiation. *Nature* **594**, 436-441 (2021).
13. Coburn, L. *et al.* Role of contact inhibition of locomotion and junctional mechanics in epithelial collective responses to injury. *Phys Biol* **15**, 024001 (2018).

14. Del Poggetto, E. *et al.* Epithelial memory of inflammation limits tissue damage while promoting pancreatic tumorigenesis. *Science* **373**, eabj0486 (2021).
15. Nissen, N.I., Karsdal, M. & Willumsen, N. Collagens and Cancer associated fibroblasts in the reactive stroma and its relation to Cancer biology. *J Exp Clin Cancer Res* **38**, 115 (2019).
16. Nia, H.T., Munn, L.L. & Jain, R.K. Physical traits of cancer. *Science* **370** (2020).
17. Paget, S. The distribution of secondary growths in cancer of the breast. 1889. *Cancer Metastasis Rev* **8**, 98-101 (1989).
18. Reuten, R. *et al.* Basement membrane stiffness determines metastases formation. *Nat Mater* **20**, 892-903 (2021).
19. Pothapragada, S.P., Gupta, P., Mukherjee, S. & Das, T. Matrix mechanics regulates epithelial defence against cancer by tuning dynamic localization of filamin. *Nat Commun* **13**, 218 (2022).
20. Vishwakarma, M. & Piddini, E. Outcompeting cancer. *Nat Rev Cancer* **20**, 187-198 (2020).
21. Moreno, E. Is cell competition relevant to cancer? *Nat Rev Cancer* **8**, 141-147 (2008).
22. Panciera, T. *et al.* Reprogramming normal cells into tumour precursors requires ECM stiffness and oncogene-mediated changes of cell mechanical properties. *Nat Mater* **19**, 797-806 (2020).
23. Hupfer, A. *et al.* Matrix stiffness drives stromal autophagy and promotes formation of a protumorigenic niche. *Proc Natl Acad Sci U S A* **118** (2021).
24. Wu, B. *et al.* Stiff matrix induces exosome secretion to promote tumour growth. *Nat Cell Biol* **25**, 415-424 (2023).
25. Sneider, A. *et al.* Small extracellular vesicles promote stiffness-mediated metastasis. *bioRxiv* (2023).
26. Bera, K. *et al.* Extracellular fluid viscosity enhances cell migration and cancer dissemination. *Nature* **611**, 365-373 (2022).
27. Tsujita, K. *et al.* Homeostatic membrane tension constrains cancer cell dissemination by counteracting BAR protein assembly. *Nat Commun* **12**, 5930

(2021).

28. Liu, Y. *et al.* Cell Softness Prevents Cytolytic T-cell Killing of Tumor-Repopulating Cells. *Cancer Res* **81**, 476-488 (2021).
29. Chang, Y. *et al.* Substrate rigidity dictates colorectal tumorigenic cell stemness and metastasis via CRAD-dependent mechanotransduction. *Cell Rep* **38**, 110390 (2022).
30. Micalizzi, D.S., Maheswaran, S. & Haber, D.A. A conduit to metastasis: circulating tumor cell biology. *Genes Dev* **31**, 1827-1840 (2017).
31. Ashworth, T.R. A case of cancer in which cells similar to those in the tumors were seen in the blood after death. *Australas. Med. J.* **14** (1869).
32. Butler, T.P. & Gullino, P.M. Quantitation of cell shedding into efferent blood of mammary adenocarcinoma. *Cancer Res* **35**, 512-516 (1975).
33. Monzo, P. *et al.* Adaptive mechanoproperties mediated by the formin FMN1 characterize glioblastoma fitness for invasion. *Dev Cell* **56**, 2841-2855.e2848 (2021).
34. Aceto, N. *et al.* Circulating tumor cell clusters are oligoclonal precursors of breast cancer metastasis. *Cell* **158**, 1110-1122 (2014).
35. Jin, T. *et al.* Association between circulating tumor cells in the peripheral blood and the prognosis of gastric cancer patients: a meta-analysis. *Ther Adv Med Oncol* **15**, 17588359231183678 (2023).
36. Danila, D.C. *et al.* Circulating tumor cell number and prognosis in progressive castration-resistant prostate cancer. *Clin Cancer Res* **13**, 7053-7058 (2007).
37. Perea Paizal, J., Au, S.H. & Bakal, C. Squeezing through the microcirculation: survival adaptations of circulating tumour cells to seed metastasis. *Br J Cancer* **124**, 58-65 (2021).
38. Baccelli, I. *et al.* Co-expression of MET and CD47 is a novel prognosticator for survival of luminal breast cancer patients. *Oncotarget* **5**, 8147-8160 (2014).
39. Paoletti, C. *et al.* Comprehensive Mutation and Copy Number Profiling in Archived Circulating Breast Cancer Tumor Cells Documents Heterogeneous Resistance Mechanisms. *Cancer Res* **78**, 1110-1122 (2018).

40. Ring, A., Nguyen-Sträuli, B.D., Wicki, A. & Aceto, N. Biology, vulnerabilities and clinical applications of circulating tumour cells. *Nat Rev Cancer* **23**, 95-111 (2023).

41. Fina, E. *et al.* Gene signatures of circulating breast cancer cell models are a source of novel molecular determinants of metastasis and improve circulating tumor cell detection in patients. *J Exp Clin Cancer Res* **41**, 78 (2022).

42. Lambert, A.W., Pattabiraman, D.R. & Weinberg, R.A. Emerging Biological Principles of Metastasis. *Cell* **168**, 670-691 (2017).

43. Crosby., D. *et al.* Early detection of cancer. *Science* **375** (2022).

44. Hansem, L.M.K. *et al.* Intratumor Heterogeneity in Interstitial Fluid Pressure in Cervical and Pancreatic Carcinoma Xenografts. *Transl Oncol* **12**, 1079-1085 (2019).

45. Deng, B. *et al.* Biological role of matrix stiffness in tumor growth and treatment. *J Transl Med* **20**, 540 (2022).

46. Forster, J.C., Harriss-Phillips, W.M., Douglass, M.J. & Bezak, E. A review of the development of tumor vasculature and its effects on the tumor microenvironment. *Hypoxia (Auckl)* **5**, 21-32 (2017).

47. Li, J. *et al.* Targeted drug delivery to circulating tumor cells via platelet membrane-functionalized particles. *Biomaterials* **76**, 52-65 (2016).

48. Ildiz, E.S., Gvozdenovic, A., Kovacs, W.J. & Aceto, N. Travelling under pressure - hypoxia and shear stress in the metastatic journey. *Clin Exp Metastasis* (2023).

49. Pereira-Veiga, T., Schneegans, S., Pantel, K. & Wikman, H. Circulating tumor cell-blood cell crosstalk: Biology and clinical relevance. *Cell Rep* **40**, 111298 (2022).

50. Huang, Q. *et al.* Fluid shear stress and tumor metastasis. *Am J Cancer Res* **8**, 763-777 (2018).

51. Lorenzo-Herrero, S. *et al.* NK Cell-Based Immunotherapy in Cancer Metastasis. *Cancers (Basel)* **11** (2018).

52. Osmulski, P.A. *et al.* Contacts with Macrophages Promote an Aggressive

Nanomechanical Phenotype of Circulating Tumor Cells in Prostate Cancer. *Cancer Res* **81**, 4110-4123 (2021).

53. Shivam Rajput., Pramod Kumar Sharma. & Malviya, R. Fluid mechanics in circulating tumour cells: Role in metastasis and treatment strategies. *Medicine in Drug Discovery* **18** (2023).
54. Regmi, S., Fu, A. & Luo, K.Q. High Shear Stresses under Exercise Condition Destroy Circulating Tumor Cells in a Microfluidic System. *Sci Rep* **7**, 39975 (2017).
55. Fan, R. *et al.* Circulatory shear flow alters the viability and proliferation of circulating colon cancer cells. *Sci Rep* **6**, 27073 (2016).
56. Xin, Y. *et al.* Mechanics and Actomyosin-Dependent Survival/Chemoresistance of Suspended Tumor Cells in Shear Flow. *Biophys J* **116**, 1803-1814 (2019).
57. Goh., A., PaI., P.C., ChenG., G., Ho., Y.P. & Lei., K.F. Modulation of cancer stemness property in head and neck cancer cells via circulatory fluid shear stress. *Microfluidics and Nanofluidics* **26:37** (2022).
58. Xin, Y., Li, K., Yang, M. & Tan, Y. Fluid Shear Stress Induces EMT of Circulating Tumor Cells via JNK Signaling in Favor of Their Survival during Hematogenous Dissemination. *Int J Mol Sci* **21** (2020).
59. Li, S.S. *et al.* Sialyl Lewis(x)-P-selectin cascade mediates tumor-mesothelial adhesion in ascitic fluid shear flow. *Nat Commun* **10**, 2406 (2019).
60. Varotsos Vrynas, A., Perea Paizal, J., Bakal, C. & Au, S.H. Arresting metastasis within the microcirculation. *Clin Exp Metastasis* **38**, 337-342 (2021).
61. Follain, G. *et al.* Hemodynamic Forces Tune the Arrest, Adhesion, and Extravasation of Circulating Tumor Cells. *Dev Cell* **45**, 33-52.e12 (2018).
62. Zhou, M., Li, K. & Luo, K.Q. Shear Stress Drives the Cleavage Activation of Protease-Activated Receptor 2 by PRSS3/Mesotrypsin to Promote Invasion and Metastasis of Circulating Lung Cancer Cells. *Adv Sci (Weinh)*, e2301059 (2023).
63. Zhao, B., Tang, M. & Lv, Y. Shear stress regulates the migration of suspended breast cancer cells by nuclear lamina protein A/C and large tumor suppressor through yes-associated protein. *Hum Cell* **35**, 583-598 (2022).

64. Follain, G. *et al.* Fluids and their mechanics in tumour transit: shaping metastasis. *Nat Rev Cancer* **20**, 107-124 (2020).

65. Azevedo, A.S., Follain, G., Patthabhiraman, S., Harlepp, S. & Goetz, J.G. Metastasis of circulating tumor cells: favorable soil or suitable biomechanics, or both? *Cell Adh Migr* **9**, 345-356 (2015).

66. Mook, O.R. *et al.* Visualization of early events in tumor formation of eGFP-transfected rat colon cancer cells in liver. *Hepatology* **38**, 295-304 (2003).

67. Glinskii, O.V. *et al.* Mechanical entrapment is insufficient and intercellular adhesion is essential for metastatic cell arrest in distant organs. *Neoplasia* **7**, 522-527 (2005).

68. Cognart, H.A., Viovy, J.L. & Villard, C. Fluid shear stress coupled with narrow constrictions induce cell type-dependent morphological and molecular changes in SK-BR-3 and MDA-MB-231 cells. *Sci Rep* **10**, 6386 (2020).

69. Furlow, P.W. *et al.* Mechanosensitive pannexin-1 channels mediate microvascular metastatic cell survival. *Nat Cell Biol* **17**, 943-952 (2015).

70. Ballermann, B.J., Dardik, A., Eng, E. & Liu, A. Shear stress and the endothelium. *Kidney Int Suppl* **67**, S100-108 (1998).

71. Jin, J., Tang, K., Xin, Y., Zhang, T. & Tan, Y. Hemodynamic shear flow regulates biophysical characteristics and functions of circulating breast tumor cells reminiscent of brain metastasis. *Soft Matter* **14**, 9528-9533 (2018).

72. Potdar., P.D. & Lotey., N.K. Role of circulating tumor cells in future diagnosis and therapy of cancer. *Journal of Cancer Metastasis and Treatment* **1** (2015).

73. Zhang, C. *et al.* Modified heparins inhibit integrin alpha(IIb)beta(3) mediated adhesion of melanoma cells to platelets in vitro and in vivo. *Int J Cancer* **125**, 2058-2065 (2009).

74. Hope, J.M. *et al.* Circulating prostate cancer cells have differential resistance to fluid shear stress-induced cell death. *J Cell Sci* **134** (2021).

75. Mitchell, M.J. *et al.* Lamin A/C deficiency reduces circulating tumor cell resistance to fluid shear stress. *Am J Physiol Cell Physiol* **309**, C736-746 (2015).

76. Ouchi, M. *et al.* Decreased lamin A and B1 expression results in nuclear

enlargement in serous ovarian carcinoma, whereas lamin A-expressing tumor cells metastasize to lymph nodes. *Pathol Res Pract* **247**, 154560 (2023).

77. Xu, Z. *et al.* Fluid shear stress regulates the survival of circulating tumor cells via nuclear expansion. *J Cell Sci* **135** (2022).
78. Fu, A. *et al.* Tumor-resident intracellular microbiota promotes metastatic colonization in breast cancer. *Cell* **185**, 1356-1372.e1326 (2022).
79. Moose, D.L. *et al.* Cancer Cells Resist Mechanical Destruction in Circulation via RhoA/Actomyosin-Dependent Mechano-Adaptation. *Cell Rep* **30**, 3864-3874.e3866 (2020).
80. Kechagia, J.Z., Ivaska, J. & Roca-Cusachs, P. Integrins as biomechanical sensors of the microenvironment. *Nat Rev Mol Cell Biol* **20**, 457-473 (2019).
81. Wang, N., Butler, J.P. & Ingber, D.E. Mechanotransduction across the cell surface and through the cytoskeleton. *Science* **260**, 1124-1127 (1993).
82. Rehman, S. & Dimri, M. Biochemistry, G Protein Coupled Receptors, in *StatPearls* (StatPearls Publishing

Copyright © 2023, StatPearls Publishing LLC., Treasure Island (FL) ineligible companies. Disclosure: Manjari Dimri declares no relevant financial relationships with ineligible companies.; 2023).

83. Qin, L. *et al.* Roles of mechanosensitive channel Piezo1/2 proteins in skeleton and other tissues. *Bone Res* **9**, 44 (2021).
84. Barbarino, F. *et al.* Targeting spectrin redox switches to regulate the mechanoproperties of red blood cells. *Biol Chem* **402**, 317-331 (2021).
85. Mylvaganam, S. *et al.* The spectrin cytoskeleton integrates endothelial mechanoresponses. *Nat Cell Biol* **24**, 1226-1238 (2022).
86. Chugh, P. *et al.* Actin cortex architecture regulates cell surface tension. *Nat Cell Biol* **19**, 689-697 (2017).
87. Chugh, P. & Paluch, E.K. The actin cortex at a glance. *J Cell Sci* **131** (2018).
88. Truong Quang, B.A. *et al.* Extent of myosin penetration within the actin cortex regulates cell surface mechanics. *Nat Commun* **12**, 6511 (2021).
89. De Belly, H. *et al.* Cell protrusions and contractions generate long-range

membrane tension propagation. *Cell* **186**, 3049-3061.e3015 (2023).

90. Bergert, M. *et al.* Cell Surface Mechanics Gate Embryonic Stem Cell Differentiation. *Cell Stem Cell* **28**, 209-216.e204 (2021).
91. De Belly, H. *et al.* Membrane Tension Gates ERK-Mediated Regulation of Pluripotent Cell Fate. *Cell Stem Cell* **28**, 273-284.e276 (2021).
92. He, L. *et al.* Role of membrane-tension gated Ca(2+) flux in cell mechanosensation. *J Cell Sci* **131** (2018).
93. Hammarton, T.C. Who Needs a Contractile Actomyosin Ring? The Plethora of Alternative Ways to Divide a Protozoan Parasite. *Front Cell Infect Microbiol* **9**, 397 (2019).
94. Duszyc, K. *et al.* Mechanotransduction activates RhoA in the neighbors of apoptotic epithelial cells to engage apical extrusion. *Curr Biol* **31**, 1326-1336.e1325 (2021).
95. Gomis Perez, C. *et al.* Rapid propagation of membrane tension at retinal bipolar neuron presynaptic terminals. *Sci Adv* **8**, eabl4411 (2022).
96. Rodrigues-Oliveira, T. *et al.* Actin cytoskeleton and complex cell architecture in an Asgard archaeon. *Nature* **613**, 332-339 (2023).
97. Hohmann, T. & Dehghani, F. The Cytoskeleton-A Complex Interacting Meshwork. *Cells* **8** (2019).
98. Romet-Lemonne, G. & Jégou, A. The dynamic instability of actin filament barbed ends. *J Cell Biol* **220** (2021).
99. Rottner, K., Faix, J., Bogdan, S., Linder, S. & Kerkhoff, E. Actin assembly mechanisms at a glance. *J Cell Sci* **130**, 3427-3435 (2017).
100. Knerr, J. *et al.* Formin-mediated nuclear actin at androgen receptors promotes transcription. *Nature* **617**, 616-622 (2023).
101. Hwang, Y. & Barakat, A.I. Dynamics of mechanical signal transmission through prestressed stress fibers. *PLoS One* **7**, e35343 (2012).
102. López-Gay, J.M. *et al.* Apical stress fibers enable a scaling between cell mechanical response and area in epithelial tissue. *Science* **370** (2020).
103. Wei, F. *et al.* Stress fiber anisotropy contributes to force-mode dependent

chromatin stretching and gene upregulation in living cells. *Nat Commun* **11**, 4902 (2020).

104. Ingber, D.E., Wang, N. & Stamenovic, D. Tensegrity, cellular biophysics, and the mechanics of living systems. *Rep Prog Phys* **77**, 046603 (2014).

105. Li, Y. *et al.* Compressive forces stabilize microtubules in living cells. *Nat Mater* **22**, 913-924 (2023).

106. Nasrin, S.R. *et al.* Deformation of microtubules regulates translocation dynamics of kinesin. *Sci Adv* **7**, eabf2211 (2021).

107. Villars, A., Matamoro-Vidal, A., Levillayer, F. & Levayer, R. Microtubule disassembly by caspases is an important rate-limiting step of cell extrusion. *Nat Commun* **13**, 3632 (2022).

108. Renkawitz, J. *et al.* Nuclear positioning facilitates amoeboid migration along the path of least resistance. *Nature* **568**, 546-550 (2019).

109. Janke, C. & Magiera, M.M. The tubulin code and its role in controlling microtubule properties and functions. *Nat Rev Mol Cell Biol* **21**, 307-326 (2020).

110. Torrino, S. *et al.* Mechano-induced cell metabolism promotes microtubule glutamylation to force metastasis. *Cell Metab* **33**, 1342-1357.e1310 (2021).

111. Block, J. *et al.* Viscoelastic properties of vimentin originate from nonequilibrium conformational changes. *Sci Adv* **4**, eaat1161 (2018).

112. Tang, D.D., Liao, G. & Gerlach, B.D. Reorganization of the Vimentin Network in Smooth Muscle. *J Eng Sci Med Diagn Ther* **2**, 0108011-0108015 (2019).

113. Kreplak, L., Bär, H., Leterrier, J.F., Herrmann, H. & Aebi, U. Exploring the mechanical behavior of single intermediate filaments. *J Mol Biol* **354**, 569-577 (2005).

114. Lammerding, J. *et al.* Lamins A and C but not lamin B1 regulate nuclear mechanics. *J Biol Chem* **281**, 25768-25780 (2006).

115. Tang, Y., Zhu, L., Cho, J.S., Li, X.Y. & Weiss, S.J. Matrix remodeling controls a nuclear lamin A/C-emerin network that directs Wnt-regulated stem cell fate. *Dev Cell* **57**, 480-495.e486 (2022).

116. Seetharaman, S. *et al.* Microtubules tune mechanosensitive cell responses. *Nat*

Mater (2021).

117. Schaedel, L., Lorenz, C., Schepers, A.V., Klumpp, S. & Köster, S. Vimentin intermediate filaments stabilize dynamic microtubules by direct interactions. *Nat Commun* **12**, 3799 (2021).
118. Jiu, Y. *et al.* Vimentin intermediate filaments control actin stress fiber assembly through GEF-H1 and RhoA. *J Cell Sci* **130**, 892-902 (2017).
119. Li, Y., Tang, W. & Guo, M. The Cell as Matter: Connecting Molecular Biology to Cellular Functions. *Matter* **4**, 1863-1891 (2021).
120. Wang, N., Tytell, J.D. & Ingber, D.E. Mechanotransduction at a distance: mechanically coupling the extracellular matrix with the nucleus. *Nat Rev Mol Cell Biol* **10**, 75-82 (2009).
121. Lammerding, J., Engler, A.J. & Kamm, R. Mechanobiology of the cell nucleus. *APL Bioeng* **6**, 040401 (2022).
122. Arsenovic, P.T. *et al.* Nesprin-2G, a Component of the Nuclear LINC Complex, Is Subject to Myosin-Dependent Tension. *Biophys J* **110**, 34-43 (2016).
123. Lombardi, M.L. *et al.* The interaction between nesprins and sun proteins at the nuclear envelope is critical for force transmission between the nucleus and cytoskeleton. *J Biol Chem* **286**, 26743-26753 (2011).
124. Cho, S., Irianto, J. & Discher, D.E. Mechanosensing by the nucleus: From pathways to scaling relationships. *J Cell Biol* **216**, 305-315 (2017).
125. Walker, C.J. *et al.* Nuclear mechanosensing drives chromatin remodelling in persistently activated fibroblasts. *Nat Biomed Eng* **5**, 1485-1499 (2021).
126. Killaars, A.R., Walker, C.J. & Anseth, K.S. Nuclear mechanosensing controls MSC osteogenic potential through HDAC epigenetic remodeling. *Proc Natl Acad Sci U S A* **117**, 21258-21266 (2020).
127. Wong, X., Melendez-Perez, A.J. & Reddy, K.L. The Nuclear Lamina. *Cold Spring Harb Perspect Biol* **14** (2022).
128. Okada, Y. *et al.* Dissociation of heterochromatin protein 1 from lamin B receptor induced by human polyomavirus agnoprotein: role in nuclear egress of viral particles. *EMBO Rep* **6**, 452-457 (2005).

129. Segura-Totten, M. & Wilson, K.L. BAF: roles in chromatin, nuclear structure and retrovirus integration. *Trends Cell Biol* **14**, 261-266 (2004).

130. Sun, J. *et al.* LAP2β transmits force to upregulate genes via chromatin domain stretching but not compression. *Acta Biomater* **163**, 326-338 (2023).

131. van Steensel, B. & Belmont, A.S. Lamina-Associated Domains: Links with Chromosome Architecture, Heterochromatin, and Gene Repression. *Cell* **169**, 780-791 (2017).

132. Lochs, S.J.A., Kefalopoulou, S. & Kind, J. Lamina Associated Domains and Gene Regulation in Development and Cancer. *Cells* **8** (2019).

133. Poh, Y.C. *et al.* Dynamic force-induced direct dissociation of protein complexes in a nuclear body in living cells. *Nat Commun* **3**, 866 (2012).

134. Tajik, A. *et al.* Transcription upregulation via force-induced direct stretching of chromatin. *Nat Mater* **15**, 1287-1296 (2016).

135. Sun, J., Chen, J., Mohagheghian, E. & Wang, N. Force-induced gene up-regulation does not follow the weak power law but depends on H3K9 demethylation. *Sci Adv* **6**, eaay9095 (2020).

136. Amar, K., Wei, F., Chen, J. & Wang, N. Effects of forces on chromatin. *APL Bioeng* **5**, 041503 (2021).

137. Na, S. *et al.* Rapid signal transduction in living cells is a unique feature of mechanotransduction. *Proc Natl Acad Sci U S A* **105**, 6626-6631 (2008).

138. Zhou, J. & Papautsky, I. Viscoelastic microfluidics: progress and challenges. *Microsyst Nanoeng* **6**, 113 (2020).

139. Su, Y., Iacob, R.E., Li, J., Engen, J.R. & Springer, T.A. Dynamics of integrin α5β1, fibronectin, and their complex reveal sites of interaction and conformational change. *J Biol Chem* **298**, 102323 (2022).

140. Maurer, M. & Lammerding, J. The Driving Force: Nuclear Mechanotransduction in Cellular Function, Fate, and Disease. *Annu Rev Biomed Eng* **21**, 443-468 (2019).

141. Meng, Z. *et al.* RAP2 mediates mechanoresponses of the Hippo pathway. *Nature* **560**, 655-660 (2018).

142. Dupont, S. *et al.* Role of YAP/TAZ in mechanotransduction. *Nature* **474**, 179-183 (2011).
143. Venturini, V. *et al.* The nucleus measures shape changes for cellular proprioception to control dynamic cell behavior. *Science* **370** (2020).
144. Nava, M.M. *et al.* Heterochromatin-Driven Nuclear Softening Protects the Genome against Mechanical Stress-Induced Damage. *Cell* **181**, 800-817.e822 (2020).
145. Schneider, S.E. *et al.* Dynamic biophysical responses of neuronal cell nuclei and cytoskeletal structure following high impulse loading. *Acta Biomater* **163**, 339-350 (2023).
146. Heo, S.J. *et al.* Aberrant chromatin reorganization in cells from diseased fibrous connective tissue in response to altered chemomechanical cues. *Nat Biomed Eng* **7**, 177-191 (2023).
147. Betapudi, V. Life without double-headed non-muscle myosin II motor proteins. *Front Chem* **2**, 45 (2014).
148. Costa, A.R. & Sousa, M.M. Non-Muscle Myosin II in Axonal Cell Biology: From the Growth Cone to the Axon Initial Segment. *Cells* **9** (2020).
149. Zhai, K. *et al.* NMMHC IIA inhibition impedes tissue factor expression and venous thrombosis via Akt/GSK3β-NF-κB signalling pathways in the endothelium. *Thromb Haemost* **114**, 173-185 (2015).
150. Nguyen-Ngoc, K.V., Silvestri, V.L., Georgess, D., Fairchild, A.N. & Ewald, A.J. Mosaic loss of non-muscle myosin IIA and IIB is sufficient to induce mammary epithelial proliferation. *J Cell Sci* **130**, 3213-3221 (2017).
151. Jana, S.S., Kawamoto, S. & Adelstein, R.S. A specific isoform of nonmuscle myosin II-C is required for cytokinesis in a tumor cell line. *J Biol Chem* **281**, 24662-24670 (2006).
152. Craig, R. & Padrón, R. Structural basis of the super- and hyper-relaxed states of myosin II. *J Gen Physiol* **154** (2022).
153. O'Connell, C.B., Tyska, M.J. & Mooseker, M.S. Myosin at work: motor adaptations for a variety of cellular functions. *Biochim Biophys Acta* **1773**, 615-

630 (2007).

154. Vicente-Manzanares, M., Newell-Litwa, K., Bachir, A.I., Whitmore, L.A. & Horwitz, A.R. Myosin IIA/IIB restrict adhesive and protrusive signaling to generate front-back polarity in migrating cells. *J Cell Biol* **193**, 381-396 (2011).

155. Roy, A. *et al.* Activity of nonmuscle myosin II isoforms determines localization at the cleavage furrow of megakaryocytes. *Blood* **128**, 3137-3145 (2016).

156. Heuzé, M.L. *et al.* Myosin II isoforms play distinct roles in adherens junction biogenesis. *Elife* **8** (2019).

157. Weißenbruch, K. *et al.* Distinct roles of nonmuscle myosin II isoforms for establishing tension and elasticity during cell morphodynamics. *Elife* **10** (2021).

158. Conti, M.A. & Adelstein, R.S. Nonmuscle myosin II moves in new directions. *J Cell Sci* **121**, 11-18 (2008).

159. Brito, C. & Sousa, S. Non-Muscle Myosin 2A (NM2A): Structure, Regulation and Function. *Cells* **9** (2020).

160. Vicente-Manzanares, M., Ma, X., Adelstein, R.S. & Horwitz, A.R. Non-muscle myosin II takes centre stage in cell adhesion and migration. *Nat Rev Mol Cell Biol* **10**, 778-790 (2009).

161. Pecci, A., Ma, X., Savoia, A. & Adelstein, R.S. MYH9: Structure, functions and role of non-muscle myosin IIA in human disease. *Gene* **664**, 152-167 (2018).

162. Llinas, P. *et al.* How myosin motors power cellular functions: an exciting journey from structure to function: based on a lecture delivered at the 34th FEBS Congress in Prague, Czech Republic, July 2009. *Febs j* **279**, 551-562 (2012).

163. Woody, M.S., Winkelmann, D.A., Capitanio, M., Ostap, E.M. & Goldman, Y.E. Single molecule mechanics resolves the earliest events in force generation by cardiac myosin. *Elife* **8** (2019).

164. Cirilo, J.A., Jr., Gunther, L.K. & Yengo, C.M. Functional Role of Class III Myosins in Hair Cells. *Front Cell Dev Biol* **9**, 643856 (2021).

165. Yaron Ideses., Adar Sonn-Segev., Yael Roichmanb. & Bernheim-Groswasser, A. Myosin II does it all: assembly, remodeling, anddisassembly of actin networks are governed by myosin II activity. *Soft Matter* **9** (2013).

166. Murrell, M., Oakes, P.W., Lenz, M. & Gardel, M.L. Forcing cells into shape: the mechanics of actomyosin contractility. *Nat Rev Mol Cell Biol* **16**, 486-498 (2015).

167. Sonal *et al.* Myosin-II activity generates a dynamic steady state with continuous actin turnover in a minimal actin cortex. *J Cell Sci* **132** (2018).

168. Guha, M., Zhou, M. & Wang, Y.L. Cortical actin turnover during cytokinesis requires myosin II. *Curr Biol* **15**, 732-736 (2005).

169. Ramanathan, S.P. *et al.* Cdk1-dependent mitotic enrichment of cortical myosin II promotes cell rounding against confinement. *Nat Cell Biol* **17**, 148-159 (2015).

170. Xia, Y. *et al.* Rescue of DNA damage after constricted migration reveals a mechano-regulated threshold for cell cycle. *J Cell Biol* **218**, 2545-2563 (2019).

171. Chaubet, L., Chaudhary, A.R., Heris, H.K., Ehrlicher, A.J. & Hendricks, A.G. Dynamic actin cross-linking governs the cytoplasm's transition to fluid-like behavior. *Mol Biol Cell* **31**, 1744-1752 (2020).

172. Wang, N. *et al.* Cell prestress. I. Stiffness and prestress are closely associated in adherent contractile cells. *Am J Physiol Cell Physiol* **282**, C606-616 (2002).

173. Chan, C.J. *et al.* Myosin II Activity Softens Cells in Suspension. *Biophys J* **108**, 1856-1869 (2015).

174. Stull, J.T., Kamm, K.E. & Vandenboom, R. Myosin light chain kinase and the role of myosin light chain phosphorylation in skeletal muscle. *Arch Biochem Biophys* **510**, 120-128 (2011).

175. Tsai, M.H. & Jiang, M.J. Rho-kinase-mediated regulation of receptor-agonist-stimulated smooth muscle contraction. *Pflugers Arch* **453**, 223-232 (2006).

176. Martinsen, A., Dessy, C. & Morel, N. Regulation of calcium channels in smooth muscle: new insights into the role of myosin light chain kinase. *Channels (Austin)* **8**, 402-413 (2014).

177. Li, X. *et al.* Calcium and TRPV4 promote metastasis by regulating cytoskeleton through the RhoA/ROCK1 pathway in endometrial cancer. *Cell Death Dis* **11**, 1009 (2020).

178. Deng, Z. *et al.* RhoA/ROCK pathway: implication in osteoarthritis and therapeutic targets. *Am J Transl Res* **11**, 5324-5331 (2019).
179. Olson, M.F., Ashworth, A. & Hall, A. An essential role for Rho, Rac, and Cdc42 GTPases in cell cycle progression through G1. *Science* **269**, 1270-1272 (1995).
180. Chuang, H.H. *et al.* ROCKII Ser1366 phosphorylation reflects the activation status. *Biochem J* **443**, 145-151 (2012).
181. Zhou, M. & Wang, Y.L. Distinct pathways for the early recruitment of myosin II and actin to the cytokinetic furrow. *Mol Biol Cell* **19**, 318-326 (2008).
182. Kar, J., Kar, S., Gupta, A. & Jana, S.S. Assembly and disassembly dynamics of nonmuscle myosin II control endosomal fission. *Cell Rep* **42**, 112108 (2023).
183. Martens, J.C. & Radmacher, M. Softening of the actin cytoskeleton by inhibition of myosin II. *Pflugers Arch* **456**, 95-100 (2008).
184. Pal, K., Tu, Y. & Wang, X. Single-Molecule Force Imaging Reveals That Podosome Formation Requires No Extracellular Integrin-Ligand Tensions or Interactions. *ACS Nano* **16**, 2481-2493 (2022).
185. Smith, A.S. *et al.* Myosin IIA interacts with the spectrin-actin membrane skeleton to control red blood cell membrane curvature and deformability. *Proc Natl Acad Sci U S A* **115**, E4377-e4385 (2018).
186. Kassianidou, E., Hughes, J.H. & Kumar, S. Activation of ROCK and MLCK tunes regional stress fiber formation and mechanics via preferential myosin light chain phosphorylation. *Mol Biol Cell* **28**, 3832-3843 (2017).
187. Totsukawa, G. *et al.* Distinct roles of MLCK and ROCK in the regulation of membrane protrusions and focal adhesion dynamics during cell migration of fibroblasts. *J Cell Biol* **164**, 427-439 (2004).
188. Beach, J.R. *et al.* Actin dynamics and competition for myosin monomer govern the sequential amplification of myosin filaments. *Nat Cell Biol* **19**, 85-93 (2017).
189. Broders-Bondon, F., Nguyen Ho-Bouldoires, T.H., Fernandez-Sanchez, M.E. & Farge, E. Mechanotransduction in tumor progression: The dark side of the force. *J Cell Biol* **217**, 1571-1587 (2018).
190. Surcel, A. & Robinson, D.N. Meddling with myosin's mechanobiology in cancer.

Proc Natl Acad Sci U S A **116**, 15322-15323 (2019).

191. Ouderkirk, J.L. & Krendel, M. Non-muscle myosins in tumor progression, cancer cell invasion, and metastasis. *Cytoskeleton (Hoboken)* **71**, 447-463 (2014).

192. Ananthakrishnan, R. & Ehrlicher, A. The forces behind cell movement. *Int J Biol Sci* **3**, 303-317 (2007).

193. Warner, H., Wilson, B.J. & Caswell, P.T. Control of adhesion and protrusion in cell migration by Rho GTPases. *Curr Opin Cell Biol* **56**, 64-70 (2019).

194. Verkhovsky, A.B., Svitkina, T.M. & Borisy, G.G. Self-polarization and directional motility of cytoplasm. *Curr Biol* **9**, 11-20 (1999).

195. Pasapera, A.M. *et al.* MARK2 regulates directed cell migration through modulation of myosin II contractility and focal adhesion organization. *Curr Biol* **32**, 2704-2718.e2706 (2022).

196. Georgouli, M. *et al.* Regional Activation of Myosin II in Cancer Cells Drives Tumor Progression via a Secretory Cross-Talk with the Immune Microenvironment. *Cell* **176**, 757-774.e723 (2019).

197. Yeoman, B. *et al.* Adhesion strength and contractility enable metastatic cells to become adurotactic. *Cell Rep* **34**, 108816 (2021).

198. Isomursu, A. *et al.* Directed cell migration towards softer environments. *Nat Mater* **21**, 1081-1090 (2022).

199. Wang, A.Y. *et al.* DDR1 associates with TRPV4 in cell-matrix adhesions to enable calcium-regulated myosin activity and collagen compaction. *J Cell Physiol* **237**, 2451-2468 (2022).

200. Huang, X. *et al.* RhoA-stimulated intra-capillary morphology switch facilitates the arrest of individual circulating tumor cells. *Int J Cancer* **142**, 2094-2105 (2018).

201. Orgaz, J.L. *et al.* Myosin II Reactivation and Cytoskeletal Remodeling as a Hallmark and a Vulnerability in Melanoma Therapy Resistance. *Cancer Cell* **37**, 85-103.e109 (2020).

202. Gerum, R. *et al.* Viscoelastic properties of suspended cells measured with shear

flow deformation cytometry. *Elife* **11** (2022).

203. Kim, D.H., Hah, J. & Wirtz, D. Mechanics of the Cell Nucleus. *Adv Exp Med Biol* **1092**, 41-55 (2018).
204. Guilluy, C. *et al.* Isolated nuclei adapt to force and reveal a mechanotransduction pathway in the nucleus. *Nat Cell Biol* **16**, 376-381 (2014).
205. Newberg, J. *et al.* Isolated nuclei stiffen in response to low intensity vibration. *J Biomech* **111**, 110012 (2020).
206. Wang, X. *et al.* Intracellular manipulation and measurement with multipole magnetic tweezers. *Sci Robot* **4** (2019).
207. Kirby, T.J. & Lammerding, J. Emerging views of the nucleus as a cellular mechanosensor. *Nat Cell Biol* **20**, 373-381 (2018).
208. Elosegui-Artola, A. *et al.* Force Triggers YAP Nuclear Entry by Regulating Transport across Nuclear Pores. *Cell* **171**, 1397-1410.e1314 (2017).
209. Koushki, N., Ghagre, A., Srivastava, L.K., Molter, C. & Ehrlicher, A.J. Nuclear compression regulates YAP spatiotemporal fluctuations in living cells. *Proc Natl Acad Sci U S A* **120**, e2301285120 (2023).
210. Zimmerli, C.E. *et al.* Nuclear pores dilate and constrict in cellulo. *Science* **374**, eabd9776 (2021).
211. Andreu, I. *et al.* Mechanical force application to the nucleus regulates nucleocytoplasmic transport. *Nat Cell Biol* **24**, 896-905 (2022).
212. Lomakin, A.J. *et al.* The nucleus acts as a ruler tailoring cell responses to spatial constraints. *Science* **370** (2020).
213. Kalukula, Y., Stephens, A.D., Lammerding, J. & Gabriele, S. Mechanics and functional consequences of nuclear deformations. *Nat Rev Mol Cell Biol* **23**, 583-602 (2022).
214. Paul, C.D., Mistriotis, P. & Konstantopoulos, K. Cancer cell motility: lessons from migration in confined spaces. *Nat Rev Cancer* **17**, 131-140 (2017).
215. Nader, G.P.F. *et al.* Compromised nuclear envelope integrity drives TREX1-dependent DNA damage and tumor cell invasion. *Cell* **184**, 5230-5246.e5222 (2021).

216. Denais, C.M. *et al.* Nuclear envelope rupture and repair during cancer cell migration. *Science* **352**, 353-358 (2016).

217. Raab, M. *et al.* ESCRT III repairs nuclear envelope ruptures during cell migration to limit DNA damage and cell death. *Science* **352**, 359-362 (2016).

218. Hsia, C.R. *et al.* Confined migration induces heterochromatin formation and alters chromatin accessibility. *iScience* **25**, 104978 (2022).

219. Gerlitz, G. The Emerging Roles of Heterochromatin in Cell Migration. *Front Cell Dev Biol* **8**, 394 (2020).

220. Song, Y. *et al.* Transient nuclear deformation primes epigenetic state and promotes cell reprogramming. *Nat Mater* **21**, 1191-1199 (2022).

221. Vahabikashi, A., Adam, S.A., Medalia, O. & Goldman, R.D. Nuclear lamins: Structure and function in mechanobiology. *APL Bioeng* **6**, 011503 (2022).

222. Nagano, A. & Arahata, K. Nuclear envelope proteins and associated diseases. *Curr Opin Neurol* **13**, 533-539 (2000).

223. Chiarini, F. *et al.* Lamin A and the LINC complex act as potential tumor suppressors in Ewing Sarcoma. *Cell Death Dis* **13**, 346 (2022).

224. Dechat, T., Adam, S.A., Taimen, P., Shimi, T. & Goldman, R.D. Nuclear lamins. *Cold Spring Harb Perspect Biol* **2**, a000547 (2010).

225. Swift, J. *et al.* Nuclear lamin-A scales with tissue stiffness and enhances matrix-directed differentiation. *Science* **341**, 1240104 (2013).

226. Vahabikashi, A. *et al.* Nuclear lamin isoforms differentially contribute to LINC complex-dependent nucleocytoskeletal coupling and whole-cell mechanics. *Proc Natl Acad Sci U S A* **119**, e2121816119 (2022).

227. Danielsson, B.E. *et al.* Nuclear lamina strain states revealed by intermolecular force biosensor. *Nat Commun* **14**, 3867 (2023).

228. Harada, T. *et al.* Nuclear lamin stiffness is a barrier to 3D migration, but softness can limit survival. *J Cell Biol* **204**, 669-682 (2014).

229. Cho, S. *et al.* Mechanosensing by the Lamina Protects against Nuclear Rupture, DNA Damage, and Cell-Cycle Arrest. *Dev Cell* **49**, 920-935.e925 (2019).

230. Earle, A.J. *et al.* Mutant lamins cause nuclear envelope rupture and DNA

damage in skeletal muscle cells. *Nat Mater* **19**, 464-473 (2020).

231. Wang, Y.J. *et al.* Lamin A/C and Vimentin as a Coordinated Regulator during Amoeboid Migration in Microscale Confined Microenvironments. *Nano Lett* (2023).

232. Fu, Y. *et al.* Nanotube patterning reduces macrophage inflammatory response via nuclear mechanotransduction. *J Nanobiotechnology* **21**, 229 (2023).

233. Buxboim, A. *et al.* Matrix elasticity regulates lamin-A,C phosphorylation and turnover with feedback to actomyosin. *Curr Biol* **24**, 1909-1917 (2014).

234. Fan, Y., Wang, J., Kim, J., Maeda, E. & Matsumoto, T. Dependency of deformation of cell nucleus on stretch direction of tissue: Relation to anisotropic response of aortic media to hypertension. *J Mech Behav Biomed Mater* **133**, 105326 (2022).

235. Hazel, A.L. & Pedley, T.J. Vascular endothelial cells minimize the total force on their nuclei. *Biophys J* **78**, 47-54 (2000).

236. Pogoda, K. *et al.* Unique Role of Vimentin Networks in Compression Stiffening of Cells and Protection of Nuclei from Compressive Stress. *Nano Lett* **22**, 4725-4732 (2022).

237. Takaki, T. *et al.* Actomyosin drives cancer cell nuclear dysmorphia and threatens genome stability. *Nat Commun* **8**, 16013 (2017).

238. Purushothaman, D. *et al.* The transcription factor PREP1(PKNOX1) regulates nuclear stiffness, the expression of LINC complex proteins and mechanotransduction. *Commun Biol* **5**, 456 (2022).

239. Zhang, Y. *et al.* Net39 protects muscle nuclei from mechanical stress during the pathogenesis of Emery-Dreifuss muscular dystrophy. *J Clin Invest* **133** (2023).

240. Fernandez, A., Bautista, M., Wu, L. & Pinaud, F. Emerin self-assembly and nucleoskeletal coupling regulate nuclear envelope mechanics against stress. *J Cell Sci* **135** (2022).

241. Jung-Garcia, Y. *et al.* LAP1 supports nuclear adaptability during constrained melanoma cell migration and invasion. *Nat Cell Biol* **25**, 108-119 (2023).

242. Gilbert, H.T.J. *et al.* Nuclear decoupling is part of a rapid protein-level cellular

response to high-intensity mechanical loading. *Nat Commun* **10**, 4149 (2019).

243. Wang, X. *et al.* Mechanical stability of the cell nucleus - roles played by the cytoskeleton in nuclear deformation and strain recovery. *J Cell Sci* **131** (2018).

244. Danielsson, B.E. *et al.* Chromatin condensation regulates endothelial cell adaptation to shear stress. *Mol Biol Cell* **33**, ar101 (2022).

245. Chala, N. *et al.* 4D Force Detection of Cell Adhesion and Contractility. *Nano Lett* **23**, 2467-2475 (2023).

246. Elliot Jokl. *et al.* PAK1-dependant mechanotransduction enables myofibroblast nuclear adaptation and chromatin organisation during fibrosis. *bioRxiv* (2023).

247. Arsenovic, P.T. & Conway, D.E. Using Nesprin Tension Sensors to Measure Force on the LINC Complex. *Methods Mol Biol* **1840**, 59-71 (2018).

248. Chen, T.W. *et al.* Ultrasensitive fluorescent proteins for imaging neuronal activity. *Nature* **499**, 295-300 (2013).

249. Zhang, Y. *et al.* Interfacing 3D magnetic twisting cytometry with confocal fluorescence microscopy to image force responses in living cells. *Nat Protoc* **12**, 1437-1450 (2017).

250. Liu, J. *et al.* Soft fibrin gels promote selection and growth of tumorigenic cells. *Nat Mater* **11**, 734-741 (2012).

251. Matta, H. *et al.* Development and characterization of a novel luciferase based cytotoxicity assay. *Sci Rep* **8**, 199 (2018).

252. Hsieh, M.H. & Nguyen, H.T. Molecular mechanism of apoptosis induced by mechanical forces. *Int Rev Cytol* **245**, 45-90 (2005).

253. Gray, K.M. & Stroka, K.M. Vascular endothelial cell mechanosensing: New insights gained from biomimetic microfluidic models. *Semin Cell Dev Biol* **71**, 106-117 (2017).

254. Meng, S. *et al.* Circulating tumor cells in patients with breast cancer dormancy. *Clin Cancer Res* **10**, 8152-8162 (2004).

255. Kumar, R., Saha, S. & Sinha, B. Cell spread area and traction forces determine myosin-II-based cortex thickness regulation. *Biochim Biophys Acta Mol Cell Res* **1866**, 118516 (2019).

256. Barnes, J.M., Nauseef, J.T. & Henry, M.D. Resistance to fluid shear stress is a conserved biophysical property of malignant cells. *PLoS One* **7**, e50973 (2012).

257. Colville, K., Tompkins, N., Rutenberg, A.D. & Jericho, M.H. Effects of poly(L-lysine) substrates on attached Escherichia coli bacteria. *Langmuir* **26**, 2639-2644 (2010).

258. Humphries, J.D. *et al.* Vinculin controls focal adhesion formation by direct interactions with talin and actin. *J Cell Biol* **179**, 1043-1057 (2007).

259. Kim, G.B., Park, K.H. & Kim, S.J. Hemodynamics and Wall Shear Stress of Blood Vessels in Aortic Coarctation with Computational Fluid Dynamics Simulation. *Molecules* **27** (2022).

260. Surcel, A. *et al.* Pharmacological activation of myosin II paralogs to correct cell mechanics defects. *Proc Natl Acad Sci U S A* **112**, 1428-1433 (2015).

261. Kovács, M., Tóth, J., Hetényi, C., Málnási-Csizmadia, A. & Sellers, J.R. Mechanism of blebbistatin inhibition of myosin II. *J Biol Chem* **279**, 35557-35563 (2004).

262. Narumiya, S., Ishizaki, T. & Uehata, M. Use and properties of ROCK-specific inhibitor Y-27632. *Methods Enzymol* **325**, 273-284 (2000).

263. Baek, J. *et al.* Egr1 is a 3D matrix-specific mediator of mechanosensitive stem cell lineage commitment. *Sci Adv* **8**, eabm4646 (2022).

264. Fabian, L., Troscianczuk, J. & Forer, A. Calyculin A, an enhancer of myosin, speeds up anaphase chromosome movement. *Cell Chromosome* **6**, 1 (2007).

265. Debaugnies, M. *et al.* RHOJ controls EMT-associated resistance to chemotherapy. *Nature* **616**, 168-175 (2023).

266. Safaei, S. *et al.* Tumor matrix stiffness provides fertile soil for cancer stem cells. *Cancer Cell Int* **23**, 143 (2023).

267. Shah, P. *et al.* ATM Modulates Nuclear Mechanics by Regulating Lamin A Levels. *Front Cell Dev Biol* **10**, 875132 (2022).

268. Dos Santos, Á. *et al.* DNA damage alters nuclear mechanics through chromatin reorganization. *Nucleic Acids Res* **49**, 340-353 (2021).

269. Peiris-Pagès, M., Sotgia, F. & Lisanti, M.P. Doxycycline and therapeutic

targeting of the DNA damage response in cancer cells: old drug, new purpose. *Oncoscience* **2**, 696-699 (2015).

270. Prokocimer, M. *et al.* Nuclear lamins: key regulators of nuclear structure and activities. *J Cell Mol Med* **13**, 1059-1085 (2009).

271. Srivastava, L.K., Ju, Z., Ghagre, A. & Ehrlicher, A.J. Spatial distribution of lamin A/C determines nuclear stiffness and stress-mediated deformation. *J Cell Sci* **134** (2021).

272. Buchwalter, A. Intermediate, but not average: The unusual lives of the nuclear lamin proteins. *Curr Opin Cell Biol* **84**, 102220 (2023).

273. Botello-Smith, W.M. *et al.* A mechanism for the activation of the mechanosensitive Piezo1 channel by the small molecule Yoda1. *Nat Commun* **10**, 4503 (2019).

274. Kim, T.J. *et al.* Distinct mechanisms regulating mechanical force-induced Ca^{2+} signals at the plasma membrane and the ER in human MSCs. *Elife* **4**, e04876 (2015).

275. Zheng, M., Jin, G. & Zhou, Z. Post-Translational Modification of Lamins: Mechanisms and Functions. *Front Cell Dev Biol* **10**, 864191 (2022).

276. Xiong, Y. *et al.* Myosin Light Chain Kinase: A Potential Target for Treatment of Inflammatory Diseases. *Front Pharmacol* **8**, 292 (2017).

277. Watanabe, H. *et al.* An essential role of myosin light-chain kinase in the regulation of agonist- and fluid flow-stimulated Ca2+ influx in endothelial cells. *Faseb j* **12**, 341-348 (1998).

278. Wu, Y. *et al.* ROCK inhibitor Y27632 promotes proliferation and diminishes apoptosis of marmoset induced pluripotent stem cells by suppressing expression and activity of caspase-3. *Theriogenology* **85**, 302-314 (2016).

279. Mazumder, A., Roopa, T., Basu, A., Mahadevan, L. & Shivashankar, G.V. Dynamics of chromatin decondensation reveals the structural integrity of a mechanically prestressed nucleus. *Biophys J* **95**, 3028-3035 (2008).

280. Mazumder, A. & Shivashankar, G.V. Emergence of a prestressed eukaryotic nucleus during cellular differentiation and development. *J R Soc Interface* **7**

Suppl 3, S321-330 (2010).

281. Hamza, B. *et al.* Measuring kinetics and metastatic propensity of CTCs by blood exchange between mice. *Nat Commun* **12**, 5680 (2021).
282. Benjamin, D.C. *et al.* YAP Enhances Tumor Cell Dissemination by Promoting Intravascular Motility and Reentry into Systemic Circulation. *Cancer Res* **80**, 3867-3879 (2020).
283. Fischer, T., Hayn, A. & Mierke, C.T. Effect of Nuclear Stiffness on Cell Mechanics and Migration of Human Breast Cancer Cells. *Front Cell Dev Biol* **8**, 393 (2020).
284. Grashoff, C. *et al.* Measuring mechanical tension across vinculin reveals regulation of focal adhesion dynamics. *Nature* **466**, 263-266 (2010).
285. Brenner, M.D. *et al.* Spider Silk Peptide Is a Compact, Linear Nanospring Ideal for Intracellular Tension Sensing. *Nano Lett* **16**, 2096-2102 (2016).
286. Mierke, C.T. Viscoelasticity, Like Forces, Plays a Role in Mechanotransduction. *Front Cell Dev Biol* **10**, 789841 (2022).
287. Katsuta, H. *et al.* Actin crosslinking by α-actinin averts viscous dissipation of myosin force transmission in stress fibers. *iScience* **26**, 106090 (2023).
288. Humphrey, D., Duggan, C., Saha, D., Smith, D. & Käs, J. Active fluidization of polymer networks through molecular motors. *Nature* **416**, 413-416 (2002).
289. Truong, T., Sun, G., Doorly, M., Wang, J.Y. & Schwartz, M.A. Modulation of DNA damage-induced apoptosis by cell adhesion is independently mediated by p53 and c-Abl. *Proc Natl Acad Sci U S A* **100**, 10281-10286 (2003).
290. Mammoto, A., Mammoto, T. & Ingber, D.E. Mechanosensitive mechanisms in transcriptional regulation. *J Cell Sci* **125**, 3061-3073 (2012).
291. Stephens, A.D., Banigan, E.J., Adam, S.A., Goldman, R.D. & Marko, J.F. Chromatin and lamin A determine two different mechanical response regimes of the cell nucleus. *Mol Biol Cell* **28**, 1984-1996 (2017).
292. Stephens, A.D., Banigan, E.J. & Marko, J.F. Separate roles for chromatin and lamins in nuclear mechanics. *Nucleus* **9**, 119-124 (2018).
293. Elamin, E., Masclee, A., Dekker, J. & Jonkers, D. Ethanol disrupts intestinal

epithelial tight junction integrity through intracellular calcium-mediated Rho/ROCK activation. *Am J Physiol Gastrointest Liver Physiol* **306**, G677-685 (2014).

294. Barcelo, J., Samain, R. & Sanz-Moreno, V. Preclinical to clinical utility of ROCK inhibitors in cancer. *Trends Cancer* **9**, 250-263 (2023).